Master's thesis

NTNU
Norwegian University of Science and Technology
Faculty of Engineering
Department of Marine Technology

Emilie H. T. Wittemann

Hybrid Observers for Autonomous Surface Vessels Experiencing Varying Operational Conditions

Master's thesis in Marin Teknikk
Supervisor: Dong Trong Nguyen
June 2021

NTNU
Norwegian University of
Science and Technology

Emilie H. T. Wittemann

Hybrid Observers for Autonomous Surface Vessels Experiencing Varying Operational Conditions

Master's thesis in Marin Teknikk
Supervisor: Dong Trong Nguyen
June 2021

Norwegian University of Science and Technology
Faculty of Engineering
Department of Marine Technology

NTNU
Norwegian University of
Science and Technology

NTNU
Kunnskap for en bedre verden

Department of Marine Technology

Hybrid Observers for Autonomous Surface Vessels Experiencing Varying Operational Conditions

Author:
Emilie H. Thirud Wittemann

Main supervisor:
Dong Trong Nguyen

June 10, 2021

NTNU Trondheim
Norwegian University of Science and Technology
Department of Marine Technology

MSC THESIS DESCRIPTION SHEET

Name of the candidate: Emilie Wittemann

Field of study: Marine control engineering

Thesis title (Norwegian): Hybride Observere for Autonome Skip Utsatt for Varierende Operasjoner

Thesis title (English): Hybrid Observers for Autonomous Surface Vessels Experiencing Varying Operational Conditions

Background
An autonomous surface vessel sailing from a calm sea state environment at quay towards open sea will experience a varying sea state. In addition, the vessel will operate at varying speeds; and therefore the well-developed simulator used in the zero-speed regime are not applicable. Hence, a realistic simulation of a vessel sailing from quay to open sea will be subjected to varying sea state as well as varying loads due to increased speed. This thesis will first focus on further developing the MCSim model by implementing modules applicable for a vessel at higher speeds. The next task of the thesis is to develop a hybrid control scheme for the autonomous surface vessel operating in varying operational conditions. This hybrid control scheme will be validated through both simulations and model scaled ship, Cybership 3, at the MCLab.

Work description
1. Perform a background and literature review to provide information and relevant references on
    - Autonomous ships
    - Control for varying operational conditions
    - Hybrid control systems
    - Resetting Observer
    - Time-Varying Model-Based Observer

2. Write a list with abbreviations and definition of terms, explaining relevant concepts related to the literature study and thesis.

3. Develop a simulation model for a Cybership 3 in transit going from low speed to high speed. Where the focus must be on the following points to gain a sufficient simulation model:
    - Improving/changing the current reference model
    - Better handling of transient in wave drift forces and RAO, flip-flop model, together with velocity input to the wave drift block.

4. Develop hybrid controller from quay to open sea, using velocity measurements from GPS. Velocity measurements are available when the vessel is not in zero-speed regime.
    - Implement controller and observer for autopilot.
    - Conduct a formal stability analysis of the new controller and observer.
    - Conduct a simulation in MCSim for preparation of model experiments.

5. Conduct model experiment with Cybership 3 in MCLab of the vessel sailing from quay to open sea to verify simulation results.

Specifications
The scope of work may prove to be larger than initially anticipated. By the approval from the supervisor, described topics may be deleted or reduced in extent without consequences with regard to grading.

The candidate shall present personal contribution to the resolution of problems within the scope of work. Theories and conclusions should be based on mathematical derivations and logic reasoning identifying the various steps in the deduction.

The report shall be organized in a logical structure to give a clear exposition of background, results, assessments, and conclusions. The text should be brief and to the point, with a clear language. Rigorous mathematical deductions and illustrating figures are preferred over lengthy textual descriptions. The report shall have font size 11 pts., and it is not expected to be longer than 60-80 A4 pages, from introduction to conclusion, unless otherwise agreed upon. It shall be written in English (preferably US) and contain the following elements: Title page, abstract, acknowledgements, thesis specification, list of symbols and acronyms, table of contents, introduction with objective, background, and scope and delimitations, main body with problem formulations, derivations/developments and results, conclusions with recommendations for further work, references, and optional appendices. All figures, tables, and equations shall be numerated. The original contribution of the candidate and material taken from other sources shall be clearly identified. Work from other sources shall be properly acknowledged using quotations and a Harvard citation style (e.g. *natbib* Latex package). The work is expected to be conducted in an honest and ethical manner, without any sort of plagiarism and misconduct. Such practice is taken very seriously by the university and will have consequences. NTNU can use the results freely in research and teaching by proper referencing, unless otherwise agreed upon.

The thesis shall be submitted with a printed and electronic copy to the main supervisor, with the printed copy signed by the candidate. The final revised version of this thesis description must be included. The report must be submitted according to NTNU procedures. Computer code, pictures, videos, data series, and a PDF version of the report shall be included electronically with all submitted versions.

Start date: 11 January, 2021 **Due date:** 10 June, 2021

Supervisor: Dong Trong Nguyen
Co-advisor(s): TBD

Trondheim, _____

Dong Trong Nguyen
Supervisor

Preface

This thesis is written in spring 2021 at the Department of Marine Technology at the Norwegian University of Science and Technology (NTNU), Trondheim. The thesis concludes the five-year master program Marine Technology with Marine Cybernetics as a specialization field. Further, the thesis is a continuation of a thesis assignment written in fall 2020 on the same topic.

Working on the topic in this thesis has allowed me to investigate and deepen my knowledge about the opportunities to use hybrid framework in cybernetics, and especially in marine applications. In addition, I have gained a broad perspective of the journey towards the future autonomous surface vessel, mostly trough academic research, but also in industry projects. Therefore, this thesis has been a great and rewarding experience, from literature review to practical work at the laboratory.

Acknowledgments

During this thesis and project thesis, my supervisor, Dong Trong Nguyen, has never been further away than a video call. I want to express my gratitude to him for being available for guidance in both scheduled and non-scheduled meetings. Further, I want to thank Torgeir Wahl for his support and help in the laboratory. In addition, for fixing a new designated Cybership 3 computer on short notice, as the previous went out of order. I am also grateful for having a lab partner, Hans Sande, during the two intense weeks.

In addition, I wish to thank my parents for all their advice, encouragement, support during the five years, and for proofreading both the project thesis and master thesis. I wish to thank Henrik Heien for being an anchor in these strange times, always bringing a positive mindset and challenging me both academically and intellectually. Finally, I want to thank my office mates!

Trondheim, Thursday 10^{th} June, 2021
Emilie H. Thirud Wittemann

Abstract

This thesis investigates the topic of applying hybrid control theory to improve observer performance in transients due to varying operational conditions for marine surface vessels.

The thesis begins by conducting a literature review about the future autonomous surface vessels and levels of autonomy before further investigating hybrid control theory and links this together with the development of autonomous marine systems. Hybrid control allows for operations in harsher environments, more complex operations, increased safety, and reduced costs. Further, hybrid observers are explained and linked to the motion control system. The mechanisms and ideas of the observers of interest are presented. The thesis investigates today's alternatives and research on the topic of observers handling transients. In addition, the observer's bias mechanisms are explained to allow for better implementation of the bias load. As the observers do not include a high fidelity simulation model but rather a simplified version, the observer needs to include an appropriate bias load, accounting for the unmodelled loads and dynamics.

As a continuation of the literature review, the thesis presents five different test scenarios where the vessel is subjected to transit due to varying operational conditions. Each test is first investigated in the high fidelity simulation environment, Marine Cybernetics Simulator (MCSim). In addition, an extension of the environment was made to allow for varying sea states i varying surge speeds. Then model-scale experiments were conducted at the Marine Cybernetics Laboratory (MCLab) at the Department of Marine Technology (IMT), NTNU. After the tests, the observer performance was evaluated using a cost function.

The thesis concludes that the improvement of handling transients is significant in all occurrences of transients. The improvements were clear from both high fidelity simulations with the extension of varying sea states and in the model-scale laboratory experiments. In addition, a justification is made about which observer benefits in the different varying operational conditions.

Sammendrag

Denne masteroppgaven tar for seg bruk av hybrid kontrollteori for å forbedre observer-ytelse i transienter på grunn av varierende operasjonelle forhold for marine overflatefartøy.

Oppgaven begynner med litteraturstudie om de fremtidige autonome overflatefartøyene. Videre følger undersøkelse av hybrid kontrollteori, som knyttes sammen med utviklingen av autonome marine kontrollsystemer. Hybridkontroll muliggjør operasjoner i tøffere miljøer, mer komplekse operasjoner, økt sikkerhet og reduserte kostnader. Videre blir hybride observere forklart og presentert. Konseptet til observerene som undersøkes i denne masteroppgaven presenteres. Oppgaven undersøker dagens alternativer og forskning gjort på temaet hånderting av transienter av observere. I tillegg forklares observerenes bias-mekanismer for å muliggjøre en tilpasset implementering av bias-last avhengig av de operasjonelle forholdene. Ettersom observerene ikke inkluderer en presis simuleringsmodell, men snarere en forenklet versjon, må observeren inneholde en passende bias-last som tar hensyn til ikke-modellert dynamikk og last.

Som en fortsettelse av litteraturstudiet presenterer oppgaven fem forskjellige testscenarier hvor fartøyet utsettes for transiter på grunn av varierende operasjonelle forhold. Hver test blir først undersøkt i simuleringsmodellen Marine Kybernetikk Simulator (MCSim). I tillegg blir det gjort en utvidelse av simuleringsmodellen MCSim, for å gjøre det mulig å ha varierende sjøtilstander og varierende fremover-hastigheter. Deretter blir testene utført på Marine Kybernetikk Labratoriet (MCLab) ved Institutt for Marin Teknikk (IMT), NTNU. Etter testene blir observerens ytelse evaluert ved hjelp av en kostfunksjon.

Oppgaven konkluderer med at forbedringen av håndtering av transienter er signifikant i alle tilfeller av transienter. Forbedringene var tydelige fra både simuleringer og laboratorieeksperiementer. I tillegg er det gitt en begrunnelse for hvilken observer som gjør seg best i de forskjellige operasjonelle forhold, og dermed for hvilke fartøy det kan være hensiktsmessig å bruke disse observerene.

Contents

List of Figures

List of Tables

Abbreviation

CPM	Control Plant Model
CS3	Cybership 3
DOF	Degree of Freedom
DP	Dynamic Positioning
GES	Gloablly Exponentially Stable
GNSS	Global Navigation Satellite System
IMT	Department of Marine Technology
IMU	Inertial Measurement Unit
LF	Low-Frequency
LOA	Level of Autonomy
LP	Low Pass
MCSim	Marine Cybernetics Simulator
MCLab	Marine Cybernetics Laboratory
NPO	Nonlinear Passive Observer
OSC	Outer Semi-Continuous
PID	Proportional-Integral-Derivative
PM	Position Mooring
PPM	Process Plant Model
RAO	Response Amplitude Operator
RM	Reference Model
TVNPO	Time-varying Nonlinear Passive Observer
UGAS	Uniformally Gloablly Asymptotically Stable
UGpAS	Uniformally Globally pre-Asymptotic Stable
USV	Unmanned Surface Vessel
VOCs	Vessel Operational Conditions
WF	Wave-Frequency

Symbols

$\eta^b = [x\ y\ z]$	Position in body-fixed frame
$\eta^n = [N\ E\ D]$	Position in North-East-Down frame
$\eta^e = [\phi\, \theta\ \psi]$	Euler angles
$\nu = [u\ v\ r]$	velocity
τ	Generalized force vector
$R(\psi)$	Euler Angle Rotation matrix
M	Inertia matrix
M_{RB}	Rigid-body inertia matrix
M_A	Added mass matrix
C_{RB}	Rigid-body Coriolis matrix
D	Damping matrix
$G(\eta)$	Gravity matrix
T_{jj}	Quadratic hydrodynamic transfer-functions
A_j	Wave amplitude
ω_j	Wave frequency
β	Mean wave direction
ϵ_j	Random phase
η_{Rw}	Wave-frequency motion in hydrodynamic frame
η_w	Wave-frequency motion in the Earth-fixed frame (NED)
ξ	Wave motion
b	Bias Dynamics State
Δ	Relative damping ratios
Ω	Natural Frequencies
r	Reference input
$\mathcal{C}^n$	n-degrees of freedom
$\mathcal{A}$	Set of attraction
K_2, K_2, K_3, K_4	Gain injection gain matrices for NPO
K_P	Proportional gain
K_D	Derivative gain
K_I	Integral gain
u	Actuator input

Chapter 1

Introduction

This chapter will introduce the thesis with a background review, including the primary motivations for conducting this study. Following is a shortened version of the literature review undertaken in chapter 2. Next, the thesis's scope and objectives are presented, along with the main contributions of the thesis. Finally, the organization of the thesis is presented.

1.1 Background

Motivations for increased autonomy are improved safety for crew, passengers, and others involved in a marine operation and the opportunity for lower fuel consumption and overall better performance. In addition, the demands for marine operations are increasing. The demand results in operations in harsher environments and a demand for increased weather windows to conduct all-year marine operations such as subsea installation, drilling, and pipe-laying. The operations can be time-consuming and sensitive to the varying environment, such as a change in sea states. By implementing a hybrid control system, the autonomous process becomes more complex but facilitates the opportunity of a smoother autonomous operation (Sørensen [2011]).

Research on the topic *hybrid dynamical control* begun already in the 1960s by Witsenhausen. Up until today, research over a wide range of applications is conducted. Hybrid dynamical control is highly beneficial for marine systems because of the large diversity in the dynamical behavior of the various marine operations. When discussing hybrid systems, three vessel operational conditions (VOCs) are defines for a vessel: changes in the environment, operational mode, and speed. The VOCs are used as a boundary when discussing the application area of controllers and observers when discussing performance monitoring and switching logic.

The term *transit* has slightly different meanings depending on the setting. In the Cambridge Dictionary, transit is *the movement of goods and people from one place to another.* While in academia, transit is the phase between two steady-states, i.e., the transition phase. This could e.g., be the transition in thermodynamic processes or the acceleration between two speeds for a car. In the commercial industry of marine operations, transit often refers to the transit of a vessel between steady states due to environment, operation or speed, such as when e.g., carrying a wind turbine for offshore installation.

Hence, the benefits of improving the transient behavior for an autonomous surface vessel depend on the objective. For a commercial vessel conducting offshore installations, improving transit behavior would allow the vessel to sail at higher speeds, improving efficiency and reducing

cost. Further developments of improved autonomy could allow for the vessel to sail unmanned offshore with equipment. In addition, improved behavior in transients will allow for operations in harsher environments. Marine operations are not limited by the weather in the same way as before, as improved control systems can resist quick accelerations. Hence, transit in terms of operational conditions is the combination of change in environment, operational mode, and speed. Furthermore, the phase after a quick change in load has disturbed the steady-state, and the control system converges to steady-state again.

Behavior during transients of marine control systems has received more attention over recent years. Several researchers have been investigating how to improve performance and improve transient behavior. Several papers have been written on the topic of hybrid observers for dynamic positioning and low-speed maneuvering for vessels. The concept of time-varying gains observer gains [Værnø et al., 2017], acceleration feedforward [Skjetne and Øivind K. Kjerstad, 2016], switching between a model-based and signal-based observer [Brodtkorb et al., 2018d], and the resetting observer [Torben, 2019] discuss how transient performance can be improved with different technologies.

For a marine surface vessel, safe and stable behavior can be challenging to ensure compared to a car, as the car can quickly stop moving when unsure if a situation is safe. However, a vessel at quay or in offshore operations can not stop moving to ensure safety as the dynamics and environment are much more complicated. The transient events discussed in this thesis are due to different varying operational conditions. Hence it will be possible to indicate which observers are suited for what. Further, this thesis can work as guidance for choosing a suitable observer depending on the type of operations and the type of vessel. Figure 2.1 presents the different components of autonomous surface vessels which need to be autonomous or automatic. In addition, the four levels of autonomy can divide this process into four phases. Different methods and approaches will be used to obtain autonomy. E.g., situational awareness using artificial intelligence and optimization and control theory for motion and actuator control. Hence, it is evident that the future autonomous surface vessel will combine data science and control theory worlds. This thesis contributes to improving the automatic motion control system, a part of the comprehensive autonomous system

1.2 Shortened Literature Review

Sørensen [2011] conducts a review about the mature dynamical positioning (DP) technology design in addition to perspectives and possible future designs and challenges regarding future autonomy in the marine vessel. It is established that there is a variety of taxonomy used when addressing autonomy, and this thesis uses the four levels of autonomy defined by the National Institute of Standards and Technology. Further, these levels can be used to categorize the development into four phases. Hence, hybrid control systems can be addressed in these terms and put into the big picture of future autonomous surface vessels.

The development of autonomous surface vessels has begun, both in academia and in the commercial world. The approach varies depending on the purpose of the vessel, either dynamic positioning, position mooring, improved transit behavior, or tug vessels.

Hybrid dynamical systems in this context are control systems consisting of at least two controllers or observers. Hence, the control system based on a predefined performance monitoring and switching logic will automatically change to the appropriate controller or observer. This will allow for improved performance depending on the objective. Often, the objectives regarding hybrid control are in terms of the vessel operating conditions (VOCs): change in environment,

operational mode, and speed.

Hybrid control has been researched since the 1960s and has gained serious attention concerning marine vessel control systems in the previous years. The research has resulted in different technologies and approaches. Among the research objectives are expanding the operational window as this is highly motivated by the industry. Expanding the operational window will allow for conducting operations further offshore and in more adverse conditions. An example is that the hybrid control system will, by the help of sea state estimation, be able to automatically switch the controller or observer appropriate for the current sea state.

When researching and testing control systems for a marine surface vessel, the simulation model is of importance. The fidelity of the model has a significant impact on the validity of the results. The simulation model is crucial to know when creating extensive simulations for testing and verifying marine control systems; it needs to be accurate and reliable. *Marine Cybernetics Simulator* (MCSim) is a simulator created at the Department of Marine Technology in cooperation with the Department of Engineering Cybernetics in Matlab/Simulink. MCSim is a modular system simulator, resulting in a realistic environment for studying sea transportation, offshore oil and gas operations, fishery, and aquaculture.

The terms bias load and bias dynamics are introduced in the control plant model to capture unknown forces and moments. The knowledge of the simulation model is relevant as the control plant models are simplified versions of the process plant model in real life and need to include several unmodeled loads. If the control system is reliable, then the control system needs to be accurate and react appropriately. Due to its importance, there are different approaches to tackle this obstacle. The bias state is often designed to be slowly varying to capture the slowly varying environmental loads, but this has limited performance when the vessel is subjected to a rapid load.

Hybrid observers are a further development in hybrid dynamics, and these are observers based on a defined performance monitoring and switching logic changing its dynamics, resets, or changes gains. Four different hybrid observer technologies are in focus: the acceleration feedforward observer (Skjetne and Øivind K. Kjerstad [2016]), the switching between a model-based and signal-based observer (Brodtkorb et al. [2018d]), the resetting observer (Torben [2019]), and the time-varying model-based observer (Værnø et al. [2017]).

When implementing these technologies, either controller or observer, tuning of the control parameters is in order. The performance of controllers and observers is susceptible to operation, sea state, and these parameters must fit the objective. When conducting the tuning, there is a particular approach that allows for fine adjustment to infinity. Hence, it is beneficial to have settled an approach to find the optimal tuning and know when to be satisfied with the behavior.

The observers researched further in this thesis are the resetting observer (Torben [2019]) and the time-varying model-based observer (Værnø et al. [2017]). This thesis conducts a high-fidelity simulation of the two observers subjected to a transit phase.

1.3 Objective and Scope

The objective of the thesis is to give an overall understanding of today's alternatives to hybrid observers regarding the improvement of behavior in transients, i.e., in varying operational conditions. In addition, the objective includes developing the resetting observer and gain a scheduling observer for vessels experiencing transient conditions. A high-fidelity model-scale simulator and experiments will validate the proposed setup.

The scope of the thesis has been to

- Perform a background and literature review to provide information and relevant references on autonomous ships, control for varying operational conditions, hybrid control systems, resetting observer, and time-varying model-based observer.
- Further develop the simulation environment *Marine Cybernetics Simulator* (MCSim). The improvements were varying wave drifts and RAO due to varying sea states, including velocity input to the wave drift block, and improve and add new reference model(s). Then, implement the hybrid controller and test a vessel subjected to various operational conditions.
- Verify simulation results with a model-scaled experiment at the *Marine Cybernetics Laboratory* (MCLab) at the Department of Marine Technology. Both simulation and model-scaled experiments were conducted on the supply vessel Cybership 3 (CS3).
- Conduct a fair comparison and evaluation using a cost function.

1.4 Contribution

This thesis researches the case of a vessel experiencing transit due to varying operational conditions. This thesis develops a controller and observer scheme with hybrid observers to investigate the observers' performance. A high-fidelity simulator and laboratory experiments validate the controller scheme and hybrid observers. Hence, these results provide an indication of behavior in transient, to be used in observer choice decisions for different marine surface vessels.

The thesis further develops the existing MCSim, with increased fidelity, allowing varying sea states with varying surge speeds using a flip flop and nested flip flop model.

Experimental data of the motion control system using the hybrid resetting observer was also collected for the paper *A resetting observer for LTV systems with application to dynamic positioning of marine surface vessels*, Appendix B.

1.5 Organization

This thesis begins with a literary review in Chapter 2, covering the relevant research and work conducted on future unmanned surface vessels and autonomous ships, hybrid systems, and hybrid observers, including control for varying operational conditions.

Chapter 3 presents the relevant mathematical modeling of autonomous surface vessels used in simulation and experiments. Chapter 3.5 investigates the two observers further, presenting the mathematical model of the two observers, in addition to short stability analysis of the two observers, in hybrid framework.

Chapter 4 presents the methods used in the high-fidelity simulation study. First, the vessel characteristics of Cybership 3 are given. Then the hybrid observer test scenarios are presented and put in context. Next, the simulation setup is presented. In addition, the flip-flop model approach is explained using a motivational example. Further, the experimental setup is presented. Finally, a method to evaluate the observer's performance is presented.

Chapter 5 presents the results from the simulation, including modeling varying wave loads acting on the vessel due to the varying sea states. Chapter 6 shows the results from the model experiment conducted at the Marine Cybernetics Laboratory. Chapter 7 discusses the results from both sections and presents some challenges from the laboratory.

Chapter 8 concludes the thesis by sewing the literature review and the simulation and experiment and results and suggests future work.

Chapter 2

Literature Review

2.1 Autonomous Ships

The interest in autonomous marine vessels has increased both from academia and the industry. The main reasons are increased safety, reduced costs, and opening up for a broader range of operation possibilities. E.g., the surface vessel would be allowed to work in harsher environments further offshore, or an underwater vehicle could potentially do sea-floor mapping under the ice far north.

The unmanned surface vessel is a part of the journey towards autonomous ships. Different researchers and companies use different taxonomy when it comes to autonomy. This thesis uses a four-level definition defined by the US National Institute of Standards and Technology (as described in Sørensen [2018]). These levels of autonomy (LOA) are defined as follows.

1. Automatic operation (remote control)
2. Management by consent (teleoperation)
3. Semi-autonomous or management by exception
4. Highly autonomous

Furthermore, the architecture of the autonomous components can be illustrated as in Figure 2.1, this is defined from Zeabuz [1]. It shows all the necessary components and how they are sewed together from left to right. E.g., situational awareness allows the vessel to sense and perceive. Motion planning will create the optimal route, while motion control will find the optimal control input to the actuator control, which distributes these controller inputs to rotations at the propeller. Hence, improving the behavior in transients is regarding improving the motion control component, marked in red, in Figure 2.1

Ferries are becoming more autonomous. The ferry operates with different objectives than a platform supply vessel, as it sails a fixed and relatively short distance. The ferry may be subjected to more trafficked areas and more collision objects. The busiest ferry in Norway sailing between Horten and Moss has received an *auto-pilot* to navigate the vessel to quay. Due to safety measures, the crew is still present, meaning that they interfere with the control system if needed. However, the crew may now be able to conduct other tasks in addition.

[1] www.zeabuz.com

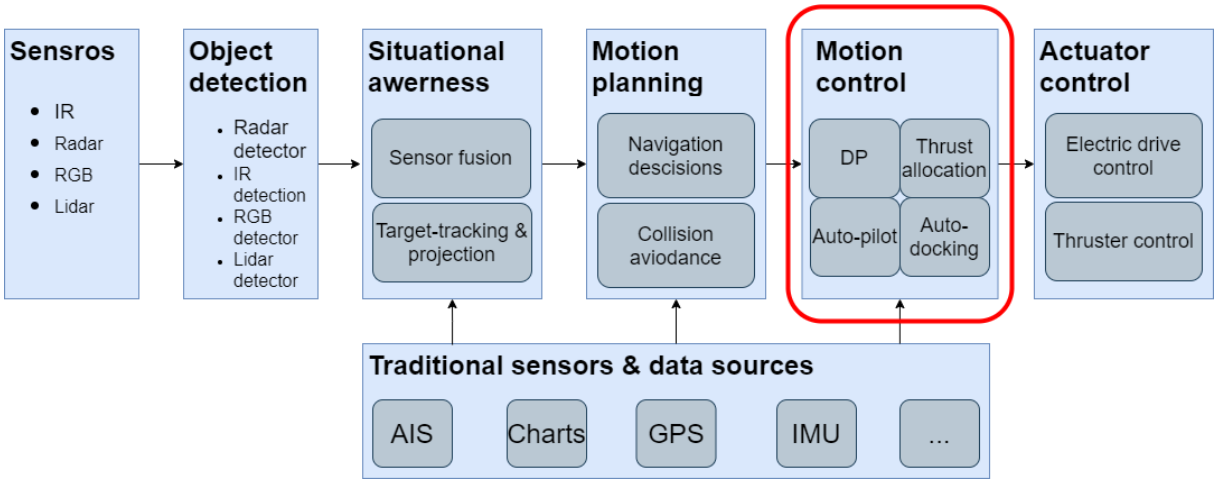

Figure 2.1: TMR06 - Autonomous Marine Systems: zeabuz lecture - Øyvind Smogeli, *NTNU Autonomy lecture*, 2020-10-26.

Another recent development is the Abu Dhabi Ports project with the naval architects at Robert Allan to develop unmanned autonomous tugs to operate in port (Hand). These tugs are meant to serve in more adverse weather conditions and increase operational safety. In addition to the development in Abu Dhabi, Singapore Port, in co-operations with Keppel and ABB, is developing the technology for autonomous vessels and retrofit a (32-meter) tugboat with digital solutions (Liang). The development is divided into different phases. The initial phase is to complete a series of navigational tasks in a designated area in Singapore Port remotely operated from onshore. The next phase is vessel performance concerning collision avoidance tasks while under remote supervision. The port of Singapore has 130 000 vessels calling annually, and one of the busiest ports there is, adding another complexity to the technology trials.

Further, the operation and development of offshore wind farms have increased over the years. This development uses research and technology developed for the oil and gas industry, meaning the operations are mature and available. Hence, the installation of offshore wind farms will happen further and further offshore, and the installations have strict safety requirements, and the vessels used need to have a reliable autonomous control. In addition to this, with improved control systems behavior during transients, the vessels will be able to sail at a possible higher speed or at the speed that offers the best efficiency, meaning savings in both emissions and cost.

Hence, this thesis distinguishes between the objectives of

1. A vessel operating at zero-speed regime maneuvering at the quay, e.g., the tugs boats, the ferry.

2. A vessel in transit mode, e.g., a supply vessel or a ferry.

These control systems have different needs, objectives, and approaches. However, both control systems need to be safe and reactive. During docking, the transit situation also needs to be addressed with a similar approach to the supply vessel in transit between two quays.

2.2 Hybrid Dynamical Control Systems

The development of hybrid dynamical theory began in the 1960s by Witsenhausen, where continuous and discrete systems were modeled and analyzed. For the last 20 years, a large amount of research has been conducted. A large toolbox with mathematical models, stability analysis, and robustness has been established. Examples are impulsive differential equations, systems with distinct logical states (also called hybrid automata), switching control systems, resetting control algorithms, synchronized behavior in biological systems, and systems in networks. Hence, there are many frameworks for the mathematical modeling of hybrid systems. This thesis uses the framework of Goebel et al. [2012] is used. The concept of hybrid theory has been implemented in various industries, such as in control of airplanes and land-based vehicles (Sørensen [2011]).

The hybrid dynamic control system is highly relevant at *the Department of Marine Technology* (IMT) at NTNU and NTNU AMOS (Autonomous Marine Operations and Systems). Many marine applications can benefit from using a hybrid dynamical framework, as the applications often have a large diversity in dynamical behavior for various vessel operational conditions. The complex dynamics can be captured using different sub-models merged into one hybrid system. Fall 2019 Andrew Teel, co-author of the subject book *Hybrid Dynamical Systems* (Goebel et al. [2012]) came to IMT to teach a course on the topic. After this, the course was further developed by Astrid Brodtkorb to be held for the master's students. It is giving a theoretical foundation and an insight into current applications and research. The interest in hybrid control towards marine application has grown over the last 15 years, and after the concept of the hybrid controller to switch based on different environmental changes (Nguyen et al. [2007]), then for switching automatically between controllers for different speed ranges (Nguyen et al. [2008]), an approach that differs from the hybrid concept, is to consider a robust control by multiple model adaptive controller.

The term hybrid control represents a system with more than one controller or observer. Depending on the situation, the control system automatically switches to the most appropriate component, introducing performance monitoring and switching logic. Hence hybrid control allows improved automatic control systems.

As the number of system functions that switch automatically increases, it is essential to know that the dynamics triggered by a switch are well behaved. A hybrid control system that can evaluate different control strategies, and choose the best one on its own, will improve system reactivity, safety, and performance relative to having an operator change the use mode and vessel speed. Hybrid dynamical control theory implies that there exists a performance monitoring and switching logic.

A reactive control system often requires that the power system deliver much power over a short time, which could solve this by integrating a battery-driven energy source. This solution would also benefit the vessel and give better working conditions for both systems (in combination with, e.g., a generator) (Sørensen [2018]).

2.2.1 Vessel Operational Conditions

When discussing hybrid theory, vessel operational conditions (VOC) are often used. The operation conditions are operation mode, environment, speed, and load. The three former conditions are often depicted in a three-dimensional figure, illustrated as a 3D axis system. Operation mode addresses the differences for a vessel, e.g., in station-keeping versus low-speed maneuvering. The environment establishes the changes in sea state, wind, current, ice. E.g., the control objective

of dynamic positioning (DP) vessel from calm to the moderate sea is to keep its position and heading by compensating for low-frequency (LF) motion only. As the sea state increases, wave-frequency (WF) motion is induced by waves with lower dominant frequencies, especially swelling in the North Sea and Barents Sea (Sørensen [2011]). Subsequently, the control objective is to compensate for both LF and WF. The speed condition addresses the significant change that will occur in the dynamic response of the vessel. E.g., nonlinear damping effects can be neglected in the zero speed regimes but should be included in the controller design for higher speed regimes.

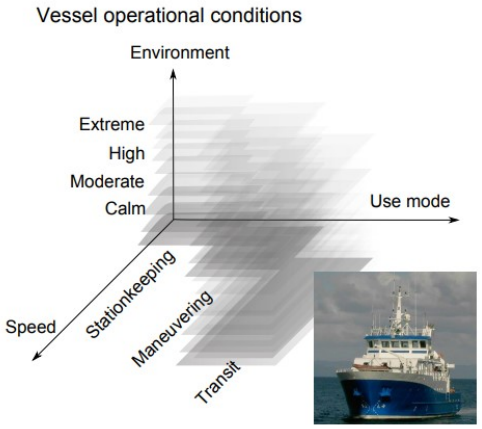

Figure 2.2: Illustration of the vessel operational conditions (VOCs): speed, environment, and operation mode (Sørensen [2018]).

A coarse division can be made for the research conducted on adaptive controllers. There are controllers for changing environmental conditions. There are automatically switching between controllers for different speed ranges. Lastly, there are proposed controllers for changing environmental conditions by the use of the hybrid framework. Further there are three areas for the changing strategies within hybrid theory with focus on improving transient performance: resetting (Tutturen and Skjetne [2015]), jumping between estimates from different observer types based on performance (Brodtkorb et al. [2018d], Brodtkorb et al. [2016b]), hybrid signal-based observers (Brodtkorb et al. [2015], Brodtkorb et al. [2016a]). Other areas for application are supervisory control for thrust allocation and hybrid systems control of top-tension risers.

The vessel operational conditions (VOC) in this thesis refers to

1. Change in vessel speed - introducing change in hydrodynamic loads
2. Change in environmental conditions - mostly due to high sea states because of wind, but due to current, also introduce changes in hydrodynamic loads
3. Change in operation mode - e.g., in DP, low-speed maneuvering, transit.

2.3 Expanding the Operation Window

With improved technology and increased knowledge, we can operate in harsher environments and new territory while conducting offshore oil and gas operations and installations and new technology of offshore wind farms. When conducting installations, maintenance, and surveillance, the weather can be an expensive burden, limiting the operation window due to safety. As the technology has developed, safety is maintained, but the operation window can be expanded, introducing operation cost reductions.

Brodtkorb et al. [2014] expands the operational window by creating a hybrid control system including four sets of controllers and observers tuned for four different environmental conditions (sea states). A sea state estimate is calculated in the jump-dynamics based on spectral analysis of the vessel wave frequency response, adding up the switching logic. Brodtkorb et al. [2014] models in *Increasing the Operation Window for Dynamic Positioned Vessels Using the Concept of Hybrid Control* a hybrid controller for a DP vessel in a varying sea state using the hybrid dynamical system frameworks from Goebel et al. [2012]. Switching will be based on spectral analysis of the vessel wave frequency motions. The motivation is to expand the operational window for vessels in dynamic positioning. The paper concludes that the hybrid controller can switch when exposed to higher sea states performs better than the single controller going from calm to extreme. In comparison, the single controller with adaptive wave filtering became unstable in extreme seas due to the filtering of low-frequency motions.

Hence, by addressing the varying operational conditions, new solutions may allow for expanding the offshore operating window. When introducing hybrid systems, the performance and switching logic are introduces as two new system variables. In the last article, the performance and switching depended on a spectral analysis of the vessel wave-frequency motions. Further development of this introduces the sea state estimation approach, addressed in the following section.

In short, the term of vessel operational conditions are highly relevant when discussing increasing the operational window as these are two sides of the same coin. When expanding the operational window, the vessel will operate in increasing environment, speeds, and operations. Hence, e.g., when improving the vessel's performance in transit, all three VOCs can be addressed and should be defined when discussing what is meant by improved performance or expanded operational window. With improved technology and increased knowledge, we can operate in harsher environments and new territory. This is regarding offshore oil and gas operations and installations and the new technology of offshore wind farms. When conducting installations, maintenance, and surveillance, the weather can be an expensive burden, limiting the operation window due to safety. As the technology has developed, safety is maintained, but the operation window can be expanded, introducing operation cost reductions.

2.3.1 Sea State Estimation

Many studies have been conducted for the last 12-14 years to establish a sea state estimation approach. The purpose varies, but the motivation is to have a fast and reliable method for obtaining an on-site sea state estimate. With this, it would be possible to let the control system adapt while at sea by using hybrid control performance monitoring and switching logic. It would also be possible to assist in a decision-making process either by system or operator, either on-site or off-site. As the DP forces cancel the horizontal plane motions, the motion measurements of heave, roll, and pitch are suitable for sea state estimation.

Brodtkorb et al. [2018a] presented a method to online calculate a sea state estimation algorithm by finding the wave spectrum estimate from the motion measurements by iterative solving a set of linear equations. This is a further development of Brodtkorb et al. [2018b], which introduces the point-wise wave spectrum estimation by iteration procedure based on motion measurements of a vessel in DP, no forward speed, in a long-crested sea state. This approach was then extended by Brodtkorb et al. [2018c] to include a correction for forwarding rate and short-crested sea states. Because both these approaches run on data obtained from full-scale vessel motion data or simulations post-process, they are both offline methods. However, this was solved in the paper mentioned earlier by Brodtkorb et al. [2018a], which estimates the sea state online.

The article also contributed to the estimation procedure's sensitivity analysis, focusing on the iteration procedure's gains. The calculation of response spectra from measurement time series was included. All approaches have vessel parameters and motion transfer functions as input and are signal-based. There exist no assumptions on the wave spectrum shape, so that the method is computationally efficient. Brodtkorb et al. [2018a] conclude that their algorithm works well and states that it would be interesting to develop a form of auto-tuning regarding the gains and tolerances in the algorithm.

However, this is early in the research process, and there is still much work to do. There are yet no commercial companies that have applied this control strategy to the author's knowledge. Model-testing has been done for offline calculations, but online estimates remain as the algorithm needs to calculate rapidly, and the existing algorithms are not completely satisfied yet.

2.4 Simulation Structure

The process plant model (PPM) is the core of the simulation environment, also called the simulation model in some literature. The PPM will give the necessary detailed mathematical description of the simulation system consisting of the vessel dynamics systems, components, and surroundings. The model needs to be as detailed as possible using high-fidelity models to simulate the real plant dynamics. Hence, this model will lay the foundation for the accuracy and reliability of the simulation results. Due to a lack of knowledge and, consequently, models, the control plant model (CPM) is often used as PPM in practice, makings the process more available, but the results are somewhat questionable. In some instances, a calibration model is used to describe the PPM, and nominal or CPM is used to describe the CPM.

Formulating the process plant model for simulation in a marine situation includes the mathematical model of the vessel dynamics and the external forces and moments in terms of environmental loads, thruster forces, and mooring forces acting on the vessel (Sørensen [2018]). As mentioned, a feasible and high-fidelity model of the system is necessary. A vessel in DP interactive with high sea-ice concentrations has substantially different dynamics from a conventional open water DP system. Further, it has been shown from full-scale, model-scale, and numerical experiments that positioning is possible when feasible ice conditions and a reactive DP system are present (Skjetne and Øivind K. Kjerstad [2016]).

When saving computational power or creating a model for the control system, a CPM excludes terms making the model linear and adding a bias term that accounts for all the unmodelled forces and moments. These are, in most scenarios, typically slowly-varying loads due to weather, but can also be due to sudden rapid loads due to lifting operations or weather. The bias dynamics are accounted for in different ways, depending on the objective of the control system. However, it will become clear that the industry standard for vessels as DP is to use integral action. A further elaboration on how the bias dynamics can be accounted for is in section 2.6.

2.5 The Maneuvering Problem

A vessel in DP will vary from a vessel maneuvering or following a trajectory. At DP, the vessel automatically maintains its position exclusively through thruster force in zero speed regime. The thruster force will account for the mean and slowly-varying loads. Hence the oscillating first-order waves forces are not accounted for, and one reason is to avoid fatigue on the thruster. Therefore a vessel at DP has low speed or no speed, so there are well-established wave drift force

equations for a DP vessel. However, the same toolbox is not available when concerning a vessel with a certain speed because the same assumptions are no longer necessarily valid.

It is possible to use hydrodynamic programs using strip theory or the indirect integration method to find wave drift coefficients at different speeds. Still, the equations are not the same for the forces.

As mentioned, the vessel operational conditions (VOC) will change the vessel's objective, and the vessel response dynamics will change with a change in speed.

An area of research that has become more relevant in the last years is vessel maneuvering and accounting for vessel dynamics and the wave drift forces. Today a relatively simple hydrodynamic model is applied for a vessel in zero speed-regime, expressed by Faltinsen [1990] in *Sea Loads on Ships and Offshore Structures*.

2.6 The Bias Dynamics

It is beneficial to understand how bias dynamics work when improving a control system's transient response, as this is a crucial factor in transients' slow behavior. In a control plant model, the bias should account for any unmodeled loads. In practice, it is often designed to capture slowly varying environmental loads and unmodeled dynamics in the controller and subsequently the observer. Bias loads are due to sudden large wave trains, ice loads, frequent setpoint changes. As mentioned, marine operations today are exposed to harsher environments, and the operations must still be performed safely. In all the mentioned instances, it is beneficial with a reasonable and accurate bias compensation. Further, it is essential that the control plant model also captures an unmodeled and rapid load, i.e., not slowly varying, e.g., during heading change. Hence, bias dynamics has been an area of research that has gained attention.

Research has been conducted on the best approach to compensate for this bias load by Værnø et al. [2019]. The investigation is done to give insight into the methods' efficiency and make conclusions on when the best overall closed-loop performance is obtained. The paper conducted a case study based on four different approaches to compensate for the bias load. Today, for a DP vessel, the common practice is to use integral action for bias. However, in the last years, there has been a growing focus on transient conditions. The result is that it is asked whether applying integral action is the most suitable way to go.

The first of the four approaches investigated in the paper is compensating the bias load by using the bias estimate from a separate observer tuned to estimate position and velocity. Second, a wave-filtered version of this estimate is applied. In the third approach, the estimate from an independent observer tuned for working well for estimating the bias loads is applied. Fourth an integral action is tested.

As mentioned, the integral action can be considered an *industry standard* for designing output feedback because of the assumption that the observer's bias estimate is too oscillatory to give good performance when used in feedback. Integral action is therefore applied and tuned such that it is slow, calm (meaning small oscillations), and works well in steady state.

Using the bias estimate from a model-based observer instead of the standard integral action on the output tracking errors has several benefits. The windup issues in the integrator will no longer be a potential problem. The windup issue refers to a significant change in setpoint (e.g., transient occurs), and the integral term accumulates a substantial error during the windup. This results in overshooting and continuing to increase as this accumulated error is unwound.

Moreover, the tuning will be more accessible when using the separate bias estimates, as it only needs an offline data series. Subsequently, when adding a separate observer to estimate the bias load, another complexity similar to the anti-windup filter's complexity appears. An advantage of using integral action is that it can be tuned independently of the bias response time. So the integral action can be adjusted to slowly account for steady-state offsets, whereas the observer's bias estimate can be made faster and let it live its own life. This tuning separation also applies if there is a separate observer to estimate the bias load.

With the in-depth study done in Værnø et al. [2019] of the four practices, the comparison is made fair by optimizing all observers' tuning and tuning the controller and integral action. Later the four practices are implemented in a case study and simulated. The simulation model includes a detailed process plant model (PPM). Further, two maneuvers are performed—both with environmental conditions. The first is a training maneuver used to tune the observers and controller, and one test maneuver uses the same tuning to verify that the tuning is not an over-fit to the training maneuver.

The study results show that the bias from the biased observer is the best solution, both in steady-state and is transient. The standard integral action matches the steady-state performance but is, as expected, slower in transient. The observer's estimate for position and velocity is fast in transients but too oscillatory in the bias state. Simultaneously, the wave-filtered version of the bias has more minor oscillations but has an added phase lag from the extra wave filter, which is not wanted. The paper's goal was so when creating a simulation. The creator can make a scientific decision regarding how to compensate for the bias.

Another interesting study for compromising the unknown was done in Du et al. [2015]. A robust controller for a marine dynamic positioning system using a high-gain observer is implemented. In addition to this, neural networks are used to compensate for unknown environmental disturbances. It does not require a priori knowledge of the ship's dynamics and environment disturbances using the adaptive radial basis function (RBF) neural networks and the adaptive laws with a leakage term.

2.7 Hybrid Observers

Over the last years, several observers and controllers to improve transient performance have been proposed, and most are for surface vessels at DP. The observer choice and tuning typically depend on the varying operational conditions (VOCs). They also cope with the bias force in various manners. Presented here is a selection of a few other hybrid observers and their significant differences.

One practical approach has been to use velocity measurements in the observer. As already stated, it is not always possible to gain high-quality measurements of the velocity without expensive additional sensors. To cope with this, it is proposed by Skjetne and Øivind K. Kjerstad [2016] to use acceleration feedforward. The first following section elaborates on what the paper investigates and concludes, which is interesting because it is an alternative way to improve the transients. Next, switching between a model-based and a signal-based observer (Brodtkorb et al. [2018d]) is presented. Then the following section will address the time-varying model-based observer. There is the approach of implementing time-varying observer gains (Værnø et al. [2017]). Finally, the hybrid observer with resetting mechanism is presented, from Torben [2019].

2.7.1 Disturbance Rejection by Acceleration Feedforward for Marine Surface Vessels

This section is based on the paper *Disturbance Rejection by Acceleration Feedforward for Marine Surface Vessels* of Skjetne and Øivind K. Kjerstad [2016]. This paper concerns how to handle harsh and rapidly varying exogenous disturbances due to loads from sea-ice on a dynamically positioned vessel was the objective of the Arctic DP project that initiated this study. Here a particular emphasis is put on DP. This is interesting as the research replaces the conventional integral action and enables unmeasured external loads and unmodelled dynamics to be counteracted with low time lag. Further, the control system uses this to improve the transient behavior of the control system.

The ability to handle unmodelled dynamics and environmental disturbances is limited to integral action based on state feedback. Since the state measurements hold time integrals on the force, there is an inherent lag before it propagates significantly to adapt the system. This mechanism will work very well for slowly-varying systems, but when rapid and substantial force transients occur, the control precision can be severely affected.

The paper discusses two approaches to deal with the challenge of transients. First, by extending the model used in control to describe additional physics. However, as mentioned earlier, this is not developed as a result of complex environmental situations. The corresponding complex physical process can not be modeled simply. The second approach covered in this paper is extending the sensor suite for the vessel to capture the phenomena in question. Hence, acceleration signals are investigated.

To apply acceleration signals in the control design require a sensor suite containing accelerates. This acceleration equipment is found in various applications such as consumer electronics, vibration sensing of large structures, impact detection, and navigation, i.e., this is mature technology (Sørensen [2018]). Here the distinction is that the full acceleration vector is found. This vector enables kinematic and sensor models in the state observer and forms an acceleration feedforward signal used in the control law to compensate a disturbance directly. This approach will provide a powerful and reactive tool for developing robust control systems operating in harsh environments where traditional control designs are not well suited.

The paper presents a control system design that uses acceleration measurements for rigid body marine motion control subject to harsh environments. The challenges of obtaining total state measurements of the dynamic acceleration were addressed with four accelerometers placed in a specific configuration that serves as input to the state observer. The paper's main contribution is the novel method for integrating dynamic acceleration as an acceleration feedforward in the control law to compensate disturbances and unmodeled dynamics better. The proposed design was investigated with both experimental and high-fidelity simulations, showing the feasibility and effectiveness of the proposed control setup. The experimental results verify the load estimation and the measurement setup show the feasibility of these methods.

In summary, this controller is mainly for the operation mode of DP in ice and at a zero speed regime. The environment differs from the regular vessel at the open sea, and PPM and CPM need to be modified. The integral action is challenged and replaced in this controller setup.

2.7.2 Switching Between a Model-Based and a Signal-Based Observer

In the paper *Hybrid Controller Concept for Dynamic Positioning of Marine Vessels with Experimental Results* of Brodtkorb et al. [2018d] a study is conducted which establishes a hybrid control

concept for switching between candidate observers and controllers, customized for transients and steady-state behavior of DP vessels. The motivation for this study was that marine operations are moving into harsher environments. Consequently, requirements for the vessel's operational window, safety functions, and energy efficiency become stricter Sørensen [2011]. Brodtkorb et al. [2018d] discuss that the concept of hybrid control can provide a scalable and stringent methodology for designing real industrial control applications dealing with several control objectives and changing environmental and operational conditions.

The candidates are a model-based observer from Fossen [2011] and a signal-based observer based on Grip et al. [2015]. The paper also uses a controller and a switching logic combined to improve the transient response. The model-based observer is especially suited for steady-state. The signal-based observer is more reactive during transients even though the signal-based is more sensitive to signal noise.

During marine operations, both variations in stationary dynamics and transient behavior are essential to account for in an all-year operation philosophy subject to changing weather, sea loads, and modes of operation (Perez et al. [2006]). As mentioned, various unknown factors may cause transients in the vessel response, such as environmental disturbances (e.g., wave trains and wave gusts) or transients due to operation (e.g., heading changes or crane operations of heavy goods). The use mode includes algorithms that satisfy different control objectives such as station-keeping, maneuvering, and target-tracking.

The performance monitoring and switching logic block include monitoring of the environment, power system, observer performance, position precision, signal health, and more. There are high requirements for system reconfiguration, fault tolerance and redundancy, and testing and verification of performance for safety reasons.

When evaluating the hybrid system's performance, the difference in estimation error in position is used as performance monitoring. By saving the n past differences in a shift register with state m, switching is based on the states' average of the states m to get a smoother signal to base switching on. Then the performance monitoring signal, the average of m, is sent to the switching logic. There are two thresholds chosen, one for steady-state and one for the transient. The former holds a larger value than the latter. By doing this, there is some margin to provide hysteresis that suppresses switching back and forth. This mechanism adds up to be the reactive part of the switching logic. There is also the proactive switching by choosing to use the signal-based observer in a closed-loop when the desired yaw rate is larger than some other threshold.

The paper's main contribution is developing a hybrid control concept for proper switching of candidate observers and controllers, customized for DP vessels' transients and steady-state behavior.

In the model-scale experiments, the vessel model was pushed off the setpoint using a boat hook. The first time the observer was fixed used the model-based observer. The second time a switch was triggered, and the signal-based was used. During the first time, especially the velocity measure uses a long time coming back to the setpoint. The second time, the observer estimates are more accurate, but some switch back and forth. The heading reaches steady-state somewhat faster when the signal-based observer is in the loop. The signal-based made the thrust more oscillatory, as expected.

In summary, this hybrid control system is made for a vessel at DP or low-speed maneuvering. The sea state is not discussed. The integral action is employed to compensate for the bias force.

2.7.3 The Resetting Observer

The resetting observer from Torben [2019] introduces a new hybrid mechanism for better handling unmodelled dynamics and reactiveness to external disturbance without compromising steady-state performance. The observer exploits the challenge of DP observers not to have too high injection gains.

It examines the hybrid observer design by enforcing a jump in the state estimate if the estimation error exceeds a predefined bound. In implementing the resetting observer, there are different ways to implement the bias load. Some define it by the bias time constant matrix, other sets it equal to the zero matrices in the control plant model. A bias time constant matrix is used by Fossen [2011] to be able to establish the stability of the system.

In summary, this hybrid controller is mainly for the operation mode of a vessel at DP. The resetting observer was simulated while in DP and experiencing an impulsive sway disturbance. The bias estimation is modeled to be compensated for by integral action.

2.7.4 The Time-Varying Model-Based Observer

In Værnø et al. [2017], the goal was again to improve the relationship between transient and steady-state performance by using time-varying gains for a model-based observer. The gains will be more aggressive for transient and relaxed in steady-state to lower the oscillations. In the model-based observer, to compensate for the bias term integral action approach is used. If the bias load is off, the position and velocity estimates will be influenced by this. As mentioned, rapid bias load changes include wave trains, rotational currents, sea-ice loads, or mode changes in the DP system's operation.

The paper defines three situations that will create transient behavior. First is when there occurs a heading change. It is then experienced that the loads in NED change significantly, even with constant parameters and current. A reason for this is the ship hull geometry, as this is not accounted for in the bias model. This illustrates that if the vessel changes headings, the common slowly-varying assumptions of the bias model in the NED frame do not apply in transients. The second situation is when there is a change in the environmental disturbances. This will be recognized through a deterioration of the observer's performance. The third situation is when there is an error due to the initialization of the observer. Together this is expressed mathematically and is the basis of the performance monitoring and switching logic.

In summary, this hybrid controller is mainly for the operation mode of a vessel at DP. However, it was simulated for low-speed maneuvering performing the four corner test. To compensate for the bias load, the integral action approach was implemented.

2.8 Hybrid Systems in Practical Uses

Today researchers and commercial companies work together to develop high-end dynamical positioning systems (e.g., Kongsberg). They are often used for offshore supply or maintenance vessels. Still, this is not a fully autonomous operation, and there is still a need for an operator to oversee the operation. In regards to regulations, there are some rules in regards to DP. In commercial systems, there are typically three gain settings; low, medium, and high (Værnø et al. [2017], Bray et al. [2020]).

For reference, some typical vessels with dynamic positioning are the platform supply vessel (PSV), drillships, cable lay and repair vessels, floating production storage and offloading unit (FSPO).

In addition, a dynamical positioning system today often has different settings depending on the operational condition. The operator has to change between these settings manually. Implementing performance monitoring and switching logics in a hybrid control system will ensure stable switching to appropriate settings without operator interference. This would increase the level of autonomy from automatic operation to management by consent (or management by exception) for the motion control unit in Figure 2.1.

Chapter 3

Mathematical Modeling

This chapter contains the relevant derivation of mathematical expressions used to model and control marine surface vessels in this thesis.

First are the governing representation of the vessel in a simulation environment, named *the process plant model* (PPM), presented. Following is the simplified model applied in the control system, named *the control plant model* (CPM), presented. Then the reference models used for guidance are presented, followed by the mathematical description of the relevant controllers.

Next, the preliminary hybrid theory is presented, with a mathematical framework for modeling and stability analysis.

Further, calculation of the second-order wave loads are explained, and varying sea states. The first-order motions are also explained, and the first-order motion transfer functions are used. Then, relevant aspects regarding transitioning from calm sea to open sea relevant for the work done in the simulation study conducted in this thesis/relevant for the work of the thesis).

Finally, the relevant hybrid observers' mechanisms, hybrid setup, and formal stability analysis is presented.

3.1 The Marine Surface Vessel

3.1.1 Reference Frames

When working with the surface vessel two reference frames appear, illustrated in Figure 3.1.

- The body-fixed reference frame where all motions and loads acting on the vessel is defined. The body-fixed frame is fixed to the vessel body, with positive x-axis forward, positive y-axis starboard and z-axis is positive downwards.
- The inertial Earth reference frame used for position, orientation and distance. Its directions are the true North, true East and down, hence named the NED-frame.

Subsequently, a combination of reference frames appears. Hence an Euler angle transformation solves this issue expressing the relationship between body- and NED-frame. Where it is not clear, variables will be noted with superscript b if it is in body-frame or superscript n if it is in NED-frame.

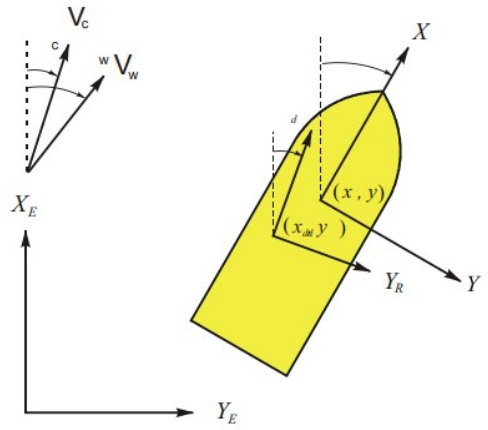

Figure 3.1: Definition of frames: Earth-fixed, reference-parallel and body-fixed.

$$\dot{\eta} = R(\psi)\nu,\ R^{-1}(\psi) = R^T(\psi) \tag{3.1}$$

$$R(\psi) = \begin{bmatrix} cos(\psi) & -sin(\psi) & 0 \\ sin(\psi) & cos(\psi) & 0 \\ 0 & 0 & 1 \end{bmatrix} \Rightarrow \nu^n = R(\psi)\nu^b \tag{3.2}$$

This transformation is valid for the horizontal motions surge, sway, and yaw. Note that Euler angle transformation introduces nonlinearities.

3.1.2 Process Plant Model

The process plant model (PPM), also named the simulation model, is a high fidelity, comprehensive description of the actual process. The objective is to create a model to simulate the vessel as similar as possible to the real world. The accuracy of the PPM constitutes a vital role in the validity of the simulation.

The vessel is modeled in two sets of frequencies, illustrated in Figure 3.2

- the low-frequency (LF) nonlinear motions caused by wind, current, and second-order wave forces.
- the wave-frequency (WF) linear motions caused by first-order wave loads. As the mean of the first-order wave loads is equal to zero, these wave loads will be filtered out with a wave filter to reduce unnecessary wear and tear on the actuators.

The resulting nonlinear six degrees of freedom body-fixed coupled equations of the low-frequency motion in surge, sway, heave, roll, pitch, and yaw are

$$\dot{\eta} = R(\psi)\nu \tag{3.3a}$$

$$M\dot{\nu} + C_{RB}(\nu)\nu + C_A(\nu_r)\nu_r + D(\nu_r) + G(\eta) = \tau_{wind} + \tau_{wave2} + \tau_{moor} + \tau_{ice} + \tau_{thr} \tag{3.3b}$$

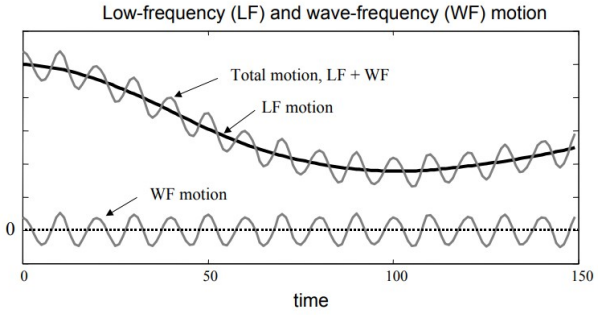

Figure 3.2: The total motion of a ship is modeled as a low-frequency (LF) response with the wave-frequency (WF) response added as an output disturbance.

$\eta \in \mathbb{R}^6$ is the position and orientation in NED frame, $\nu \in \mathbb{R}^6$ is the linear and angular velocities in the body-frame. $R(\psi) \in \mathbb{R}^{6\times6}$ is the Euler angle transformation matrix. $M = M_A + M_{RB}$ is the vessel mass matrix, C is the Coriolis and centripetal matrix, D is the damping matrix. On the right hand side are the forces acting on the vessel, $\tau_{wind}, \tau_{wave2}, \tau_{ice}$ are environmental forces, while τ_{thr} are the thruster forces. Subscript A and RB are short for the added mass and rigid-body, respectively.

The low-frequency wave loads τ_{wave2} are nonlinear motions, which are divided into three groups: mean, slowly-varying (difference frequencies), and rapidly-varying (sum frequencies) wave loads. For the modeling of a surface vessel, rapidly-varying nonlinear motions are neglected. Hence, we are interested in the nonlinear wave drift loads, a combination of the two former wave loads, mean and slowly-varying. Wave drift forces contribute a significant part of the total excitation force in the low-frequency model.

The mean wave load is

$$\bar{F}_i^{SV} = \sum_{j=1}^{N} A_j^2 T_{jj}^{ic} \tag{3.4}$$

so $A_j^2 T_{jj}^{ic}$ is the mean wave load in direction i due to regular waves of amplitude A_j and circular frequency ω_j.

Mean drift loads can approximate the slowly-varying loads. Subsequently, the computation becomes simpler and less time-consuming. Wave drift loads are found to be expressed with Newman's approximation. However, this implies high-frequency effects with no physical background, which have no influence when studying slow drift response.

$$\begin{aligned} \tau_{wave2}^i &= \bar{\tau}_{wm}^i + \tau_{wsv}^i \\ &= 2\left(\sum_{j-1}^{N} A_j \Big(T_{jj}^i(\omega_j, \beta_{wave} - \psi) \Big)^{1/2} cos(\omega_j t + \varepsilon_j) \right)^2 \end{aligned} \tag{3.5}$$

Where τ_{wave2}^i are wave drift forces for every degree of freedom, $i = 1, ..., 6$. While $\bar{\tau}_{mw}^i$ is the mean wave load component, and τ_{wsv}^i is the slowly-slowly varying component, each varies for every degree of freedom, $i = 1, ..., 6$. A_j is the incident wave amplitude, ω_j is the wave frequency, ε_j is the random phase, β_{wave} is the mean wave direction.

Further, the linear six degrees of freedom wave-frequency (WF) motions in surge, sway, heave,

roll, pitch, and yaw are

$$\dot{\eta}_w = J(\bar{\eta}_2)\dot{\eta}_{Rw} \tag{3.6a}$$
$$M(\omega)\ddot{\eta}_{Rw} + D_p(\omega)\dot{\eta}_{Rw} + G\eta_{Rw} = \tau_{wave1} \tag{3.6b}$$

where $\eta_{Rw} \in \mathbb{R}^6$ is the WF motion vector in the hydrodynamic frame, $\eta_w \in \mathbb{R}^6$ is the WF motion vector in the Earth-fixed frame (NED), and $\bar{\eta}_2 = [0\ 0\ \psi_d]^T$. $\tau_{wave1} \in \mathbb{R}^6$ is the first-order wave excitation vector, dependent on the vessel heading relative to the incident wave direction. As WF motions are assumed linear, the potential theory is valid and neglecting viscous effects. Hence motion and force response amplitude operators (RAOs) can be calculated using linear programming and software like ShipX.

Generally, results from model tests and computer programs such as ShipX for vessel response analysis are often in transfer functions and table of coefficients. To a large extent, linear theory (strip theory, etc.) are sufficient for describing wave-induced motions and loads on vessels. For moderate sea states, this is valid. However, with increasing sea states and irregular seas, the vessel's response may be calculated by adding regular waves of different amplitudes, frequencies, and directions. The nonlinear effects are increasingly important in extreme seas, and this is still a research subject. Subsequently, understanding the hydrodynamics and vessel response is an important tool for the marine cybernetics engineer.

3.1.3 Control Plant Model

The low fidelity control plant model is a product of simplifying the process plant model. This will contain only the main properties and thus works well for the control system, hence the name.

Only 3 degrees of freedom (DOF) are considered for the conventional surface vessels: surge, sway, and yaw. Hence the PPM for 6 DOFs are simplified to 3 DOFs, $\eta = [N,\ E,\ \psi]^T$ and $\nu = [u,\ v,\ r]^T$. The rotation from Equation 3.2 is applicable. Assuming low speed, Coriolis and centripetal forces are negligible, and the linear damping terms dominate, and the resulting model is as follows

$$\dot{\xi} = A_w\xi + E_w w_w \tag{3.7a}$$
$$\dot{\eta} = R(\psi) \tag{3.7b}$$
$$\dot{b} = -T_b^{-1}b + w_b \tag{3.7c}$$
$$M\dot{\nu} + D\nu = \tau + R^T(\psi)b \tag{3.7d}$$
$$y = \eta + C_w\xi + v_y \tag{3.7e}$$

$b \in \mathbb{R}^3$ is the bias vector accounting for both slowly varying disturbances and unmodelled dynamics, and E_b is a diagonal scaling matrix. This bias model uses a first-order Markov model. It is necessary that the bias capture any unmodeled loads. $w_b \in \mathbb{R}^3$ is the zero-mean Gaussian white noise vector. $T_b^{-1} \in \mathbb{R}^{3\times3}$ is a diagonal matrix consisting of the bias time constants. The output of the CPM, $y \in \mathbb{R}^3$, is the position and heading of the vessel, assumed

to be a superposition of the WF ($C_w\xi$) and LF motion (η). $v \in \mathbb{R}^3$ is the measurement noise vector. Equation 3.7a is the second-order harmonic oscillator called the wave-frequency filter. Wave-filtering should not always be implemented, for instance, when there is a heavy sea with long wavelengths (low wave frequencies), as this will filter out the low wave frequencies. This will appear in extreme seas or swell domains.

Note that we are only interested in low-frequency motions because controlling the total motion causes extra wear and tear on the thrusters. In most cases, it will not be possible to counteract the first-order wave-induced motions.

3.2 Guidance Systems

Guidance systems are used in motion control to obtain a reference trajectory. In its simplest form, open-loop guidance systems for marine crafts are used to generate a reference trajectory. The guidance system works closely with the motion control system; hence a feasible guidance system is essential. Feasible in the sense that the trajectory created needs to be physically *available* for the vessel.

In this section, a basic positing and attitude reference model is presented, followed by a reference model presented in the doctoral thesis *An output feedback motion control system for ROVs: guidance, navigation, and control* by Fernandes [2015]. The latter reference model is based on optimal curve shapes.

3.2.1 Position and Attitude Reference Model

The position and attitude reference model are of third order for filtering the steps in the reference r^n, resulting in a cascaded system composed of a first-order low-pass filter and a mass-damper-spring system, Equation 3.8. The low pass (LP) filter ensures a smooth reference signal.

$$\eta_d^{(3)} + (2\Delta + I)\Omega\ddot{\eta}_d + (2\Delta + I)\Omega^2\dot{\eta}_d + \Omega^3\eta_d = \Omega^3 r^b \tag{3.8}$$

r^b denotes the operator input expressed in {n}-frame (NED-frame), while $x_d := [\eta_d^T,\ \dot{\eta_d}^T]^T \in \mathbb{R}^{2n}$ is the desired state vector. The accelerations, velocities, and positions are in the NED-frame. Further, these are then transformed to a moving reference parallel frame that follows the desired NED position and heading trajectory.

The mass-damper-spring system is used to obtain a smooth reference trajectory, as it is a physically motivated model, where ζ_i is the relative damping ratios and ω_{n_i} are the natural frequencies. Critically damped system are equivalent to $\zeta_i = 1$ and $\Delta = I$.

$$\Delta = diag\{\zeta_1, \zeta_2, ..., \zeta_n\} \tag{3.9}$$
$$\Omega = diag\{\omega_{n_1}, \omega_{n_2}, ..., \omega_{n_n}\} \tag{3.10}$$

It is beneficial to include saturating elements for acceleration and velocity based on the physical constraints of the vessel in order for the reference trajectory to be feasible.

3.2.2 Reference Model Using Optimal Shape Curves

Fernandes [2015] presents a reference model based on optimal curve shapes is introduced and motivated by a generation of sufficiently smooth position, velocity, and acceleration references for guiding the motion of an ROV along purposefully defined curvature-continuous paths in automated missions.

The paper of Fernandes [2015] introduces two contributions to literature about guidance. First, a reference model generates a single DOF motion which is *easy* to tune. Second, it introduces more advanced reference path generations based on the former reference model, but this allows for steady multiple DOF reference motions.

Further, the reference model synthesizes position ($\mathcal{C}^2$-class), velocity ($\mathcal{C}^1$-class), and acceleration ($\mathcal{C}^0$-class) for guiding a single DOF motion in a sub-optimal manner. The notation $\mathcal{C}^n$ where $n = 0, 1, 2$ indicating the degree of continuity. While sub-optimally indicates that the constraints in the reference model have to reflect the constraints indicated with the ROV (vessel).

The optimal curve shapes have, as mentioned, a requirement to have a certain degree of continuity. Further, the optimal curve shapes are described with a straight line position path traversed, limiting velocity and acceleration. The velocity is optimal in the sense that it yields the shortest traveling time. Finally, the acceleration and deceleration are symmetric in order to simplify without losing generality. This introduces the following reference model presented in Figure 3.3.

The reference model also wishes to obtain the maximum (or minimum) velocity for as long as possible. This will introduce more steady hydrodynamic effects and fewer plant parameter variations. Finally, induct high overall motion accuracy and demand steadier thrust force and momentum from the propulsion system, which implicitly introduces energy savings.

Another advantage of this reference model is that the tuning parameters are meaningful, hence simple to implement. The tuning parameters are divided into two categories: the first includes all parameters set depending on the operation's objective. In contrast, the second is tuned for a particular ROV (or vessel). These are summarized in table Table 3.1, the four first are the first category, and the four following are the tuning parameters of category two.

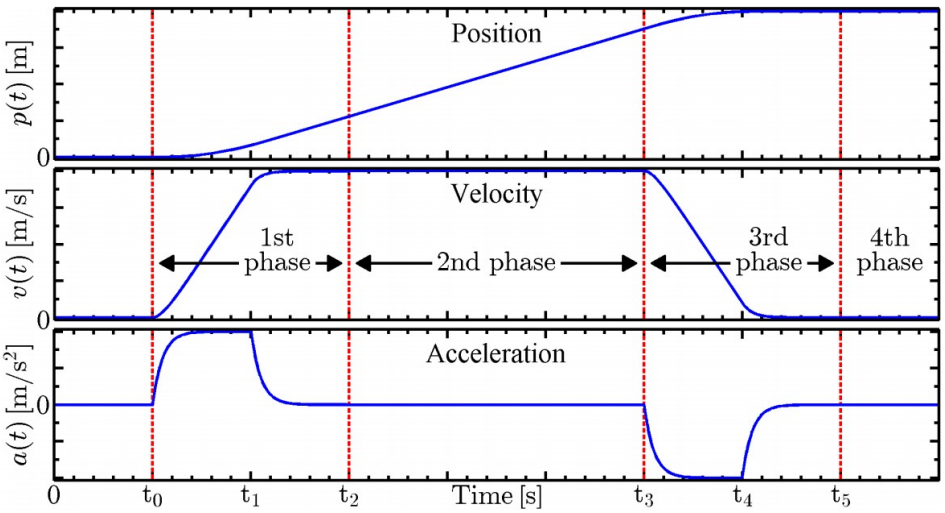

Figure 3.3: Shapes of the reference synthesized by Fernandes [2015], including the four different phases of the three curves.

The reference model is divided into four phases,

$$p(t) = p_1(t) + p_2(t) + p_3(t) + p_4(t) \tag{3.11a}$$
$$v(t) = v_1(t) + v_2(t) + v_3(t) + v_4(t) \tag{3.11b}$$
$$a(t) = a_1(t) + a_2(t) + a_3(t) + a_4(t) \tag{3.11c}$$

where $i \in [1, 4]$ represents the different phases, as illustrated using vertical lines in Figure 3.3. 1 is the acceleration phase, 2 is the constant velocity phase, 3 is the deceleration phase, and 4 is the constant position phase. Summarized in the illustration in Figure 3.3.

The first phase is when the velocity reference model increases from zero to the desired cruise velocity. The acceleration reference model has two sub-phases, first increase from zero to virtu-

ally maximum acceleration, and the decrease to zero again. The second phase keeps the cruise velocity constant, and the acceleration is zero. The third phase is the deceleration phase and is symmetric to the second phase (acceleration). The fourth and final phase is characterized by a constant reference frame with zero velocity.

L	path length
V_d	desired cruised velocity
T_a	desired minimum time to reach V_d
T_d	desired minimum time to stop from V_d
ϵ_L	minimum fraction of L to be traversed at v_m
θ_a	function switching threshold
θ_d	function switching threshold
θ_0	function switching threshold

Table 3.1: Tuning parameters for Ferandes' reference model, Fernandes [2015].

This is a 1-DOF reference model implemented in MCSim with decomposition, and this results in a 3 DOF reference model. Input to the reference model is one setpoint in NED-frame, then this is fed into the simulation, including this reference model. An appropriate reference model can be obtained for the vessel based on this and the desired cruise velocity and time parameters. This allows using the synthesized reference model for other application areas than 6 DOF ROVs, such as a 3 DOF surface vessel.

3.3 Controllers

For a marine surface vessel, the control system (in the motion control system Figure 2.1) needs to compute the thruster forces appropriate for the objective. Depending on the objective of the operation, the controllers will have different properties. The thesis works with a PID controller, in addition to a heading and speed controller, which will be presented in the mentioned order.

3.3.1 DP Controller

PID control methods are available for setpoint regulations and trajectory-tracking control for marine crafts. More specifically, autopilot design, station-keeping, position mooring systems, cross-tracking control, and line-of-sight (LOS) control systems.

The PID controller is widely used for these operations as it is easy to implement and requires no prior knowledge of the model. It is developed for control of horizontal motions, surge, sway, and yaw. The control equation is defined as

$$\tau = K_p R^T(\psi)\tilde{\eta} + K_d\tilde{\nu} + K_i \int_0^t R^T(\psi)\tilde{\nu}(\tau)d\tau \tag{3.12}$$

where $\tilde{\eta} = \eta - \eta_d$, η being the estimated or measure position, and η_d the reference position.

Even though the PID controller is easy to implement, it is only tuned for one environmental condition and one specific operation. The same PID controller will therefore not be applicable for both maneuvering and dynamic positioning operations.

This motivates the implementation of a hybrid control system, allowing automatic switching to a new tuning when entering the appropriate area decided by performance monitoring and switching logic.

3.3.2 Heading Controller

When maneuvering, the PID introduced above is often simplified to concern the heading. For maneuvering, only the heading angle is essential; hence, this is the only state used for the control law.

However, the vessel's lateral distance to the path will depend on the magnitude of the environmental forces for this control law, and the environmental forces will induce a sideslip angle β.

$$\beta = \frac{v}{U} \tag{3.13}$$

$$U = \sqrt{u^2 + v^2} \tag{3.14}$$

In order to find appropriate desired heading, ψ_d, the sideslip has to be taken into account.

$$\psi_d = \chi_d - \beta \tag{3.15}$$
$$\chi_d(e) = \chi_p + \chi_r(e) \tag{3.16}$$
$$\chi_p = \alpha \tag{3.17}$$
$$\chi_r(e) = arctan(-K_p - K_i \int_0^t e(\tau)d\tau) \tag{3.18}$$

χ_d is the course angle steering, $\chi_p = \alpha_k$ is the path tangential angle, and $\chi_r(e)$ is the velocity-tangential line. The control objective is to obtain the steering angle, by transforming the commanded course angle to a heading angle command by using the Equation 3.18.

$$\tau_\psi = -K_p\tilde{\psi} - K_d\dot{\tilde{\psi}} - K_i \int_0^t \tilde{\psi}d\tau \tag{3.19}$$

$\tilde{\psi} = \psi - \psi_d$, ψ is the heading estimate or measurement.

3.3.3 Speed Controller

The speed controller can be implemented to control the speed of the vessel. In particular this would be used to control the surge speed and calculate the necessary force in x-direction. The speed controller often only has PI-terms due to poor velocity measurements.

$$\tau_x = -K_p\tilde{u} - K_i\tilde{u} \tag{3.20}$$

where $\tilde{u} = u - u_d$, u_d is the desired surge speed. u is the velocity estimate, which are available when entering higher speed regimes.

3.4 Hybrid Dynamical Systems

Hybrid dynamical systems are relevant for marine systems as marine environments are complex, and hence the properties of the hybrid theory are highly suitable. In the following, hybrid theory and framework are presented, including the terms performance monitoring and switching logic. The hybrid control system is applied to improve the performance of the control system. More precise, in this thesis the objective is to improve the transient phase by improving the bias load term in Equation 3.7c.

Hybrid systems consists of designing the system dynamics in a combination of continuous-time and discrete-time. The model in continuous-time is modeled as a *constrained differential inclusion*, while the discrete-time is modeled as a *constrained difference inclusion*.

$$x \in C \qquad \dot{x} \in F(x) \tag{3.21a}$$

$$x \in D \qquad x^+ \in G(x) \tag{3.21b}$$

The differential and difference inclusions $\dot{x} \in F(x)$ and $x^+ \in G(x)$ are generalizations of the differential and difference equations $\dot{x} = f(x)$ and $g^+ = g(x)$. When the state x is in the flow set C, it will flow accordingly to the set-valued mapping $\dot{x} = f(x)$ for some $f \in F$. When x is in the jump set D, it jumps according to set-valued mapping $x^+ = g(x)$ for some $g \in G$. x^+ denotes the value of x after a jump.

Solutions of hybrid systems are called *hybrid arcs* and are in the *hybrid time domain*. The hybrid arcs evolve in continuous time $t \in \mathbb{R}_{\geq 0}$ and in discrete time $j \in \mathbb{N}$, where j denotes the number of jumps. Only specific subsets pf $\mathbb{R}_{\geq 0} \times \mathbb{N}$ can correspond to the evolution of hybrid systems and belong in the hybrid time domains (Goebel et al. [2012]).

Further, to establish a toolbox for analysing the complex system a general requirement regarding the definition and existence of the hybrid system called *the hybrid basic conditions* are defined as following (Goebel et al. [2012], Assumption 6.5)

(A1) C and D are closed subsets of $\mathbb{R}^n$

(A2) $F : \mathbb{R}^n \rightrightarrows \mathbb{R}^n$ is outer semi-continuous (OSC) and locally bounded (LB) relative to C, $C \subset domF$, and $F(x)$ is convex for every $x \in C$

(A3) $G : \mathbb{R}^n \rightrightarrows \mathbb{R}^n$ is outer semi-continuous (OSC) and locally bounded (LB) relative to D, and $D \subset domG$.

A vessel at sea can be described by the vessel operational conditions (VOCs): environment, operation mode, speed, and load. The three first VOCs are frequently used when describing hybrid systems on marine applications; see Figure 3.4. The switching logic needs to be established for these three VOCs to help provide robustness for measurement noise and system error. Figure 3.5 illustrates parts of the functionality that can be found within the performance monitoring and switching block in a hybrid system. The performance monitoring detects and diagnoses. The switching logic re-configures the blocks in the hybrid control system, meaning decided what set of configurations to use.

There are some key challenges to be aware of when constructing the performance monitoring and switching logic. First, there is the difficulty of switching during transients. Mainly a switch

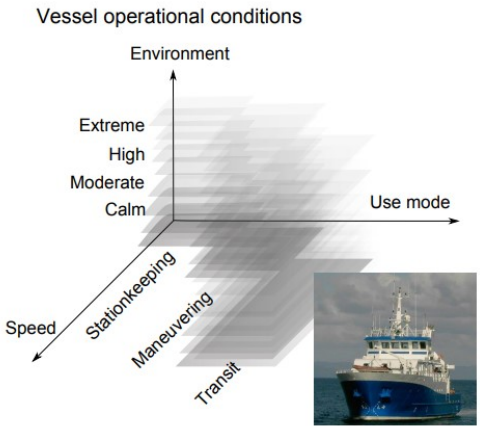

Figure 3.4: Vessel operational conditions: environment, use mode and speed

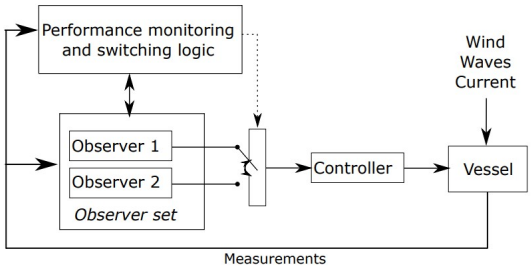

Figure 3.5: Hybrid Observer for transient performance improvement (Sørensen [2018]).

during transients is unwanted as the transient phase may be *premature* steady-state condition, meaning that the phase could be due to initialization or change of heading setpoint, or due to previous set point. This can result in instability and unwanted changes. In some applications (Værnø et al. [2017]), three pre-defined transient modes have been established to avoid any uncertainties, whether it is a proper transient phase or not. Another challenge is *chattering*. This is when there appear rapid changes back and forth. This can be solved by switching logic based on a timer, such as dwell-time or average dwell-time dynamics, or based on system variables, hysteresis. Both performance monitoring and switching logic are further discussed for each of the hybrid systems in respectively section 3.5.1 and section 3.5.2.

In control theory, the stability properties and analysis of the equilibrium points of a system is desired. When conducting the analysis, it is from Goebel et al. [2012] specified to define a set $\mathcal{A}$, because for a hybrid system the equilibrium is a set of points.

The goal of the stability analysis for hybrid control systems is to gain qualitative information about the properties of the system and so-called 'long term trends', which will also include information on the robustness of the system. For hybrid systems that meet the hybrid basic conditions (A1 - A3), then it is implied that if they are GAS, then they are also robust GAS. In marine systems, we want this to be satisfied, as there often are disturbances creating perturbations in the system. If the system is robust, we will have established that the perturbations will not disturb the system further, and the system will still be able to converge towards its set of attraction, $\mathcal{A}$.

3.5 Observers

This section begins with an explanation of observers and their use. Then two observers are presented thoroughly. These two observers will first be presented by their main mechanisms, followed by the mathematical model according to the framework presented in section 3.4 (Goebel et al. [2012]) along with stability analysis. First, the resetting observer for LTV systems is described, obtained from Torben [2019]. Following the time-varying model-based observer is described, obtained from Værnø et al. [2017].

Observers, also named state-estimators, are used in motion control systems to account for states needed in the controller which are not available. Typically the velocity measurements are poor, and hence it is appropriate to implement an observer to estimate the unknown states. The observer will then reconstruct the unmeasured states, and different observers have different approaches. Usually, they are based on a physical model of the system. In addition, the observers can work as filters for noisy measurements, reduce wear and tear, and reconstruct measurements that were not captured for some reason. Hence, the observers will reduce risk as they provide security to the motion control system if there is a measurement failure.

The state-estimators require the system model to be *observable*. If the system is observable, it is possible to infer the internal states from knowledge of its external outputs. Hence the system will use the position measurements to estimate, e.g., the velocity states. The control plant model used in the observers is observable; proof can be found in Fossen [2011].

3.5.1 Resetting Observer

The resetting observer consists of two Luenberger observers. The two observer estimates the states $z_i,\ i = 1, 2$ with two different tuning motivations. The first is an observer tuned for the steady-state model of the states (a *relaxed* tuning), while the second observer is tuned more aggressively and is supposed to work better in the transient phase. The observer will switch when the output estimate is too large, expressed by $|y - Cx| > \epsilon$. Next, using the two state estimates z_1 and z_2, we can find the true system state, $z(t_1)$.

The most straightforward state estimator is designed as a fixed gain observer where the ultimate goal of the observer is to reconstruct the unmeasured state vector $\hat{x}$ from the measurements u and y of a dynamical system, Figure 3.6.

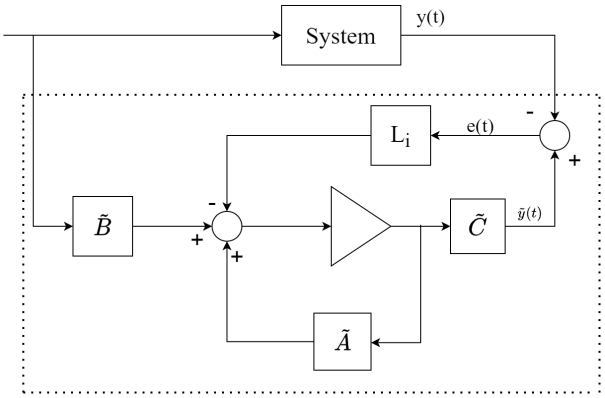

Figure 3.6: Block diagram presenting the dynamics of a system with a Luenberger observer.

When the state output error exceeds the given expression, z_1 and z_2 are reset to the true system state. Otherwise, the two state estimates are *synchronized*. This is done by setting z_2 equal

to z_1. *This is so the resulting observer reacts quickly and resets the state to the correct values.* The mechanism of the resetting observer resembles an integral action, in addition, it gives a reasonable estimation of a sudden disturbance.

Observer Design

This hybrid observer design is composed of two Luenberger observers. This section will establish the relevant equations that will later be applied in the hybrid system framework. The governing state space for a linear time-varying (LTV) system equations are as follows.

$$\dot{z} = A(t)z + B(t)u \tag{3.22a}$$
$$y = C(t)z \tag{3.22b}$$

with states $z \in \mathbb{R}^n$ and output $y \in \mathbb{R}^m$. The states z contains all states from Equation 3.7. $u \in \mathbb{R}^n$, $A(t) \in \mathbb{R}^{n\times m}$ and $C(t) \in \mathbb{R}^{p\times n}$ are all piece-wise continuous and bounded functions, and $(A(t), C(t))$ form an observable pair for each time $t \in [0, \infty)$. Hence there exists a unique solution to the LTV system, and these solutions are bounded for all time (Khalil [2002]).

Using the definition of a Luenberger observer we will have the following equations for the states. $i \in [1, 2]$ for the two observers.

$$\dot{z}_i = A(t)z_i + B(t)u + L_i(t)(y - C(t)z_i) \tag{3.23a}$$
$$\dot{e}_i = \dot{z} - \dot{z}_i = A(t)z + B(t)u - A(t)z_i - B(t)u - L_i(t)C(t)(z - z_i) \tag{3.23b}$$
$$= A(t)e_i - L_i(t)C(t)e_i = (A(t) - L_i(t)C(t))e_i = A_i(t)e_i \tag{3.23c}$$

From linear theory it can be established that the solution is

$$e_i(t) = \phi_i(t, 0)e(0) \tag{3.24}$$

Later it will become necessary to find the solution after a time δ, which will be a part of the *true* state. The observers will be initialized with the same value $\rightarrow e(0)$ will be the same for both.
There are now two unknowns $e(0)$ and $z(\delta)$, and two equations for Equation 3.24 $i \in [1, 2]$.

$$\phi_1(\delta, 0)e(0) = z(\delta) - z_1(\delta) \Rightarrow e(0) = \phi_1^{-1}(\delta, 0)(z(\delta) - z_1(\delta)) \tag{3.25a}$$
$$\phi_2(\delta, 0)e(0) = z(\delta) - z_2(\delta) \tag{3.25b}$$

Insert these equations in each other, get the result

$$z(\delta) = (I - \phi_2(\delta, 0)\phi_1^{-1}(\delta, 0))^{-1} \begin{bmatrix} -\phi_2(\delta, 0)\phi_1^{-1}(\delta, 0) & I \end{bmatrix} \begin{bmatrix} z_1 \\ z_2 \end{bmatrix} \tag{3.26}$$

Equation 3.26 gives an expression for the true state at time δ by using the two estimates from the observers.

Next the state transition matrices are calculated recursively, based on $\dot{x} = \phi(t,0)x(0)$. Differentiating

$$\dot{x}(t) = A(t)x(t) = A(t)\phi(t,0)x(0) = \dot{\phi}(t,0)x(0) \tag{3.27a}$$

$$\Rightarrow \dot{\phi}(t,0) = A(t)\phi(t,0),\ \phi(0,0) = I \tag{3.27b}$$

In the Hybrid Framework

Next, these expressions are implemented to express the resetting mechanism. Subsequently, the hybrid system will be stated according to the framework presented in section 3.4. The state-vector x consists of the following states

$$x = (z, z_1, z_2, \phi_1, \phi_2, \zeta, \tau) \in N \times \mathbb{R}^n \times \mathbb{R}^n \times M \times M \times \mathbb{R}_{\geq 0} \times \mathbb{R}_{\geq 0} \tag{3.28}$$

where z is the true state, assumed to live in the compact set $N \subset \mathbb{R}^n$. $z_i \in \mathbb{R}^n, i \in [1,2]$ are the Luenberger observer estimates. $\phi_i, i \in [1,2]$ are the respective state transition matrices, and ζ and τ are scalar time variables. Equation 3.23a states the expression for z_i, and Equation 3.27b states an expression for ϕ_i, note that the state transition matrices are periodically reset to identity, and will live in the the compact set $M \subset \mathbb{R}^{n\times n}$. With the states in the state vector defined as mentioned, the differential functions $f(x)$ and difference functions $g(x)$ can be stated as:

$$\dot{x} = f(x) = \begin{bmatrix} A(\tau)z + B(\tau)u \\ A_1(\tau)z_1 + B(\tau)u + (A(\tau) - A_1(\tau))z \\ A_2(\tau)z_2 + B(\tau)u + (A(\tau) - A_2(\tau))z \\ A_1(\tau)\phi_1 \\ A_2(\tau)\phi_2 \\ 1 \\ 1 \end{bmatrix},\ x^+ \in G(x) = \begin{bmatrix} z \\ \{KJ(x) + (I-K)z_1, z_1\} \\ \{KJ(x) + (I-K)z_1, z_1\} \\ I \\ I \\ 0 \\ \tau \end{bmatrix} \tag{3.29}$$

where $J(x) = (I - \phi_2 - \phi_1^{-1})^{-1}[\phi_2\phi_1^{-1}\ I][z_1\ z_2]^T$ and K is a diagonal gain matrix with $0 < k_{ij} < 1$. As for the time variable t, it is not replaced with the scalar time variable τ. Further the jump map and flow map may now be stated as:

$$C = N \times \mathbb{R}^n \times \mathbb{R}^n \times M \times M \times [0,\delta] \times \mathbb{R}_{\geq 0} \tag{3.30}$$

$$D = N \times \mathbb{R}^n \times \mathbb{R}^n \times M \times M \times \delta \times \mathbb{R}_{\geq 0} \tag{3.31}$$

This means:

- z_1, z_2 will jump to either $z_1 + K(J(x) - z_1)$ or z_1, depending on whether the output estimation error exceeds the ϵ-bound, expressed as $|y - C(t)z_1| \geq \epsilon_i$ for $i \in [1,2,...,p]$.

- Now, this would yield a jump map that is not outer semi-continuous (OSC), and the hybrid system would not satisfy the hybrid basic conditions, but this is overcome by using a set-value mapping that contains both values in the jump map.
- C and D are closed sets $\Rightarrow$ (A1) is satisfied, section 3.4.
- $F = f(x)$ is locally bounded, OSC and has convex values for every $x \in C$ by virtue of being a singleton set-valued mapping containing only a continuous function $\Rightarrow$ (A2) is satisfied, section 3.4.
- $G(x)$ is locally bounded and OSC for every $x \in D \Rightarrow$ (A3) is satisfied, section 3.4.
- The continuity of $J(x)$ follows from the fact that the matrix inverse is a continuous function for non-singular matrices, and that continuity is conserved through products, sums and compositions with other continuous functions.
- This shows that the hybrid system satisfies the hybrid basic conditions (section 3.4) and, therefore, constitutes a well-posed hybrid system.

The tasks of the switching logic consist primarily of ensuring safe switching to the candidate algorithms indicated by the performance measures. So for the vessel with the resetting observer mechanism, this means that the switching logic makes sure we are using the preferred Luenberger observer. This is indicated by the performance measures being the deviation from true state. The switch is now called a jump. To avoid chattering, dwell-time is applied in this system, and this is a *timer* which keeps track of the time from the last switch and does not allow a new switch until a certain time has passed. This is also necessary as the Luenberger observer needs some time to initialize before doing another jump.

3.5.2 Time-Varying Model-Based Observer

The time-varying observer gains consist of a nonlinear passive observer (NPO). This observer consists of a *copy* of the familiar CPM (3.7) with added *injection-gains* in wave-filter, velocity, bias force and position. The time-varying gains are the velocity and bias injection gains. First presented in Værnø et al. [2016] where only the bias injection-gain K_3 varied with time, it was argued that the transient performance would be even better with a velocity injection-gain K_4 varied with time as well. A time-varying K_4-gain was then presented in Værnø et al. [2017]. This observer is presented here.

The time-varying model-based observer is not hybrid as it is not constructed with the hybrid framework presented. However, it carries some of the properties, such as it *switches* from one set of tuning to another. This *switching* also needs to be defined by a switching logic, performance monitoring, and prevent chattering.

The NPO benefits as opposed to other observers as it has significantly reduced number of parameters to tune. It requires only one set of observer gains to be tuned to cover the whole space and the wave filter, which is directly coupled to the wave frequency.

Observer Design

K_1 and K_2 gains depend on the peak frequency of the wave spectrum. Værnø et al. [2017] states that it is important that the injection-gain $K_4(t)$ in the velocity dynamics (3.32d) is high enough to dominate the feedback control action. In addition, the injection gain $K_3(t)$ (in 3.32c)

must be high enough in order for the bias estimate to more accurately track the bias load value during the transient. However, it is not wanted to keep these injection gains high at all times. This will result in oscillatory estimates (and subsequently diverge) of the bias and velocity in a steady state.

$$\dot{\hat{\xi}} = A_w\hat{\xi} + K_1\tilde{y} \tag{3.32a}$$
$$\dot{\hat{\eta}} = R(\psi)\hat{\nu} + K_2\tilde{y} \tag{3.32b}$$
$$\dot{\hat{b}} = -T_b^{-1}\hat{b} + K_3(t)\tilde{y} \tag{3.32c}$$
$$M\dot{\hat{\nu}} = -D\hat{\nu} + R(\psi)^T\hat{b} + \tau + K_4(t)R(\psi)^T\tilde{y} \tag{3.32d}$$
$$\hat{y} = \hat{\eta} + C_w\hat{\xi} \tag{3.32e}$$

$\hat{\xi} \in \mathbb{R}^5 \times \mathbb{S}^1$, $\hat{\eta} \in \mathbb{R}^2 \times \mathbb{S}$, $\hat{b} \in \mathbb{R}^3$, $\hat{\nu} \in \mathbb{R}^3$ are state estimates of respectively first order wave motion, position, bias, and velocity. $K_1 \in \mathbb{R}^{6\times3}, K_2, K_3(t), K_4(t) \in \mathbb{R}^{3\times3}$ are non-negative gain matrices. The gain matrices are defined further in Equation A.8 and in Fossen [2011]. Next the time-varying injection-gains are defined to range within,

$$K_i(t) = \kappa(t)K_{i,max} + (1-\kappa(t))K_{i,min},\ i = 3,4 \tag{3.33}$$

where κ tells if the system is in steady state ($\kappa = 0$) or in a transient ($\kappa = 1$). Thus three transient events are defined,

1. Operator executed heading change, easily detected through the desired yaw rate from the guidance system.
2. A change in the environmental disturbances, detected through a deterioration of the observer performance.
3. Error due to initialization of the observer.

Mathematically expressed by

$$\kappa(t) = max\{0,\ \beta(t) - 1\}, \tag{3.34a}$$
$$\beta(t) = min\{\varepsilon_{rd}|r_d(t)| + \varepsilon_\eta|\tilde{\eta}_f(t)|,\ 2\}, \tag{3.34b}$$
$$\dot{\tilde{\eta}}_f = -T_{\eta_f}^{-1}\{\tilde{\eta}_f - \tilde{y}\}, \tag{3.34c}$$

where $\varepsilon_{r_d} \in \mathbb{R}_{>0}$ and the desired yaw rate $r_d(t) \in \mathbb{R}$ are related to a heading change. $\tilde{\eta}_f$ in 3.34b is the low pass filter 3.34c that tracks the observer output error performance, and $T_{\eta_f} \in \mathbb{R}^{3\times3}$ is a diagonal matrix of filter time constants. Thus if the observer performance deteriorate (meaning the error grows) $|\tilde{\eta}_f|$ will grow. This is tuned so that κ approaches zero at steady state. In order to avoid chattering (the rapid switching back and forth) a few considerations is done, a hysteresis is implemented

- An effect of a transient of a transient at observer start-up, $\tilde{\eta}_f$ is initialized with non-zero values.
- β in 3.34b are between zero and two.
- The maximum function in 3.34a establish a threshold such that κ will never go above zero before β is larger than one.

Chapter 4

Method

This chapter presents the methods applied to conduct the simulations and experiments of the control system containing hybrid observers to test behavior in varying operational conditions. The Cybership 3 (CS3) vessel characteristics, employed in both simulation and experiment, are first provided. The results of the tests are then reported, along with each test's objective and purpose.

Then the simulation setup is presented. In addition, the implementation of varying sea states in the *Marine Cybernetics Simulator* (MCSim) are presented and further explained. Next, the expansion of tables allows for varying hydrodynamic coefficients for finding first-and second-order wave motions and loads are included.

Then the experimental setup in the *Marine Cybernetics Laboratory* is presented, along with relevant considerations regarding the laboratory.

Figure 4.1: Cybership 3 in MCLab.

4.1 Vessel Characteristics

Cybership 3 (CS3) is a supply vessel and is model-scaled 1:30, pictured in Figure 4.1 in the Marine Cybernetics Laboratory. The model-scale of the vessel weighs 75 kg and has an overall length of 2.275 m and breadth of 0.4 m. The vessel is equipped with three thrusters, two azimuth thrusters in the stern and one in the bow, illustration of the thruster configuration can be seen in Figure 4.2. Their rotation angle is fixed, $-30°$, $30°$ and $90°$. The thrusters on Cybership 3 are over-dimensioned relative to the scale of the vessel and are hence powerful. Therefore the vessel control system includes an emergency solution for disabling the thrusters.

Cybership 3 has an onboard computer, a compact RIO (cRIO) from National Instruments (NI), that controls the three thrusters' hardware. The motion control system created in Simulink/Matlab is compiled to C code, a NI compatible format, and then transferred to the cRIO through WLAN. During the testing, the operator may monitor, log, and control through a custom workspace using a dedicated computer.

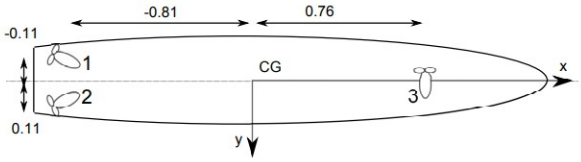

Figure 4.2: Thruster configuration of Cybership 3. Fixed angle stern $\pm 30°$, and bow $+90°$.

4.2 Hybrid Observer

In addition to work as state-estimators, the hybrid observers' objectives are to be reactive while outside steady-state and hence increase performance. Different mechanisms trigger the improved performance, i.e., different performance monitoring and switching logics as discussed in section 3.5. The objective of the case study was to test (investigate) the hybrid observer subjected to varying operational conditions. As described earlier, varying operational conditions (VOCs) are changes in the environment, operation, and speed.

The objective of the simulation and model-scale experiments are to compare the behavior during transients induced by varying operational conditions (VOC) and implementation of the resetting observer introduced in section 3.5.1 and the time-varying model-based observer presented in section 3.5.2.

The motion control system includes a dynamic positioning (DP) controller tuned for station-keeping in a moderate sea. Another tuning was also conducted for the station-keeping to work during higher sea states as well. Hence two sets of controller PID parameters exist. Tuning of controllers can constantly be improved and optimized. However, the controller performance was not of primary concern, and hence the focus was kept on the observers, i.e., the controller could have been tuned for further optimal performance.

Two reference models were used as well. The first is the position and attitude reference model as presented in section 3.2.1 and presents the second by Fernandes [2015] based on optimal curve shapes as described in section 3.2.2.

The three different observers used during testing to map the best behavior of each observer are the nonlinear passive observer, also named the nonlinear model-based observer. Then the

time-varying model-based observer, which is an extension to the nonlinear passive observer, presented by Værnø et al. [2017] and described in section 3.5.2, was tested. Finally the resetting observer presented by Torben [2019] and described in section 3.5.1 was tested. The first observer is included to work as a benchmark for the observer's behavior.

Table 4.1 presents a summary of the four tests that were conducted. The table shows the test, the goal of the test, and the various operational conditions that are being tested. Each observer was conducted one time per observer.

Testno.	Experiment	VOC
1	The vessel sailed from position A: $\eta_A = [-1\ 0\ 0]$ to position B: $\eta_B = [7\ 0\ 0]$.	Change in speed.
2	The vessel put in station-keeping, first subjected to no waves, then the waves was turned on.	Change in environment.
3	The vessel put in station-keeping at $\eta = [0\ -1\ 0]$, before suddenly pushed off setFpoint $1-2$ meters in sway direction.	Sudden unmodeled load in sway.
4	The vessel put in station-keeping at position $\eta = [0\ 0\ -30°]$ and then a setpoint change to $\eta = [0\ 0\ +30°]$, introducing a transient.	Change in operation mode.
5	(Only Simulation) - Vessel in transit going from low speed to high (max) speed, including varying sea states.	Change in speed, environment.

Table 4.1: Overview of the test scenarios.

In the first test, the changing VOCs will be the change in speed due to the change in operational mode, sailing in DP from at quay to transit to steady-state forward speed. The transit phase occurs between the two setpoints. While sailing this distance, the vessel will be subjected to an acceleration in surge speed. The nonlinear passive observer is modeled to capture the main dynamics of the situation. Further, as there may be a lag due to the transient period, the nonlinear passive observer is tuned for a specific environment where there are inaccuracies. If any estimation error grows over a certain limit due to this, the time-varying nonlinear passive observer will pick up this, and the time-varying observer gains work. The resetting observer works similarly, so when the estimation error grows over a predefined bound, the state estimates jump to a new state. The new state is found from finding the *true system value*.

In the second test, the vessel was set to station-keeping with the dynamic positioning controller to test the station-keeping capabilities with varying environmental loads. The vessel was first subjected to no waves before the moderate sea state was activated. As the sea state grows, both controllers and observers are expected to be challenged, as both units are tuned for specific environments. In addition, as the sea state grows over time, the control system does not have the time to reach a steady-state before a new sea state has begun (in the simulation), while in the laboratory, the vessel will be able to find a steady-state.

During the third test, the objective was to test and compare the handling of a sudden and unmodeled load. The vessel was at station-keeping with the DP controller tuned for moderate sea state while subjected to the moderate sea state. The vessel was pushed off approximately between $1-2$ meters in sway direction. This test scenario challenges the capability to react when an unmodeled load occurs. As the bias dynamics for observers are usually modeled as slowly varying loads, this is an acceptable assumption when the bias dynamics are meant to

capture environmental loads. Hence the observer needs to be reactive during these incidents in order to ensure safety. The nonlinear passive observer has little reactivity, but as the estimation error grows (which is part of the performance monitoring and switching logic), the time-varying observer gains will be enabled. The resetting observer will also be able to detect the estimation error and reset its states.

The fourth test was conducted to learn how the observers reacted to the transient occurrence during heading change. This was done when the vessel was set to station-keeping at a fixed angle $\eta = [0\ 0\ -30°]$ and then commanded a heading turn to $\eta = [0\ 0\ +30°]$. The heading change will induce a transient in the control system. The time-varying nonlinear passive observer has three predefined transients, which are implemented by design. One is the operator commanded heading change. Hence it is expected that the time-varying gains will ensure improved performance over the regular nonlinear passive observer. Further, the resetting observer has not predefined the heading change as a transient event. However, if the heading change introduces a large transient, the resetting observer is expected to reset the observer states.

The fifth test was a simulation of the vessel going from low speed to high speed while subjected to varying sea states using a high fidelity simulation model. This test was not conducted in the laboratory due to basin size. This test includes the nested flip-flop model, presented in section 4.3.1. Hence, the handling of the transient wave drifts forces and RAO. As the vessel reaches higher speeds, the controller will be able to use velocity measurements available from GPS. Hence estimates in acceleration and deceleration are compared, i.e., before and after the vessel uses GPS velocity measurements. During this simulation, the optimal curve shape reference model presented in section 3.2.2 is used in addition to a speed- and heading-controller.

During both simulation and experiment, model-scale tests were conducted. Hence, the results will also be presented in full-scale using Froude scaling, using the ratio $\lambda = 30$. All result plots in chapter 5 and 6 will have model-scale values in left vertical and bottom horizontal axis, while full-scale values in right vertical and top horizontal axis.

	Model-scale	Full-scale
H_s [m]	0.04	1.20
T_p [s]	0.80	0.15

Table 4.2: The moderate sea state used in simulation and experiments, using JONSWAP wave spectrum.

4.3 Simulation Setup

The control system was tested in the simulation environment *Marine Cybernetics Simulator* (MCSim). This simulator is based on Matlab/Simulink developed by the Department of Marine Technology, with the latest updates from Astrid Brodtkorb. Cybership 3 (CS3) was used in simulation as this vessel exists in model-scale in the marine cybernetics laboratory. The simulator consists of

- a vessel module containing a wave-frequency (WF) and low-frequency (LF) model.
- an environment module, containing wave-, current-, wind- and ice-loads.
- a sensor module representing the real-life sensors a vessel.

- a vessel motion controller module which includes the reference model(s), observer(s), and controller(s).
- a thruster and shaft module with thrust allocation and thruster dynamics together with a local thruster control.

4.3.1 Varying Sea States

In the *Marine Cybernetics Simulator* (MCSim) an extension was made in this thesis to allow for varying sea states and hence varying first and second order wave motions and loads, and higher speed transfer functions. This was done with creating a flip-flop model and a nested flip-flop model.

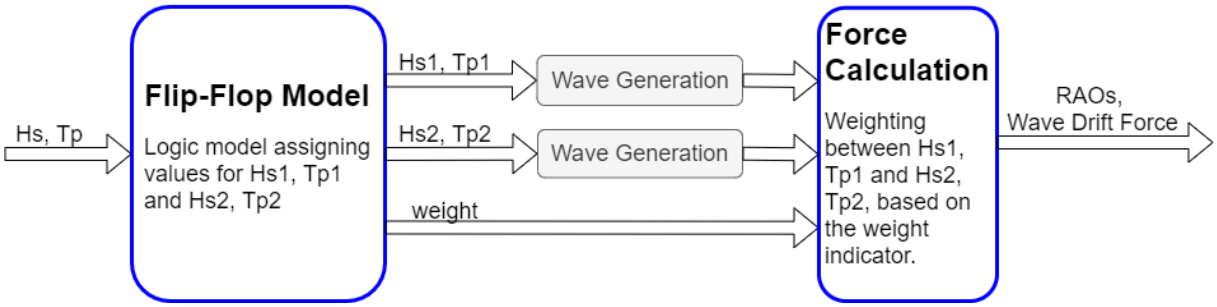

Figure 4.3: Illustration of how the flip-flop model works.

To further explain the mindset behind a flip-flop model, a motivating example is presented. The system inputs a $Value$ and outputs two new $Values$ and an on/off indicator $weight$. The on/off indicator switch signal in black in Figure 4.4 is indicating if $Value$ should converge from $Value_1$ or $Value_2$. Meaning when the signal is 0 the Value will converge from $Value_1$ to $Value_2$, and when the signal is 1 the $Value$ will converge from $Value_2$ to $Value_1$. Further, the weight function in red in Figure 4.4 ensures that there is a smooth transition between the two Values. The plots in Figure 4.4 in solid lines are the output from the flip-flop model as seen in Figure 4.3, while the dashed lines are the outputs from the *Force Calculation*-model.

The *Force Calculation*-model will calculate the wave drift motions and loads based on Equation 3.4, by using a lookup table. The lookup table maps the inputs to an output value by interpolating the table with transfer functions. The coefficients were obtained from ShipX, using Vessel Response Program (VERES). A program system for computation of added mass and damping, first-order wave excitation forces, motion transfer functions, or slender ships with forwarding speed.

Further, in MCSim, the flip-flop model inputs a sea state and outputs two sea states and a weight $w = [0, 1]$. The weight will be used in a weighting block to alter the resulting force between the two forces. Hence, the two sea states will first be used to calculate two sets of appropriate RAOs and wave forces before these are weighted, and a final RAO and wave drift motions and forces are obtained. Conceptually this is illustrated in Figure 4.3.

Further, the transfer function lookup table was extended to input surge speed in order to calculate more correct wave drift forces. The surge velocity can not be used directly in the lookup table. Hence another flip-flop model was created. Resulting in a *nested* flip-flop model, illustrated in Figure 4.5.

u_1 and u_2 are the surge speeds the model is switching between.

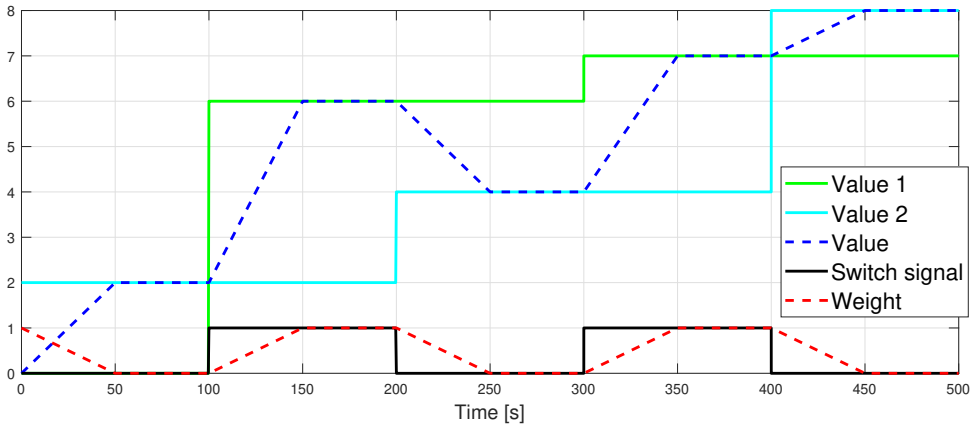

Figure 4.4: Motivating example of the flip-flop model.

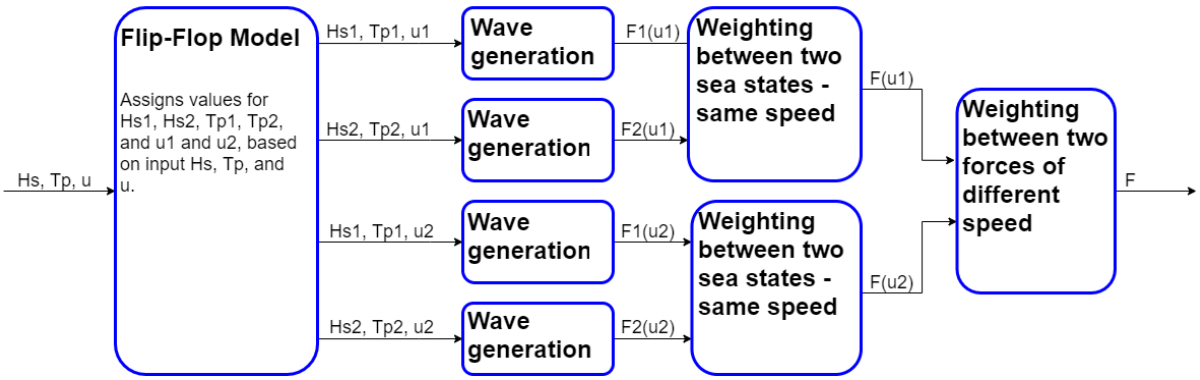

Figure 4.5: Illustration of the nested flip-flop model.

An advantage of using a flip-flop model for varying sea states is that the motion transfer functions and wave drift forces are depending on the transfer functions found in a lookup table. Hence, the flip-flop model does not increase the complexity of the calculations too much. Further, it is advantageous is to interpolate the output (e.g., the wave drift force) rather than changing the input (H_s and T_p). as this can result in unphysical output during the transition period because the output calculation is complex/complicated (integrate all wave components, Equation 3.5).

In simulation 2 (Figure 5.1), the first wave drift load model was used, while the latter model was used in simulation 5 (Figure 5.2). The results are presented in section 5.1.

4.4 Laboratory Setup

The laboratory experiments were conducted in the model test tank *Marine Cybernetics Laboratory* (MCLab) at the Department of Marine Technology, NTNU Trondheim.

The laboratory includes a DHI (www.dhigroup.com) wave-maker. The wave-maker is a single paddle wave-making machine with a width of 6 meters, and it is equipped with an Active Wave Absorption Control System (AWACS 2). A dedicated computer controls this single paddle wave generator. The machine can produce both regular and irregular waves through the DHI Wave Synthesizer system. Available spectrum are first order Stoke, JONSWAP, Pierson-Moskowitz, Bretschneider, ISSC and ITTC. The largest wave the wave-maker can produce is (H_s, T_p) =

$(0.15m,\ 1.5s)$. $H_s\ =\ 0.1$ m scales to $H_s\ =\ 3$ m full-scale for Cybership 3.

For measurement of the position of the vessel, a Qualisys camera system is used as a motion capturing unit. The four spheres on Cybership 3 captured by the camera system can be seen in Figure 4.1. The highest reflector sphere is placed $(x,\ y,\ z)\ =\ (510,\ -180,\ -860)$ mm from the center of gravity (COG). This is entered in the Qualisys camera system, which then translates the coordinate system.

Further, the signals from Qualisys can freeze, causing possible errors in data and dangerous situations in real life. This is handled by including a signal freeze detection model in the motion control system to enable dead reckoning to be included in the observers. The size of the basin is $40 \times 6.5m^2$, while the cameras attached to the towing carriage captures an area of approximately $7 \times 6m^2$.

4.5 Observer Performance Evaluation

In order to conduct a fair evaluation of the three observers, cost functions are used during simulation and experiment. These are then normalized to summarize the four tests, so the largest cost value obtains the value 100, these summaries are found in Table 5.3, 5.4 and 6.1.

$$J_\eta = \int_{t_0}^{t_f} \{|\eta_N - \hat{\eta}_N| + |\eta_E - \hat{\eta}_E| + \frac{180}{\pi}|\psi - \hat{\psi}|\}dt \tag{4.1a}$$

$$J_\nu = \int_{t_0}^{t_f} \{|u - \hat{u}| + |v - \hat{v}| + \frac{180}{\pi}|r - \hat{r}|\}dt \tag{4.1b}$$

$$\tag{4.1c}$$

where $\hat{\eta}, \hat{u}, \hat{v}$, and $\hat{r}$ are the estimates.

However as not all of these states are available in measurements a different performance evaluation was done.

Chapter 5

Simulation Results

This chapter contains the results from the simulations conducted in Matlab/Simulink in the *Marine Cybernetics Simulator* (MCSim). First, the flip-flop model results allowing varying sea states in MCSim during sim 2 and sim 5 are presented. Then the results from the five different case studies introduced in Table 4.1 are presented. For each scenario, the error over time and cost function for position and velocity are presented. Finally, the results are summarized for each observer in each test by the cost function and normalized such that the worst-performing has a score of 100, in Table 5.3 and 5.4.

5.1 The Wave Drift Loads

In simulation 2, 2nd order mean wave drift forces are enabled while the vessel is in dynamic positioning (DP). The sea states are increasing linearly from SS1 to SS2 presented in Table 5.1

	H_s [m]		T_p [s]	
	Model-scale	Full-scale	Model-scale	Full-scale
SS1	0.04	1.20	0.80	0.15
SS2	0.18	5.20	1.16	0.21

Table 5.1: Sea states used in simulation 2.

The resulting wave drift forces are in Figure 5.1. Model-scale forces are on the left vertical axis, and full-scale is on the right vertical axis. The solid lines in green and cyan in Figure 5.1 and 5.2 are the sea states the flip flop model switches between. The solid black line is the switch parameter, determining which sea state to converge towards. Further, the dashed red line shows the weighting between the sea states, and the dashed blue is the resulting wave drift force. This result is obtained from simulating the vessel at station-keeping in $\eta = [0\ 0\ 0]$.

In simulation 5, The vessel was set to accelerate to max speed and then decelerate. The resulting surge wave drift forces are presented in Figure 5.2, subjected to varying sea states. To increase the fidelity of the simulation model, the transfer coefficients found in lookup tables are now also expanded to include surge speed. Hence the nested flip flop model was used, as introduced in section 4.3.1. The sea states were set to increase linearly from SS1 to SS2, Table 5.2.

As can be seen in Figure 5.2 the wave forces decrease due to the lowering of speed. The surge speed trajectory is presented in Figure 5.10.

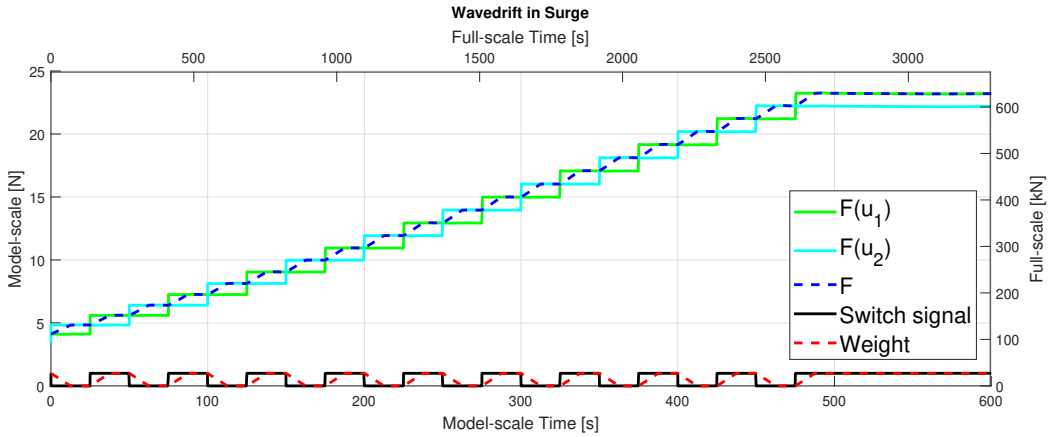

Figure 5.1: Wave drift forces in surge direction during simulation 2. In this simulation and figure, u_1 and u_2 are zero.

	H_s [m]		T_p [s]	
	Model-scale	Full-scale	Model-scale	Full-scale
SS1	0.04	1.20	0.80	0.15
SS2	0.10	3.00	1.50	0.27

Table 5.2: Sea states used in simulation 5.

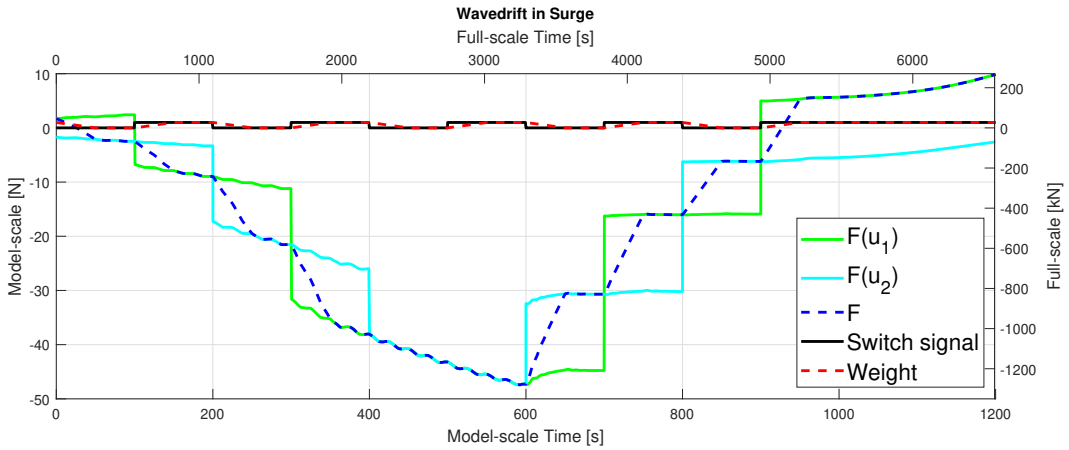

Figure 5.2: Wave drift force in surge direction during simulation 5.

5.2 Sim 1: Vessel Sailing From A - B Subjected to Waves

In the first simulation the vessel was set to sail from station-keeping in $\eta_A = [-1\ 0\ 0]$ to $\eta_B = [7\ 0\ 0]$, a distance of 8 meters in model-scale, which scales to 240 meters full-scale, illustrated in Figure 5.3 by the surge position trajectory. Moderate sea state (Table 4.2) was used. During the simulation, the vessel used the DP controller for moderate sea and the position and attitude reference model. This distance was chosen due to the laboratory camera range to have consistency in simulation and experimental tests.

The sailed distance is four times the ships-length, which would resemble a vessel doing maneuvering in real life, rather than sailing from the calm sea at quay towards the open sea. This is also true regarding the moderate sea state the vessel is subjected to. So it is instead the beginning of the journey towards open sea.

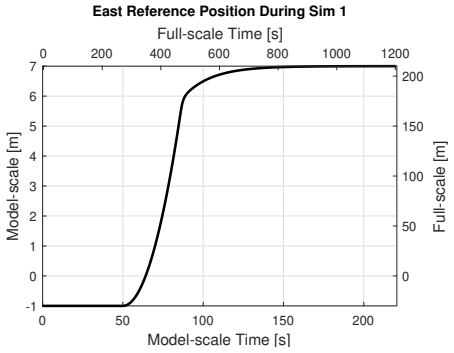

Figure 5.3: Surge Positions During Sim 1.

The vessel has a slight overshoot when it reaches the setpoint. To compensate, the vessel surge speed has to correct and undershoots and does not follow its reference speed. This occurs for all observers, as seen in Figure 5.4 (a), where a modest peak in inaccuracy arises at roughly $t = 90$.

As NPO estimates has little deviation from the measurements the time-varying gains are not activated.

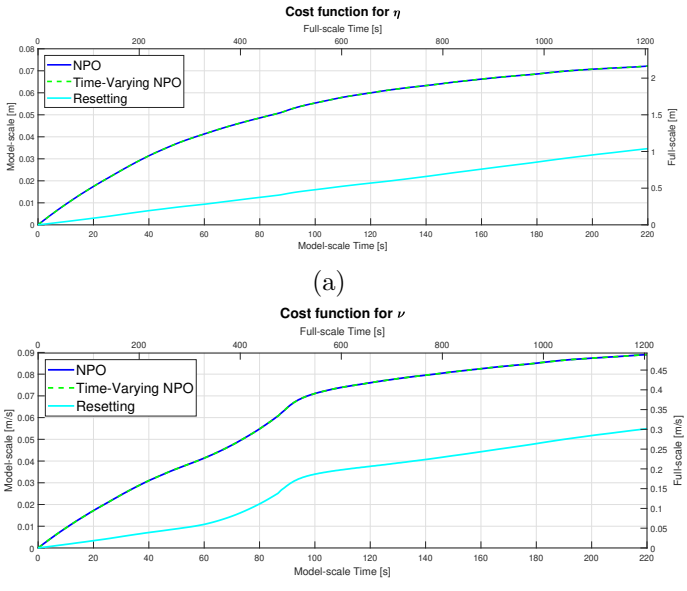

Figure 5.4: Sim 1 - Observer Performance Evaluation.

5.3 Sim 2: Vessel at DP Subjected to Varying Sea States

During the second simulation, the objective was to test the vessel's behavior with varying environmental loads, i.e., varying sea states. Hence the flip-flop model presented in section 4.3.1 was used, allowing the sea states to varying linearly from SS1 to SS2 (Table 5.1), resulting in the wave drift forces presented in Figure 5.1. The vessel was station-keeping in $\eta = [0\ 0\ 0]$ by using the DP controller tuned for moderate sea.

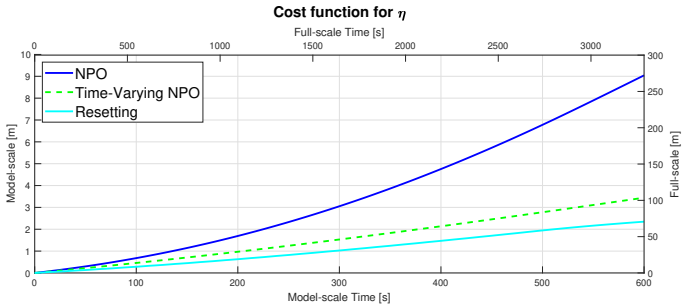

(a)

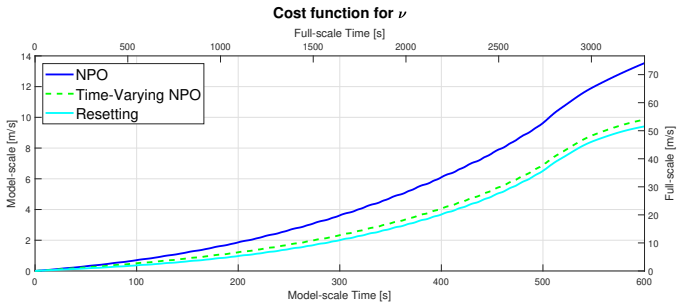

(b)

Figure 5.5: Sim 2 - Observer Performance Evaluation.

Figure 5.5 shows that the time-varying gains are activated quickly, and the regular nonlinear passive observer cost grows larger than the two other observers. The transient is detected through the deterioration of the estimates due to the varying environmental changes in the time-varying NPO.

During this test, the vessel is exposed to larger wave drift forces. Hence the thruster forces need to be larger, and the saturation of the thruster forces was increased.

5.4 Sim 3: Vessel at DP Subjected to Waves Pushed Off Set-point in Sway

This test is conducted in order to investigate the performance of the observers when subjected to an unknown and rapid load. The vessel will be disturbed at steady-state, introducing a transient phase. The vessel will be at station-keeping with the DP controller for moderate sea when the vessel is subjected to a load of $50N$ for 1 second in sway direction at $t = 40$. This results in the vessel moving approximately 1.1 meters in model-scale, which is 33 meters full-scale. The sway position are shown in Figure 5.6.

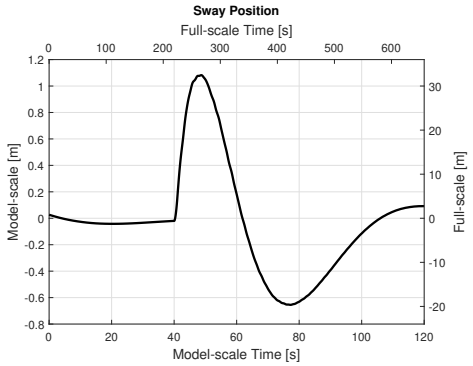

Figure 5.6: Sim 3 - Sway Position.

As an unmodeled and rapid load will generate an error in the sway estimate, both the time-varying gains for the nonlinear passive observer and the resetting mechanism and time-varying gains are expected to be enabled.

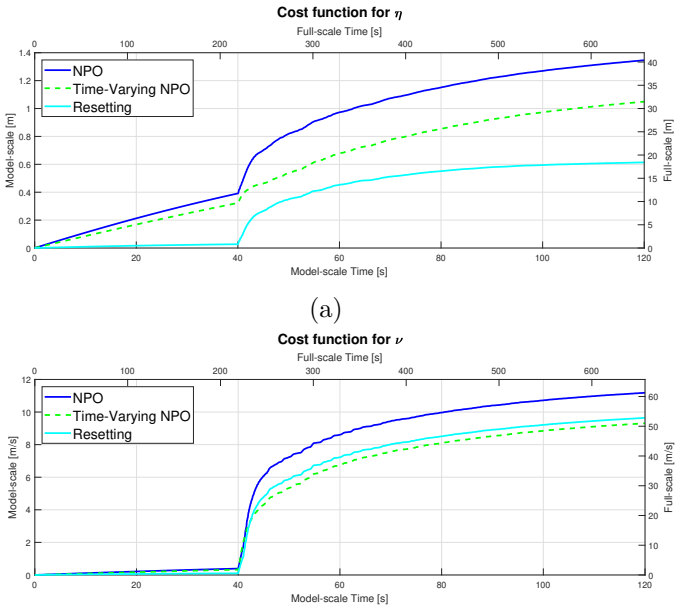

Figure 5.7: Sim 3 - Observer Performance Evaluation.

In Figure 5.7 the cost functions for the observers seem to escalate after the push. The time-varying gains improved the performance of the nonlinear passive observer by allowing for the aggressive gains to cope with the transient phase. While the resetting observer allows for capturing bias loads that are slowly varying.

5.5 Sim 4: Vessel at DP Subjected to Waves with Change in Heading Setpoint

The fourth simulation test's objective was to test handling a transient introduced by the operator through setpoint change. The position and attitude reference model was used to create a suitable reference trajectory for the heading change from $\eta = [0\ 0\ -30°]$ to $\eta = [0\ 0\ +30°]$. The heading trajectory can be seen in Figure 5.8.

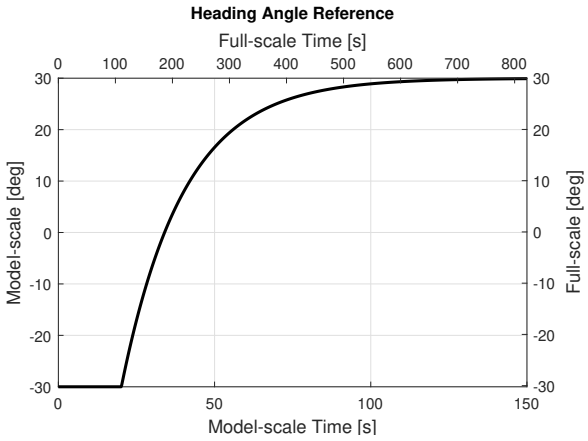

Figure 5.8: Heading during test 4.

For the time-varying nonlinear observer, a heading change is defined as a transient event. Hence the hybrid observer's performance monitoring is designed to capture this and enable the time-varying gains. This results in the time-varying observer improving the behavior of the nonlinear passive observer. In addition, in Figure 5.9 the resetting observer generates a small cost value compared to the other.

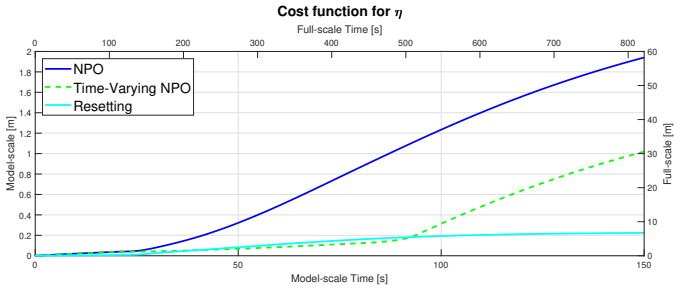

(a)

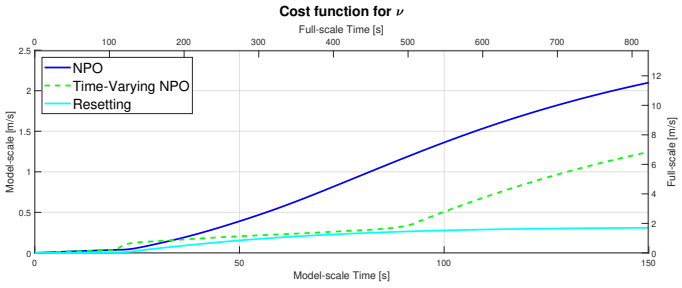

(b)

Figure 5.9: Sim 4 - Observer Performance Evaluation.

5.6 Sim 5: Vessel Subjected to Varying Sea States in Max Speed

Simulation 5 was conducted to extend the second simulation, allowing for varying sea states in varying surge speeds. In addition, a performance monitoring and switching logic were implemented to change between velocity estimates and measurements, as velocity measurements are available when the vessel enters higher speed regimes. This is illustrated in Figure 5.10, showing the surge velocity trajectory, the dashed line is where the motion control system uses estimates, and the solid line is where the motion control system uses measurements. The switching logic switches to measurements when the vessel reaches $u = 1.6$ m/s full-scale, and switches back when decelerated to $u = 0.54$ m/s full-scale.

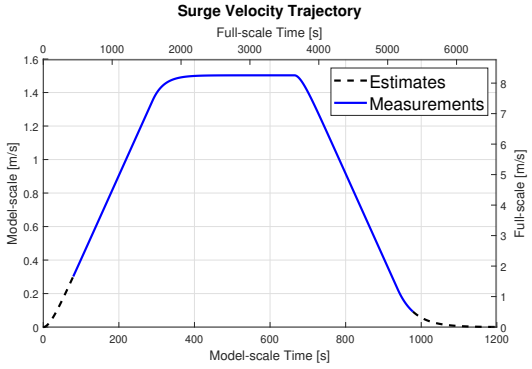

Figure 5.10: Surge velocity for simulation 5, including switch between estimates and measurements.

Hence in Figure 5.11 and A.5 the cost does not grow, and the error estimates are zero during the period when measurements are used. Further, the varying gains in the model-based observer are activated during the entire simulation.

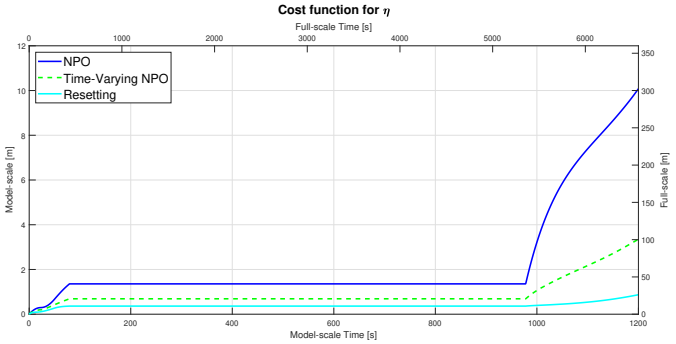

(a)

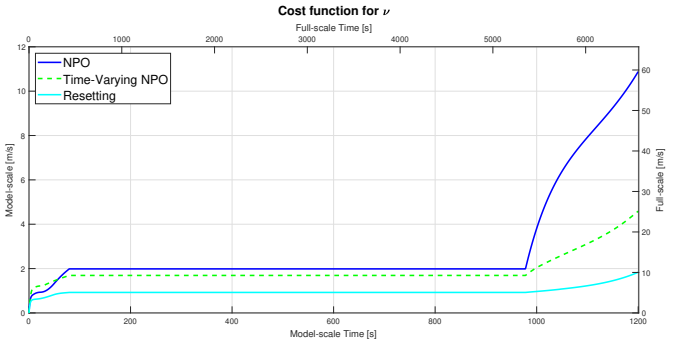

(b)

Figure 5.11: Sim 5 - Observer Performance Evaluation.

5.7 Result Summary

To compare the performance of the observers in the four different test scenarios the estimation error is summarized by the cost function defined in Equation 4.1. Further, the values are normalized such that the worst performing for each test has a score of 100, and lower scores imply better observer behavior. During simulation, the position estimates are available. In addition, the low-frequency velocity measurements are used to obtain the velocity estimate error. The results for the position estimate are presented in Table 5.3, and the velocity estimates are found in Table 5.4.

Sim	NPO	TVNPO	Resetting
1	100	100	47.99
2	100	38.07	25.95
3	100	77.94	45.60
4	100	52.54	11.52
5	100	33.23	8.64

Table 5.3: Position cost function values are normalized such that the worst performing has score of 100.

Sim	NPO	TVNPO	Resetting
1	100	100	61.69
2	100	72.86	69.55
3	100	83.26	86.23
4	100	59.29	14.74
5	100	42.18	16.89

Table 5.4: Velocity cost function values are normalized such that the worst performing has score of 100.

As mentioned, the worst-performing observer obtains a score of 100, which is indicated by red cell color. As the performance improves, the scores are lower, and the cell color is green, in Table 5.3 and 5.4.

In Table 5.3 the normalized cost function value for position estimate indicates that the resetting observer has the best performance during the first test when the vessel was in transient between two surge setpoints. As the transient does not generate a large estimate deviation the time-varying gains are not activated, and the time-varying observer gains the same score as the baseline, the nonlinear passive observer.

In the appendix the instant error over simulations are presented. Figure 5.5 (a) shows that the resetting observer resets to true state periodically trough the simulation.

The resetting observer scores better than the time-varying nonlinear passive observer in position estimates in test 2. During test 2, the vessel was subjected to a transient phase due to varying environmental loads. The bias dynamics for the nonlinear passive observer are modeled to capture slowly varying loads. Combined with aggressive tuning, this design results in good state estimation, both for position and velocity.

During test 3, the vessel is subjected to a rapid and unmodeled load, and the resetting observer has the best score. However, the scores of the resetting observer and time-varying NPO are close. The slowly varying bias dynamics cannot capture the rapid change correctly. However,

by enabling the aggressive gains, the the-varying observer improves the NPO behavior. The resetting observer captures this rapid change by finding the true system state, resulting in a more precise and improved position and velocity estimate.

The fourth test exposed the vessel to a transient trough change in the heading setpoint. This particular transient event is, as mentioned, predefined in the observer design of the time-varying nonlinear passive observer. Hence the observer enables aggressive gains when subjected to heading change, and the results are better than the nonlinear passive observer. Further, the resetting observer detects estimation error and hence resets to the true system state.

The fifth test simulates the vessel in transit between low speed and high speed while subjected to increasing sea states. During which the time-varying nonlinear observer actives its time-varying gains from the start. This indicates that the model-based observer used as a baseline could have higher gains. However, using too high gains in the model-based observer is usually not preferred as this causes oscillations in steady-state. Further, the resetting observer has good performance and can react to the varying sea states, both before and after switching when the sea states are larger.

Chapter 6

Experimental Results

This chapter contains results from the model-scale experiment conducted at the Marine Cybernetics Laboratory at the Department of Marine Technology, NTNU. The tests conducted was presented in Table 4.1, and the results are presented here in the corresponding order. Each observer and each test use the cost function to compare results presented at the end of the chapter.

6.1 Test 1: Vessel Sailing From A - B Subjected to Waves

The vessel was set to manoeuvre from set point $\eta_A = [-1\ 0\ 0]$ to $\eta_B = [7\ 0\ 0]$ with waves while subjected to moderate sea (Table 4.2). During this test the vessel will accelerate to approximately surge speed $u = 0.4$ m/s, which scales to 2.19 m/s. The vessel commences to move at $t = 30$, this can be seen in Figure 6.1, where the surge position from the three tests are collected.

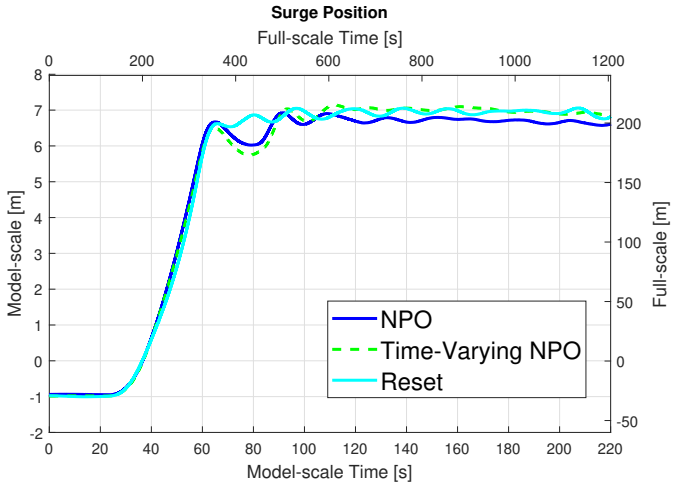

Figure 6.1: Test 1 - Surge Position.

In Figure 6.2 (a), the error for all three degrees of freedom can be seen over time. In Figure 6.2 the cumulative sum is plotted. The resetting observer has the lowest cumulative sum, and the time-varying NPO has the second-best score. However, during the commencement of the surge motion, the cost function for the time-varying observer has steeper growth than the nonlinear

passive observer, before stabilizing and obtains a lower final cost value.

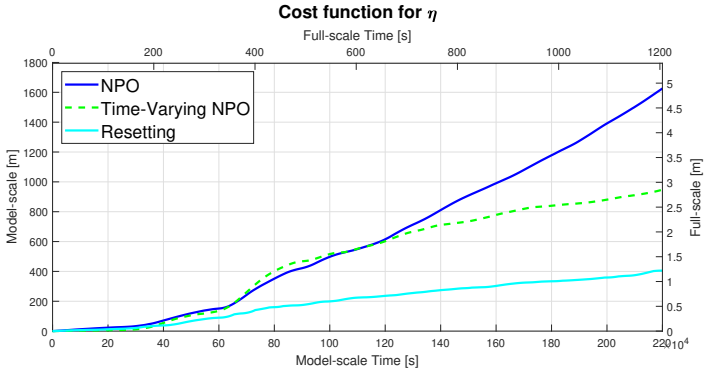

Figure 6.2: Test 1 - Observer Performance

6.2 Test 2: Vessel at DP Subjected to Varying Sea States

During the second test, the objective was to test the observers' abilities when the vessel was subjected to varying environmental conditions, in this case varying sea states. This was done by enabling the vessel to station-keeping with the DP controller tuned for a moderate sea state. The position and attitude reference model was set to have setpoint $\eta = [0\ 0\ 0]$. As Cybership 3 (CS3) does not have a waterproof top, the wave-maker was rather disabled before being enabled to work as varying environmental load. The moderate sea state (Table 4.2) was enabled at approximately $t = 50$ s.

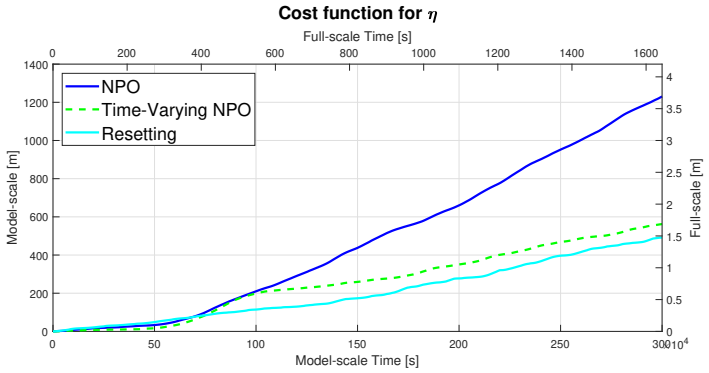

Figure 6.3: Test 2 - Observer Performance

In Figure 6.4 the horizontal motions of the vessel during the three tests are plotted, and it is possible to see that the waves are enabled at $t = 50$s in the surge motion, as the vessel meets a more significant resistance.

In Figure 6.3 (a), both estimation error for the nonlinear passive observer and time-varying observer increase as the waves meet the vessel. However, once the aggressive gains are activated, the time-varying gains correct the estimates, and the inaccuracy is reduced. Figure 6.3 (b) shows that the nonlinear passive observer has accumulated the largest error.

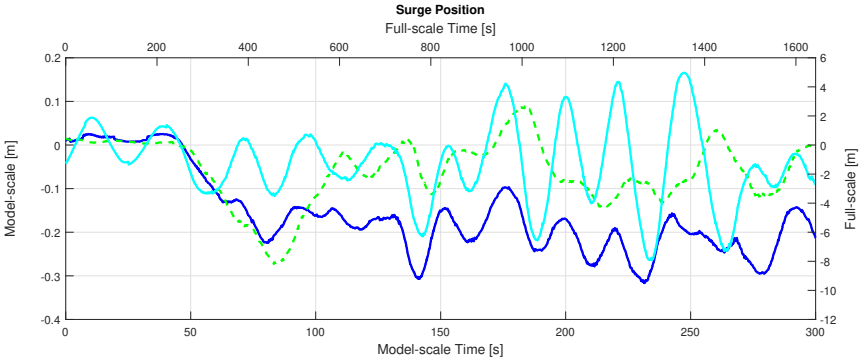

(a) Surge Position

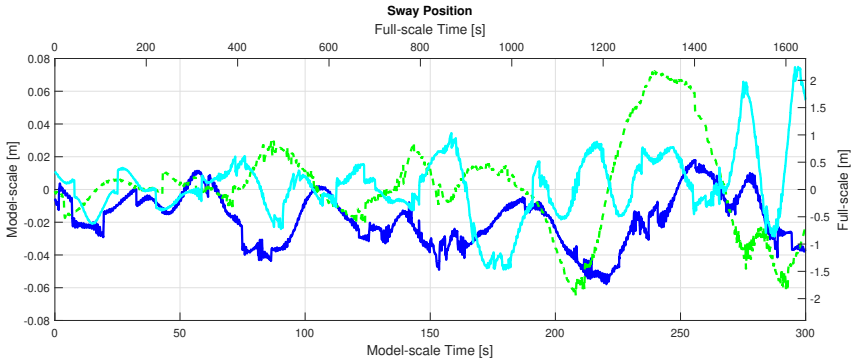

(b) Sway Position

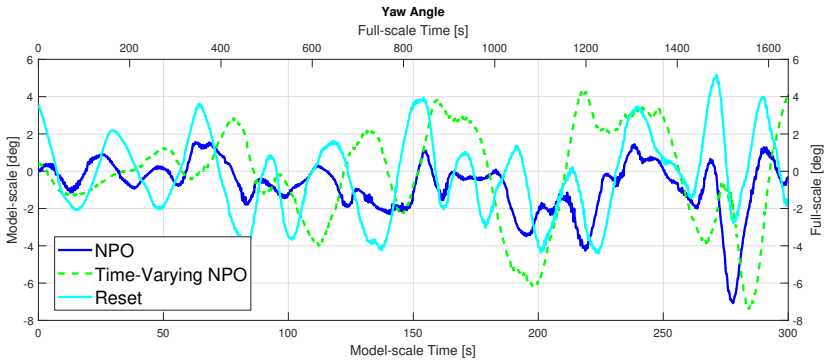

(c) Yaw Angle

Figure 6.4: Test 2 - the horizontal motions during laboratory experiment 2.

6.3 Test 3: Vessel at DP Subjected to Waves Pushed Off Setpoint in Sway

The third experiment was conducted to investigate the behavior when subjected to a sudden unmodeled load in sway direction. The vessel was pushed approximately 1 meter off setpoint at the laboratory, 30 meters in full-scale, while subjected to moderate sea. The push was done with a boat stake.

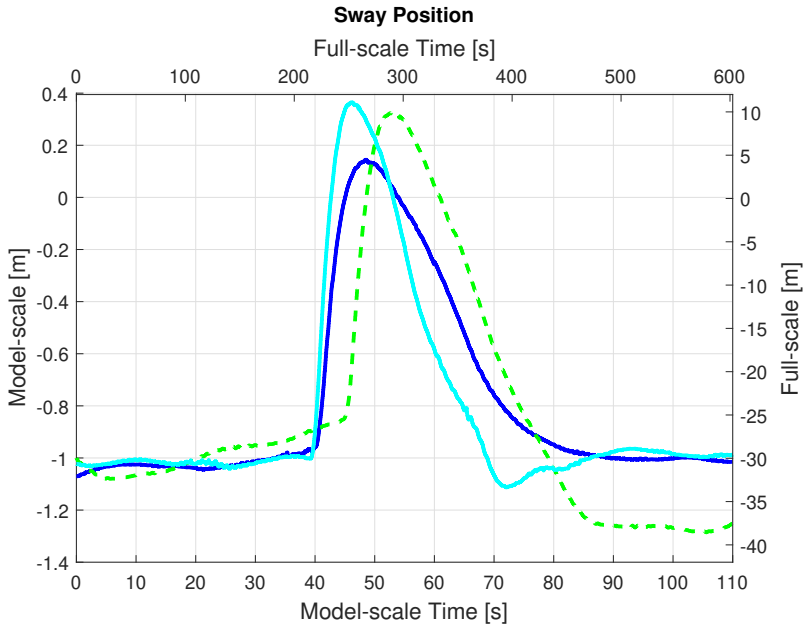

Figure 6.5: Sway position, capturing the push off setpoint in sway direction.

The sway positions measured during the test can be seen in Figure 6.5.

As the vessel is pushed at approximately $t = 40$ seconds, the nonlinear passive and time-varying observer estimates jump significantly. As the time-varying gains are activated, the estimates of the TVNPO correct. The resetting observer has a correcting effect and resets to the *true system states* which ensures that the estimates stay correct.

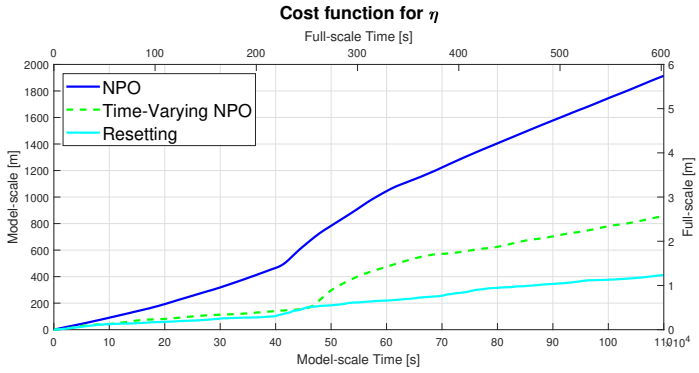

Figure 6.6: Test 3 - Observer Performance

6.4 Test 4: Vessel at DP Subjected to Waves with Change in Heading Setpoint

The fourth test was conducted to investigate the behavior during heading setpoint change. The vessel was subjected to a moderate sea state while at the station-keeping with the DP controller. The vessel begun the test in position $\eta = [0\ 0\ -30°]$, then the reference setpoint was changed to $\eta = [0\ 0\ +30°]$. The position and attitude reference model was used. The measured heading during the three tests are presented in Figure 6.7, the heading change begins at approximately $t = 20$ seconds.

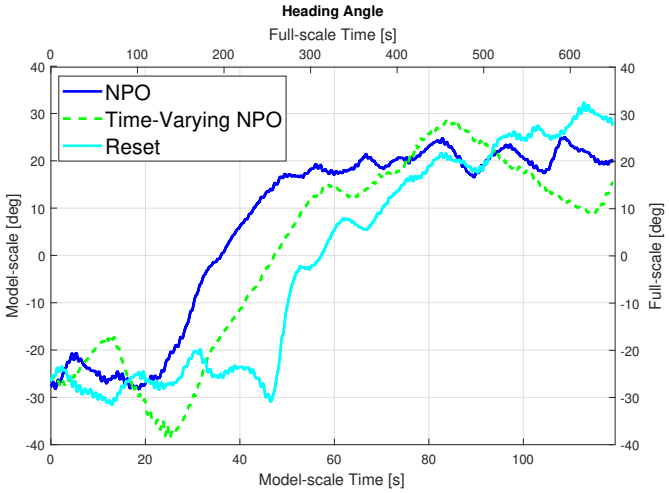

Figure 6.7: Test 4

When the vessel has heading $\pm 30°$ the waves act as head/bow sea, and the vessel is slightly more sensitive than when the waves are purely head sea. This is especially important when tuning the control system. However, the tuning for the moderate head sea was used for this position.

During the test, the time-varying nonlinear passive observer's performance monitoring will switch to the time-varying gains as the performance monitoring depends on the heading reference. This allows for improved performance compared to the regular nonlinear passive observer. However, the resetting accumulates more minor errors than the two formers.

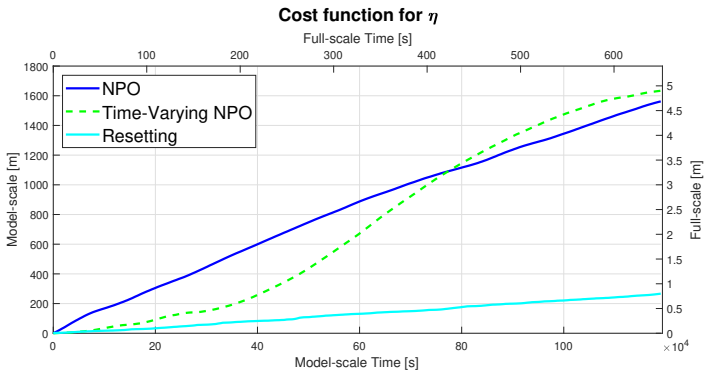

Figure 6.8: Test 4 - Observer Performance

6.5 Result Summary

In order to compare the performance of each observer during the four test scenarios, the position cost function defined in Equation 4.1 was used. The resulting figures are presented in Table 6.1, where the worst performing observer has a score 100, indicated by red cell color. The results are presented in Table 6.1.

Test	NPO	TVNPO	Resetting
1	100	58.29	24.95
2	100	45.67	39.95
3	100	44.79	21.55
4	95.63	100	16.32

Table 6.1: Position cost function values are normalized such that the worst performing has score of 100.

During the laboratory experiments, the resetting observer has overall improved performance. Further, the nonlinear passive observer scores improve performance for all but the fourth test. This means that the performance monitoring for the time-varying nonlinear passive observer enables the time-varying gains resulting in improved performance, except for in the last test where the vessel was subjected to a heading setpoint change enabled by the operator. This was unexpected as this transient occurrence should be detected by the performance monitoring of the time-varying observer and introduce the improved performance.

Chapter 7

Discussion

This chapter presents a discussion of the work conducted in this thesis. Beginning with a discussion about the method of the thesis, the varying sea states implementation for higher fidelity simulations in MCSim is discussed. Then a discussion about each test scenario, comparing the results form simulation and laboratory experiment.

7.1 Simulation Environment

The implementation of a flip flop model to enable varying sea states, in addition, the nested flip flop model presented in section 4.3.1 was successful. It allowed a gradual increase of the environment, increasing the fidelity of the simulation environment. The flip flop model interpolates the output rather than the input. The equation for varying second-order loads were presented in Equation 3.4 and 3.5. Interpolating the input may result in nonphysical wave drift force; hence the interpolating of output is preferred.

During the second simulation, varying wave drift forces are activated while the vessel is station-keeping at $\eta = [0\ 0\ 0]$. The wave drift forces in Figure 5.1 show the two wave drift forces the model flip flops between. In addition, it can be seen that the interpolating of wave drift force allows for a steady increase in sea state without introducing any nonphysical loads.

During the fifth simulation, the nested flip flop model was used. The transfer functions including the wave drift forces increase due to increased surge speed, this can be seen in Figure 5.2. Further, Figure 5.2 shows that the surge speed of the vessel has a significant impact on the wave drift force, and the wave drift force decrease significantly when the surge speed of the vessel decrease. The impact of high surge speed is more significant than the magnitude of the sea state at the end of the simulation. However, increasing the sea state to a more extreme environment or adding a current could be interesting, and result in larger wave drift loads.

7.2 Hybrid Observer

The reference model used in this thesis was the position and attitude reference model and an optimal curve shape reference model, which created adequate reference trajectories. A PID controller was used for the dynamic positioning controller, and a speed-and heading controller used for autopilot. In MCSim, simplified thruster dynamics are present. These has a predefined

saturation limit, which during simulation 2 and 5 was increased significantly in order for the vessel to provide enough propulsion. However, the increased thruster forces may not be realistic, and hence the validity of the actuator control can be questioned.

In the first test scenario the behavior in transient induced by a vessel in surge motion while maneuvering from $\eta_A = [-1\ 0\ 0]$ to $\eta_B = [7\ 0\ 0]$ was investigated. The performance monitoring of the time-varying observer gains was not enabled. This could be expected as the performance monitoring is not designed to react to this transit unless it creates an estimation error exceeding the predefined estimation error bounds. In addition, it would not necessarily have an improved effect with more aggressive gains. However the resetting observer has for the simulation a significantly lower cost function score in for both simulation and experiment, in Table 5.3, 5.4 and 6.1.

The second test was a vessel subjected to varying environmental loads by introducing varying sea states. This was included using the flip-flop model for the simulation, allowing the vessel to be exposed to moderate sea before gradually exposed to more extreme sea. In the laboratory, the Cybership 3 model did not have a waterproof top. To avoid any unfortunate incidents, the waves were at first disabled before the moderate sea state was enabled. In this test, the performance monitoring of the time-varying observer gains was expected to increase if the NPO were unable to estimate satisfactory estimates. The estimate error grew outside the predefined bound, and the time-varying gains were activated quickly, can be seen in Figure 5.5. Hence the nonlinear passive observer could have had more aggressive gains. However, using too aggressive gains can result in unwanted oscillations outside transients. In the laboratory experiment, the same happened, this can be seen in Figure 6.3. The resetting observer mechanism implies a reactive observer, which becomes clear in this test. The resetting observer resets to the true system states, and the result is minor estimation errors. It illustrates the benefit of using this observer, as the need to tune based on sea state is not present.

The third test was a vessel subjected to an unmodeled and sudden push off setpoint. For the simulation case, this was done by applying a force of 50 N in 1 second, this translated to a movement of 1.5 meters in sway direction. At the laboratory, this was done by pushing the vessel 1 meter off set point with a boat stake. As the three pushes in the laboratory were not identical, the results should only be regarded as indication of performance. The results show that the sudden load can not correctly be calculated by the bias load in the nonlinear passive observer, as the bias load is modeled to be a slowly varying load (to resemble environmental loads). Hence the estimation grows beyond the predefined bounds, and the time-varying gains are enabled, which improves the performance. For the resetting observer, this test very much illustrates another benefit. The unmodeled loads are quickly captured, and the true system state is found. Table 5.3, 5.4, and Table 6.1 shows that during both simulation and experiment, the time-varying gains allows improved performance.

For the fourth test the vessel was commanded by operator to make a heading change, as the setpoint changed from $\eta = [0\ 0\ -30°]$ to $\eta = [0\ 0\ 30°]$. During which the position and attitude reference model generated a feasible trajectory for the control system, and the DP controller managed the vessel to follow the trajectory. For the simulation, the time-varying gains were enabled, and improved the position estimates. For the experimental results, the position estimates are not improved with time-varying gains, which was not expected. In Figure A.9 the error over time shows that as the heading change commence, the time-varying gains are activated, however, without improving effect. A reason might be that the tuning is not aggressive enough, and resulting the estimates are oscillating.

During the fifth test, which only was simulated, the vessel was set to sail in increasing sea states following an increase and decrease surge velocity trajectory, as seen in Figure 5.10. Similarly

to sim and test 2, the time-varying gains are working from the beginning, which indicates that the NPO could have had more aggressive gains. As mentioned, the simulation gave satisfactory wave drift forces. Further, the autopilot control system was expanded to use GPS velocity measurements as the vessel reaches higher speeds. Figure 5.11 shows that the two hybrid observers has improved performance compared to the nonlinear passive observer.

During the five simulations the control system and observers had slightly different tuning in the performance monitoring of the time-varying observer altered from test to test. This was done to enable the aggressive gains in the expected transients. For practical reasons, it is simpler for the motion control system to keep one tuning for the observer. While the resetting observer required little altering in the tuning.

Overall, the tests gave an insight to the different transits. The results indicate that there exists hybrid observers for marine surface vessels which by improving performance of the motion control system allows for more reliable behavior.

Further, the resetting observer require knowledge of the turn yaw turn rate in addition to the yaw acceleration to prove UGES. These measurements are often not available. However in Torben [2019] presented in section 3.5.1, and Appendix B UGpAS has been established by introducing a workaround. Hence the papers conclude that there is a desire to further develop the theoretical foundation of the observer. However, most importantly there cannot exists singularities in the jump map, in hybrid terms. The resetting observer has relative simple dynamics to implement and tune. However, the observer model does not include a wave-filter as the nonlinear passive observer does. This means that the measurements needs to be notch filtered before entering the closed-loop.

A ferry operating in the fjords where there is moderate sea but occurrences of strong current could benefit from these hybrid observers. The time-varying observer has a wave filter model which works well, and the nonlinear passive observer is a mature concept which with these time-varying gains can be used in even harsher environments. Hence a platform supply vessel may be demanded to conduct all year operations in more extreme weather. The focus of a offshore operation is safety and precision, while a ferry also needs to ensure safety, it also requires precise estimation.

Chapter 8

Conclusions

This chapter presents the concluding remark of the thesis, major findings, and contributions from the thesis. All evaluated in regards to the model-scaled simulation in the *Marine Cybernetics Simulator* (MCSim) and experiments conducted at the *Marine Cybernetics Laboratory* (MCLab) at the Department of Marine Technology, NTNU.

8.1 Concluding Remarks

The objective of this thesis was to give an overall understanding of today's alternatives to hybrid observers to improve motion control systems during transients due to varying operational conditions, and trough simulation and laboratory experiments the results confirm that the hybrid observers are improving in all transients. Hence, this should be used further in the autonomous motion control system.

This thesis begins with a literature review (chapter 2) to obtain insight into the latest research and projects about autonomous surface vessels, including motivation and background to using hybrid observers and why transients are interesting. The literature review also captures research conducted in the field of hybrid control systems and hybrid observers.

In chapter 3 the derivation of relevant mathematical expression used in the case study of the thesis is presented—mathematical modeling of surface vessels, guidance systems, controllers, hybrid theory, and framework. Last, the two observers' mechanism and hybrid framework are presented.

The thesis objective to investigate hybrid observers' behavior during transients included model-scale simulations and experiments. In chapter 4 the method of the thesis is presented. Beginning with description of the vessel characteristics for Cybership 3 used in this thesis. Then the different test cases were presented (Table 4.1), including what was done and which vessel operational condition would introduce a transient. Followed by the simulation setup in the simulation environment *Marine Cybernetics Simulator* (MCSim) is presented, including the flip flop model allowing for varying sea states. Then the laboratory setup for the *Marine Cybernetics Laboratory* (MCLab) is presented. Finally, the performance evaluation method of the observer is presented.

In chapter 5 and chapter 6 the result to the five simulations and four experiments are presented. Both Chapters end with a summary of the results presented in a table with a score for each observer in each test, and the score is the normalized value of the cost function presented in Equation 4.1. Chapter 7 discussed the results of the flip flop and nested flip flop model used to

enable varying sea states before discussing the results of the simulations and experiments.

Based on the results from simulation 2 and simulation 5, which included different mission objectives, the flip flop and nested flip flop model gave satisfactory performance to varying sea states.

The observers were subjected to transients due to different varying operational conditions. This was done through a comprehensive testing scheme. This gave a suitable range of transients to investigate the motion control system behavior.The hybrid observer can improve the behavior of the motion control system in all transient events in the simulation. During experimental results, the time-varying observer did not improve the behavior of the motion control system in the fourth test, which was changing heading setpoint. Overall hybrid observers improve performance significantly. Both time-varying model-based and resetting are easy to implement.

An advantage of using the time-varying model-based observer is the wave filter, as the resetting requires a notch filter before entering the observer. The resetting is, however, more reactive. Both time-varying nonlinear and resetting observer are highly suitable in the different transients. However, as the resetting is required to have notch filtered signals, this can be difficult to filter when entering high sea states, and the notch filter can filter out the low-frequency motions. Hence, the resetting observer would benefit from ferries in fjords or tug boats that require high reactivity in port where the sea states are lower by quay. While the time-varying model-based observer based on the mature nonlinear passive observer suits well for operations at harsh sea conducting offshore operations which require high precision in all sea states and environments.

8.2 Further Work

- Establish a hybrid framework defined on the varying operational conditions, which can work as a tool for uniting hybrid observer and hybrid control research. This could allow for a more efficient study of the systems and put directly into the application of, e.g., ferries, supply vessels, tugs.
- Combine the motion control perspective to the planning and vessel specification to decide which control system to use based on vessel operational conditions.
- Further investigations for when a ferry or supply vessel can safely switch between estimates and measurements in autopilot.
- In addition, conduct a risk assessment and gain an operational perspective of a ferry or supply vessel. In this way, the transient events can be predicted, and the observer design can be fitted to the vessel.
- Expansion of the MCSim environment for improved thruster simulation for Cybership 3. While subjected to varying sea states, the vessel needs increased thruster force.

Bibliography

FNI Captain David Bray, MNI Captain John Daniels, MNI Captain Glenn Fiander, and MNI Captain Dane Foster. *DP Operator's Handbook*. The Nautical Institute, 3rd edition, 2020.

Astrid H. Brodtkorb, Asgeir J. Sørensen, and Andrew R. Teel. Increasing the operation window for dynamic positioned vessels using the concept of hybrid control. Volume 1A: Offshore Technology, 06 2014. doi: 10.1115/OMAE2014-23601. URL `https://doi.org/10.1115/OMAE2014-23601`.

Astrid H. Brodtkorb, Andrew R. Teel, and Asgeir J. Sørensen. Sensor-based hybrid observer for dynamic positioning. pages 948–953, 2015. doi: 10.1109/CDC.2015.7401995.

Astrid H. Brodtkorb, Andrew R. Teel, and Asgeir J. Sørensen. Hybrid observer combining measurements of different fidelities. *IFAC-PapersOnLine*, 49:506–511, 2016a. doi: https://doi.org/10.1016/j.ifacol.2016.10.486.

Astrid H. Brodtkorb, Svenn A. Værnø, Andrew R. Teel, Asgeir J. Sørensen, and Roger Skjetne. Hybrid observer for improved transient performance of a marine vessel in dynamic positioning. *IFAC-PapersOnLine*, 49:345–350, 2016b. doi: https://doi.org/10.1016/j.ifacol.2016.10.189.

Astrid H. Brodtkorb, Ulrik D. Nielsen, and Asgeir J. Sørensen. Online wave estimation using vessel motion measurements. *IFAC PaperOnlIne*, 51:244–249, 2018a. doi: https://doi.org/10.1016/j.ifacol.2018.09.510.

Astrid H. Brodtkorb, Ulrik D. Nielsen, and Asgeir J. Sørensen. A brute-force spectral approach for wave estimation using measured vessel motions. *Marine Structures*, 60:101–121, 2018b. doi: https://doi.org/10.1016/j.marstruc.2018.03.011.

Astrid H. Brodtkorb, Ulrik D. Nielsen, and Asgeir J. Sørensen. Sea state estimation using vessel response in dynamic positioning. *Applied Ocean Research*, 70:76–86, 2018c. doi: https://doi.org/10.1016/j.apor.2017.09.005.

Astrid H. Brodtkorb, Andrew R. Teel, Asgeir J. Sørensen, and Roger Skjetne. Hybrid controller concept for dynamic positioning of marine vessels with experimental results. *Automatica*, 93: 489–497, 2018d. doi: 10.1016/j.automatica.2018.03.047.

J. Du, X. Hu, H. Liu, and C. L. P. Chen. Adaptive robust output feedback control for a marine dynamic positioning system based on a high-gain observer. *IEEE Transactions on Neural Networks and Learning Systems*, 26(11):2775–2786, 2015. doi: 10.1109/TNNLS.2015.2396044.

Odd M. Faltinsen. *Sea Loads on Ships and Offshore Structures*. Cambridge University Press, 1990.

Daniel de Almeida Fernandes. An output feedback motion control system for rovs: guidance, navigation, and control. *Doctoral thesis at NTNU;2015:122*, 2015.

Thor Inge Fossen. *Handbook of Marine Craft Hydrodynamics ans Motion Control*. John Wiley & Sons, Ltd, 2011.

Rafal Goebel, Richardo G. Sanfelice, and Andrew R. Teel. *Hybrid Dynamical Systems: Modeling, Stability, and Robustness*. Princeton University Press, 2012.

Håvard Fjær Grip, Thor I. Fossen, Tor A. Johansen, and Ali Saberi. Globally exponentially stable attitude and gyro bias estimation with application to gnss/ins integration. *Automatica*, 51:158–166, 2015. doi: https://doi.org/10.1016/j.automatica.2014.10.076.

Marcus Hand. Abu dhabi ports to develop unmanned autonomous tugs with robert allan. URL `https://www.seatrade-maritime.com/technology/abu-dhabi-ports-develop-unmanned-autonomous-tugs-robert-allan`. (accessed: 19.04.2021).

Hassan K. Khalil. *Nonlinear Systems*. Prentice-Hall, 3rd edition, 2002.

Lee Hong Liang. Keppel, abb to bring autonomous tug operation to singapore in 2020. URL `https://www.seatrade-maritime.com/asia/keppel-abb-bring-autonomous-tug-operation-singapore-2020`. (accessed: 19.04.2021).

Dong Nguyen, Asgeir Sørensen, and Ser Quek. Multi-operational controller structure for station keeping and transit operations of marine vessels. *Control Systems Technology, IEEE Transactions on*, 16:491 – 498, 06 2008. doi: 10.1109/TCST.2007.906309.

Trong Dong Nguyen, Asgeir J. Sørensen, and Ser Tong Quek. Design of hybrid controller for dynamic positioning from calm to extreme sea conditions. *Automatica*, 43:768–785, 2007. doi: 10.1016/j.automatica.2006.11.017.

T. Perez, A. J. Sørensen, and M. Blanke. Marine vessel models in changing operational conditions - a tutorial. *IFAC Proceedings Volumes*, 39:309–314, 2006.

Roger Skjetne and Øivind K. Kjerstad. Disturbance rejection by acceleration feedforward for marine surface vessels. *IEEE Access*, 4:2656–2669, 2016. doi: 10.1109/ACCESS.2016.2553719.

Asgeir J. Sørensen. A survey of dynamic positioning control systems. *Annual Reviews in Control*, 35:123–136, 2011. doi: https://doi.org/10.1016/j.arcontrol.2011.03.008.

Asgeir J. Sørensen. *Marine Cybernetics Towards Autonomous Marine Systems and Operations*. Department of Marine Technology, the Norwegian University of Science and Technology (NTNU), Trondheim, Norway, 2018.

Tobias Torben. Control allocation and observer design for autonomous ferries, master thesis, ntnu, trondheim. 2019.

Svenn Are Tutturen and Roger Skjetne. Hybrid control to improve transient response of integral action in dynamic positioning of marine vessels. *IFAC-PapersOnLine*, 48:166–171, 2015. doi: https://doi.org/10.1016/j.ifacol.2015.10.275.

Svenn A. Værnø, Astrid H. Brodtkorb, and Roger Skjetne. Compensation of bias loads in dynamic positioning of marine surface vessels. *Ocean Engineering*, 179:484–492, 2019.

Svenn Are Værnø, Astrid H. Brodtkorb, Roger Skjetne, and Asgeir J. Sørensen. An output feedback controller with improved transient response of marine vessels dynamic positioning. *Proc. IFAC Conf. Control Appl. Marine Syst.*, 49, no. 23:133–138, 2016.

Svenn Are Værnø, Astrid H. Brodtkorb, Roger Skjetne, and Vincezo Calabrò. Time-varying model-based observer for marine surface vessels in dynamic positioning. *IEEE Access*, 5: 14787–14796, 2017. doi: 10.1109/ACCESS.2017.2731998.

Appendix A

Appendix

This appendix contains the principle hull data for Cybership 3, sea state parameters, the different matrices and wave filter used in the nonlinear passive observer. Last two screenshots from Simulink are attached, of the switching mechanism and the weighting mechanisms between two sea states.

A.1 Vessel Parameters for Cybership 3

	Model-scale	Full-scale	
Length over all	2.275	68.26	m
Length between perp.	1.971	59.13	m
Breadth moulded, B_m	0.437	13.11	m
Breadth waterline, B_{wt}	0.437	13.11	m
Draught at $L_{pp}/2$, T	0.153	4.59	m
Draught at fore perpendicular, T_{FP}	0.153	4.59	m
Draught at aft perpendicular, T_{AF}	0.153	4.59	m
Depth to main deck, D	0.203	6.10	m
Mass	85.5	2067300	kg

Table A.1: Principle hull data for Cybership 3 in model-scale and full-scale.

Full-scale	[knots]	0	4	8	12	16
	[m/s]	0	2.0576	4.1152	6.1728	8.2304
Model-scale	[knots]	0	0.7303	1.4606	2.1909	2.9212
	[m/s]	0	0.3757	0.7513	1.1270	1.5027

Table A.2: The five speeds the hydrodynamic calculations were conducted in ShipX, and results further implemented in the MCSim module. Given in full-scale and model-scale.

Thruster Configuration in Laboratory

$$a_1 = 30^\circ \text{ (port)},\ a_2 = -30^\circ \text{ (starboard)}\ a_3 = 90^\circ \text{ (bow)} \tag{A.1}$$

$$l_{1x} = -0.81m,\ l_{2x} = -0.81m,\ l_{3x} = 0.76m \tag{A.2}$$

$$l_{1y} = -0.11m,\ l_{2y} = 0.11m,\ l_{3y} = 0m \tag{A.3}$$

$$T = \begin{bmatrix} cos(a_1) & cos(a_2) & cos(a_3) \\ sin(a_1) & sin(a_2) & sin(a_3) \\ l_{1x}sin(a_1) - l_{1y}cos(a_1) & l_{2x}sin(a_2) - l_{2y}cos(a_2) & l_{3x}sin(a_3) \end{bmatrix} \tag{A.4}$$

$$\tau = Tf \tag{A.5}$$

$$\tag{A.6}$$

Figure 4.2 shows the thruster configuration. Angles are fixed. $\tau \in \mathbb{R}^3$ is the generalized force vector, $f \in \mathbb{R}^3$ are the forces for each thruster, and $T \in \mathbb{R}^{3\times3}$ is the thruster allocation matrix which distributes the forces.

A.2 Observer Matrices

The resetting observer matrices

$$A(t) = \begin{bmatrix} 0_{3x3} & 0_{3x3} & R(t) \\ 0_{3x3} & 0_{3x3} & 0_{3x3} \\ 0_{3x3} & M^{-1}R(t)^T & -M^{-1}D \end{bmatrix},\ B = \begin{bmatrix} 0_{3x3} \\ 0_{3x3} \\ M^{-1} \end{bmatrix},\ C = \begin{bmatrix} I_{3x3} & 0_{3x3} & 0_{3x3} \end{bmatrix} \tag{A.7a}$$

NPO gains:

$$\mathbf{K}_1(\omega_0) = \begin{bmatrix} diag\{\mathbf{K}_{11}(\omega_{01}), \mathbf{K}_{12}(\omega_{02}), \mathbf{K}_{13}(\omega_{03})\} \\ diag\{\mathbf{K}_{14}(\omega_{04}), \mathbf{K}_{15}(\omega_{05}), \mathbf{K}_{16}(\omega_{06})\} \end{bmatrix} \tag{A.8a}$$

$$\mathbf{K}_2 = diag\{\mathbf{K}_{21}, \mathbf{K}_{22}, \mathbf{K}_{23}\} \tag{A.8b}$$

$$\mathbf{K}_3 = diag\{\mathbf{K}_{31}, \mathbf{K}_{32}, \mathbf{K}_{33}\} \tag{A.8c}$$

$$\mathbf{K}_4 = diag\{\mathbf{K}_{41}, \mathbf{K}_{42}, \mathbf{K}_{43}\} \tag{A.8d}$$

$$\mathbf{K}_{1i}(\omega_{0i}) = -2(\zeta_{ni} - \lambda_i)\frac{\omega_{ci}}{\omega_0 i} \tag{A.9a}$$

$$\mathbf{K}_{1(i+3)}(\omega_{0i}) = 2\omega_{0i}(\zeta_{ni} - \lambda_i) \tag{A.9b}$$

$$\mathbf{K}_{2i} = \omega_{ci} \tag{A.9c}$$

Observer system matrices for the time-varying model based observer,

$$A(\psi, t) := \begin{bmatrix} A_w - K_1 C_w & -K_1 & 0 & 0 \\ -K_2 C_w & -K_2 & 0 & r(\psi) \\ -K_3(t)R(\psi)^T C_w & -K_3(t)R(\psi)^T & -T_b^{-1} & 0 \\ -M^{-1}K_4(t)R(\psi)^T C_w & -M^{-1}K_4(t)R(\psi)^T & -M^{-1}R(\psi)^T & -M^{-1}D \end{bmatrix} \tag{A.10}$$

A.3 Additional Results

In the following plots the instants estimate errors for each simulation and test are presented.

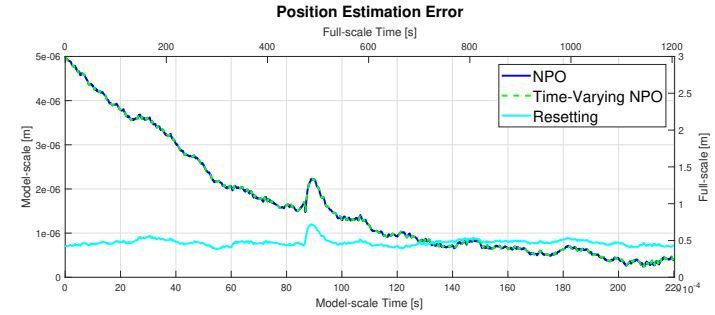

(a)

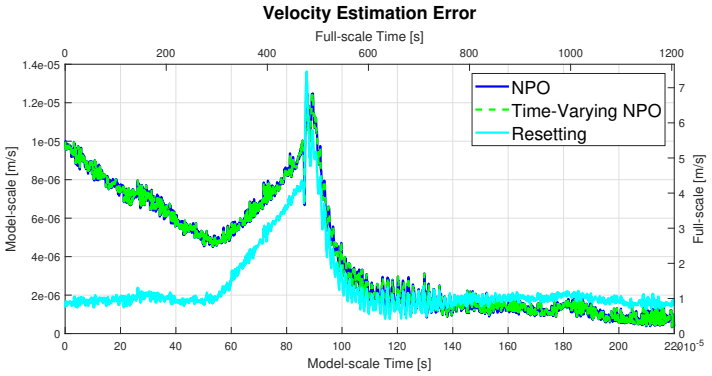

(b)

Figure A.1: Sim 1 - Position and velocity estimation error plot. Vessel sailing from A to B subjected to waves.

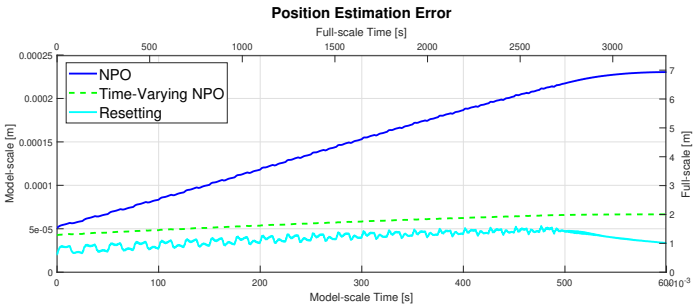

(a)

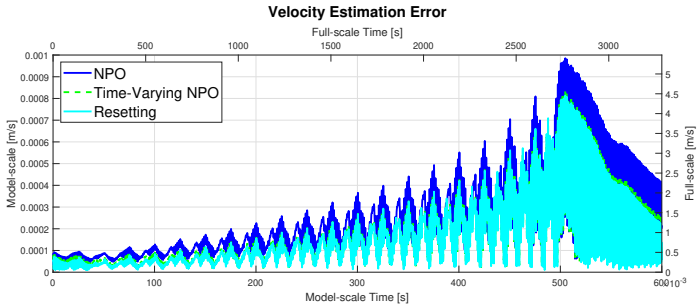

(b)

Figure A.2: Sim 2 - Position and velocity estimation error plot. Vessel at DP subjected to varying sea states.

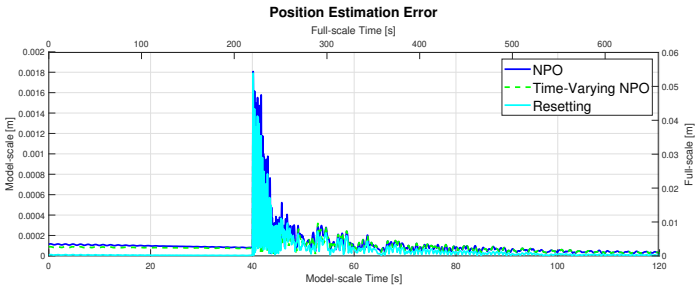

(a)

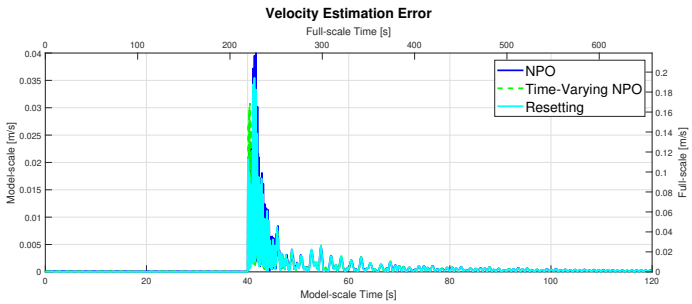

(b)

Figure A.3: Sim 3 - Position and velocity estimation error plot. Vessel at DP subjected to waves pushed off setpoint in sway.

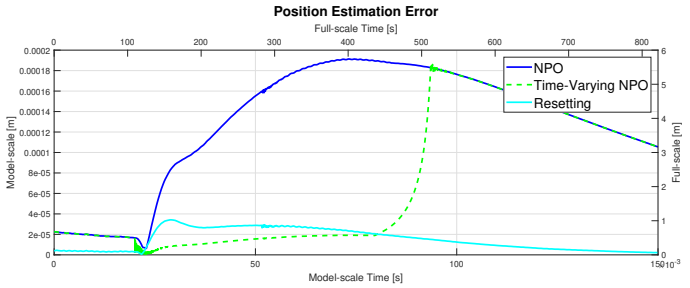

(a)

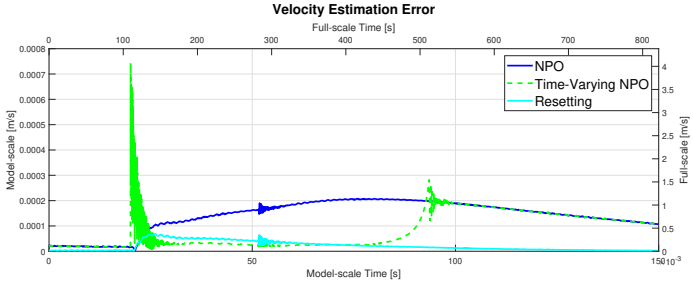

(b)

Figure A.4: Sim 4 - Position and velocity estimation error plot. Vessel at DP subjected to waves with change in heading setpoint.

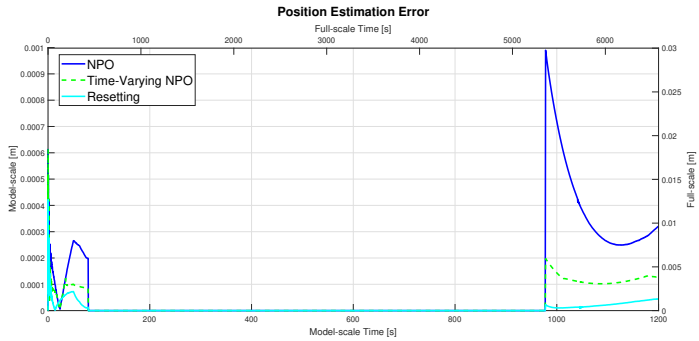

(a)

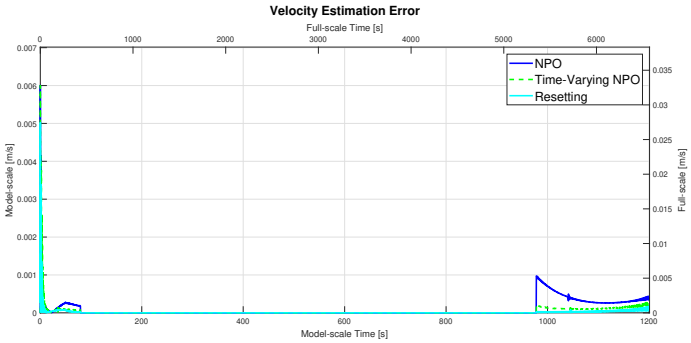

(b)

Figure A.5: Sim 5 - Position and velocity estimation error plot. Vessel subjected to varying sea states in max speed.

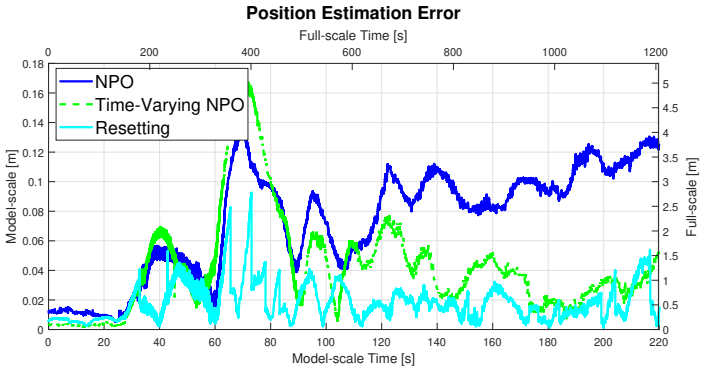

Figure A.6: Test 1 - Position and velocity estimation error plot. Vessel sailing from A to B subjected to waves.

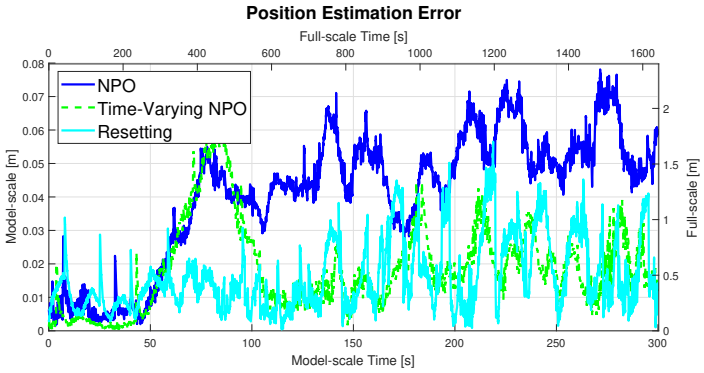

Figure A.7: Test 2 - Position and velocity estimation error plot. Vessel at DP subjected to varying sea states.

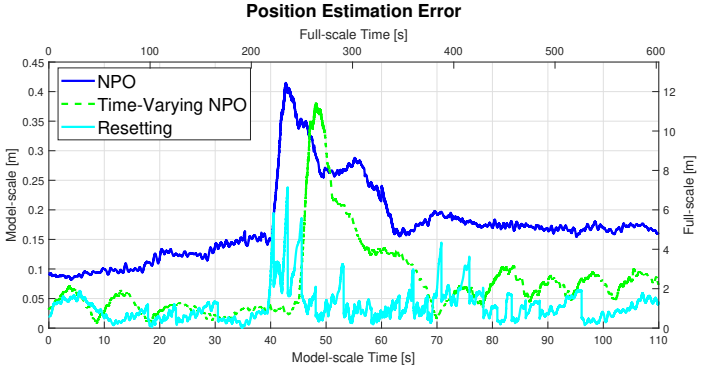

Figure A.8: Test 3 - Position and velocity estimation error plot. Vessel at DP subjected to waves pushed off setpoint in sway.

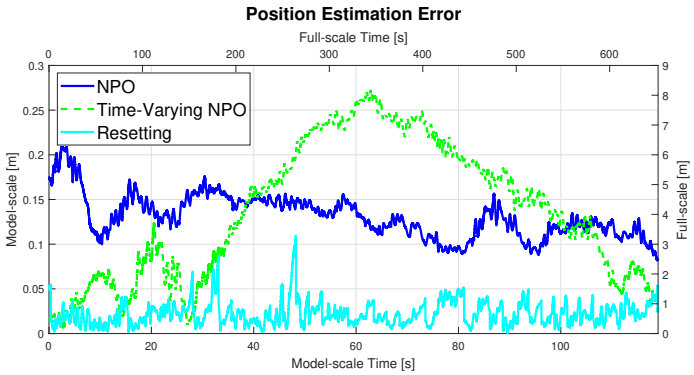

Figure A.9: Test 4 - Position and velocity estimation error plot. Vessel at DP subjected to waves with change in heading setpoint.

Appendix B

Appended Paper

B.1 A resetting observer for LTV systems with application to dynamic positioning of marine surface vessels

A resetting observer for LTV systems with application to dynamic positioning of marine surface vessels*

Tobias R. Torben[1], Øivind K. Kjerstad[3], Emilie H. T. Wittemann[1] and Roger Skjetne[1]

Abstract— **This paper presents a resetting observer for linear time-varying systems. The motivation for this is better handling of unmodelled dynamics and reactiveness to external disturbance without compromising steady-state performance. A reset is triggered if the output estimation error exceeds predefined bounds. The jump map for the reset uses a finite-time observer approach. The finite-time equations are derived for LTV systems, and a method for calculating the state transition matrices online is presented. The observer equations are formulated in a hybrid dynamical systems framework, and sufficient conditions for Uniform Global pre-Asymptotic Stability are given. The method is applied to observer design for dynamic positioning of marine surface vessels. Numerical simulations as well as model scale experiments of this application show promising results, with improved transient performance compared to state-of-the-art continuous-time observers.**

I. Introduction

Observers play a vital role in many control systems. The main objective of an observer is to estimate the states of a system based on limited measurements. Also, an observer may have a signal processing role, where it filters noise and unwanted frequency components before the signal enters the control loop. Dynamic Positioning (DP) of a marine vessel is the process of keeping its position and heading by use of its thrusters. Model-based observers are state-of-the-art in industrial DP systems. These observers are input only position and heading measurements, and estimate position, velocity and a bias load. In addition, a DP observer has a wave filtering function [1]. A challenge for DP observers is to handle unmodelled dynamics and external disturbances in a reactive manner, without using too high injection gains. This has the potential to improve the transient behaviour of the control system and may reduce fuel consumption.

Several applications today call for DP systems able to more rapidly handle changing disturbances and transients. Examples include DP in ice, anchor handling operations, subsea pipe laying and DP gangway solutions. In recent years, several observers and controllers to improve the transient DP performance have been proposed. An effective approach is to use velocity measurements in the observer. However, high-quality velocity measurements are not always available. The most common source of velocity measurement is the course and speed over ground from a GNSS receiver. These often give poor velocity measurements at low speed. Other approaches are implemented purely in software, and thus avoid the installation of expensive additional sensors. Examples include using time-varying observer gains [2], acceleration feedforward [3], switching between a model-based and a signal-based observer [4], and a resetting observer [5]. The latter has inspired our approach.

The method of *Finite-time observers* looks promising for calculating the estimated state after a reset. The concept is that for an observable linear time-invariant (LTI) system, two Luenberger observers can be designed. By comparing the outputs of these observers after some time, the exact system state can be calculated. Finite-time observers first appeared in the literature in [6]. Here, a continuous-time observer for an LTI system was developed using time-delays. Later, [7] designed a finite-time observer for LTI systems that jumps the state estimate repeatedly after a fixed time interval.

In this paper, we examine a hybrid observer design with a resetting mechanism, where we enforce a jump in the state estimates if the estimation error exceeds a predefined bound. This resetting mechanism is illustrated in Figure 1. To calculate the new state estimates after a jump, a finite-time observer approach is used. The finite-time approach is extended to cover linear time-varying (LTV) systems, and an observer for a generic LTV system is developed. We then show how this observer can be applied for DP. To the authors best knowledge, no such observer has been developed before.

The paper is outlined as follows. First, some mathematical preliminaries are given in Section II. The concept is then motivated and illustrated for a simple SISO system in Section III. The problem formulation is presented in Section IV-A. In Section IV, the novel observer design is developed and its stability is analyzed. In Section V the resetting observer is applied to a DP system and results from numerical simulations and model scale experiments are given. The results are discussed in Section VI, before concluding remarks are given in Section VII.

II. Preliminaries

A. Notation

In this paper, $\|\cdot\|$ denotes the Euclidean vector norm, and $|\cdot|$ denotes the scalar absolute value. $\|x\|_{\mathcal{A}}$ denotes the distance

*This work was supported by the Research Council of Norway through the Centres of Excellence funding scheme, project number 223254 - NTNU AMOS, and the KPN ORCAS project, project number 280655.

[1]Centre for Autonomous Marine Operations (NTNU AMOS), Department of Marine Technology, Norwegian University of Science and Technology (NTNU), Otto Nielsens vei 10, 7052 Trondheim, Norway (tobias.torben, roger.skjetne)@ntnu.no

[3]Kongsberg Maritime, Rasmus Rønnebergs gate 21, 6002, Ålesund, Norway oivind.kjerstad@km.kongsberg.com

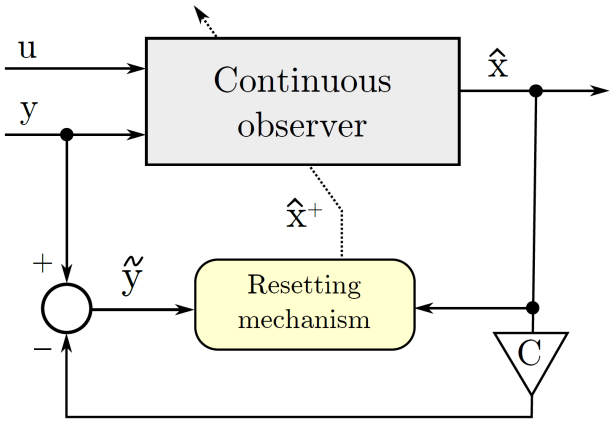

Fig. 1. The resetting mechanism concept.

from the vector x to the set $\mathcal{A}$, that is, $\|x\|_{\mathcal{A}} := \inf_{y\in\mathcal{A}} \|x-y\|$. Set-valued mappings are denoted by double arrows, for instance, $M : A \rightrightarrows B$ denotes a mapping M which maps values in A to subsets of B. The domain of a mapping is denoted $dom(\cdot)$. ∇f denotes the gradient vector of the scalar function f. Dot products are denoted by bracket notation: $\langle\cdot,\cdot\rangle$. The Cartesian product of A and B is denoted $A \times B$. $\lfloor\cdot\rfloor$ is the floor operator.

B. Linear time-varying systems

We consider LTV systems of the form

$$\dot{z} = A(t)z + B(t)u(t) + \Lambda(t)d(t) \tag{1}$$

$$y = C(t)z \tag{2}$$

with state $z \in \mathbb{R}^n$, output $y \in \mathbb{R}^p$, input $u(t) \in \mathbb{R}^m$, and disturbance $d(t) \in \mathbb{R}^q$. $u(t)$, $d(t)$, and the matrices $A(t) \in \mathbb{R}^{n\times n}$, $B(t) \in \mathbb{R}^{n\times m}$, $C(t) \in \mathbb{R}^{p\times n}$, and $\Lambda(t) \in \mathbb{R}^{n\times q}$ are piecewise continuous and bounded functions. $(A(t), C(t))$ form an observable pair for each time $t \in [0,\infty)$. Under these conditions, a unique solution to (1)-(2) exists and is bounded for all time [8].

We introduce an important stability result for LTV systems, which will be used in the stability analysis in Section IV-F. This theorem guarantees the existence of a quadratic, time-varying Lyapunov function for Uniformly Globally Exponentially Stable (UGES) LTV systems.

Theorem 1: Existence of a Quadratic Lyapunov function for UGES LTV systems ([9] Theorem 4.12)
Let $x = 0$ be the exponentially stable equilibrium point of $\dot{x} = A(t)x$. Suppose $A(t)$ is continuous and bounded. Let $Q(t)$ be a continuous, bounded, positive definite, symmetric matrix. Then, there is a continuously differentiable, positive definite, symmetric matrix $P(t)$ that satisfies

$$-\dot{P}(t) = P(t)A(t) + A^\top(t)P(t) + Q(t)$$

Hence, $V(x,t) = x^\top P(t)x$ is a Lyapunov function for the system that satisfies

$$k_1\|x\|_2^2 \le V(x,t) \le k_2\|x\|_2^2$$

and

$$\dot{V}(x,t) = \frac{\partial V}{\partial t} + \frac{\partial V}{\partial x}A(t)$$
$$= x^\top[\dot{P}(t) + P(t)A(t) + A^\top(t)P(t)]x$$
$$= -x^\top Q(t)x \le -k_3\|x\|_2^2$$

where k_1, k_2, and k_3 are positive constants.

C. Hybrid dynamical systems

To formulate the resetting observer equations and do a formal analysis, the *hybrid dynamical systems* framework of [10] is used. Only the main concepts and the results needed in our analysis is presented here. The reader is referred to [10] and references therein for further details.

In this framework, a hybrid dynamical system, $\mathcal{H} = (C, F, D, G)$, is modelled as a *constrained differential inclusion* and a *constrained difference inclusion*:

$$x \in C \quad \dot{x} \in F(x) \tag{3a}$$

$$x \in D \quad x^+ \in G(x) \tag{3b}$$

When the state x is in the *flow set* C, it *flows* according to the *set-valued mapping* $\dot{x} = f(x)$ for some $f \in F$. When x is in the *jump set* D, it *jumps* according to set-valued mapping $x^+ = g(x)$ for some $g \in G$. x^+ denotes the value of x after a jump. Solutions to hybrid systems are denoted $\phi(t,j)$, where $t \in \mathbb{R}_{\ge 0}$ is continuous time and $j \in \mathbb{N}$ is discrete time.

A special class of hybrid systems are *well-posed hybrid systems*. For these systems there exists an extensive toolbox of stability and robustness results. Sufficient conditions for $\mathcal{H} = (C, F, D, G)$ to be well-posed are provided by the *Hybrid Basic Conditions* ([10], Assumption 6.5):

- C and D are closed subsets of $\mathbb{R}^n$.
- $F : \mathbb{R}^n \rightrightarrows \mathbb{R}^n$ is outer semicontinuous and locally bounded relative to C, $C \subset dom(F)$, and $F(x)$ is a convex set for every $x \in C$.
- $G : \mathbb{R}^n \rightrightarrows \mathbb{R}^n$ is outer semicontinuous and locally bounded relative to D, and $D \subset dom(G)$.

Next, a hybrid Lyapunov theorem, which gives sufficient conditions for uniform global pre-asymptoptic stability (UGpAS) of a closed set, is stated. The theorem is a relaxed version of [10] Theorem 3.18, where it allows non-decrease in the Lyapunov function during jumps if the duration of flow is sufficiently large.

Theorem 2: Sufficient Lyapunov Conditions; Persistent Flowing ([10] Proposition 3.27)
Let $\mathcal{H} = (C, F, D, G)$ be a hybrid system and let $\mathcal{A} \subset \mathbb{R}^n$ be closed. Suppose V is a Lyapunov function candidate for $\mathcal{H}$ and there exist $\alpha_1, \alpha_2 \in \mathcal{K}_\infty$ and a continuous $\rho \in \mathcal{PD}$ such that

$$\alpha_1(\|x\|_{\mathcal{A}}) \le V(x) \le \alpha_2(\|x\|_{\mathcal{A}}) \quad \forall x \in C\cup D\cup G(D) \tag{4a}$$

$$\langle\nabla V(x), f\rangle \le -\rho(\|x\|_{\mathcal{A}}) \quad \forall x \in C, f \in F(x) \tag{4b}$$

$$V(g) - V(x) \leq 0 \quad \forall x \in D, g \in G(x) \tag{4c}$$

If, for each $r > 0$, there exists $\gamma_r \in \mathcal{K}_\infty$, $N_r > 0$ such that for every solution ϕ to $\mathcal{H}$, $\|\phi(0,0)\|_{\mathcal{A}} \in (0, r]$, $(t, j) \in dom(\phi)$, $t + j \geq T$ imply $t \geq \gamma_r - N_r$, then $\mathcal{A}$ is uniformly globally pre-asymptotically stable for $\mathcal{H}$.
The term of *pre-asymptotic* as opposed to asympotic stability and *pre-attraction* as opposed to attraction indicates the possibility of a maximal solution that is not complete.

For systems satisfying the hybrid basic conditions, UGpAS also implies robust UGpAS. This ensures that vanishing perturbations do not dramatically change the behaviour of solutions.

III. Motivating example

Consider an LTI SISO mass-damper-spring system subject to an unknown disturbance. This can be modelled by the following set of ODEs

$$m\ddot{p} + c\dot{p} + kp = b \tag{5}$$

$$\dot{b} = d(t) \tag{6}$$

$$y = p, \tag{7}$$

where p is the position, and b is a force bias to be estimated. This is excited by an unknown disturbance $d(t)$. Suppose $d(t)$ is approximately zero most of the time, but now and then it experiences an impulse that jumps the bias b to a new value. The output of the system is y, while m, c, and k are the mass, damping coefficient, and spring stiffness of the system.

Let $z = [p, \dot{p}, b]^\top$. The system can be written on state-space form according to (1)-(2) as

$$\dot{z} = Az + \Lambda d(t) \tag{8}$$

$$y = Cz, \tag{9}$$

where $A \in \mathbb{R}^{3\times3}$, $\Lambda \in \mathbb{R}^{3\times1}$, and $C \in \mathbb{R}^{3\times1}$. To estimate the system state z, a Luenberger observer can be designed by copying the nominal dynamics of the system (assuming $d(t) = 0$ so that b is constant), and injecting the measurements. Consider first a continuous-time observer with state estimate $z_c \in \mathbb{R}^3$,

$$\dot{z_c} = Az_c + L_c(y - Cz_c) \tag{10}$$

where $L_c \in \mathbb{R}^{3\times1}$ is the injection gain matrix.

A challenge with such an observer for transient performance is that it must typically be tuned in a relaxed manner to avoid measurement noise to propagate into the state estimates. Hence, it becomes less reactive to unknown disturbances. In our work, we present an approach to improve on this.

Suppose we design two Luenberger observers, with state estimates $z_i, i \in \{1, 2\}$, according to

$$\dot{z_i} = Az_i + L_i(y - Cz_i) \tag{11}$$

where the injection gains for z_1 are tuned in the normal relaxed manner, while the injection gains for z_2 are tuned more aggressively. As the developments of Section IV will show, we can use the information of both z_1 and z_2 to calculate the true system state z, given the nominal assumption $d(t) = 0$. By using the relaxed state estimate, z_1, during steady conditions and resetting to the true system state if the output estimation error grows, such that $|Cz_1 - y| > \epsilon$, we obtain reactivity to the unknown disturbances while still preserving noise-filtered state estimates.

Let $e_i := z - z_i, i \in \{1, 2\}$, so that $\dot{e} = A_i e_i$ where $A_i := A - L_i C$. In the interval $t \in [t_0, t_1]$, where $t_1 - t_0 = \delta$, it follows that the solution becomes $e_i(t_1) = \exp(A_i\delta)e_i(t_0)$ or

$$z(t_1) - z_i(t_1) = \exp(A_i\delta)(z(t_0) - z_1(t_0)). \tag{12}$$

Using both z_1 and z_2, it follows from the development in Section IV that we can calculate

$$z(t_1) = \Psi(t_0, t_1) \begin{bmatrix} z_1(t_1) \\ z_2(t_1) \end{bmatrix}, \tag{13}$$

where

$$\Psi(\delta) = ((I - \exp(A_2\delta))\exp(-A_1\delta))^{-1} \cdot \\ [-\exp(A_2\delta)\exp(-A_1\delta) \quad I] \in \mathbb{R}^{3\times6} \tag{14}$$

Let $x = (z, z_1, z_2, \zeta) \in \mathbb{Q} \times \mathbb{R}^3 \times \mathbb{R}^3 \times \mathbb{R}_{\geq0}$, where Q is a compact subset of $\mathbb{R}^3$. We propose the following hybrid observer, $\mathcal{H} = (C, f, D, g)$ for our mass-damper-spring system

$$\dot{x} = f(x) = \begin{bmatrix} Az \\ A_1z_1 + (A - A_1)z \\ A_2z_2 + (A - A_2)z \\ 1 \end{bmatrix} \tag{15}$$

$$x^+ = g(x) = \begin{bmatrix} z \\ H(x) \\ H(x) \\ 0 \end{bmatrix} \tag{16}$$

where

$$H(x) = \begin{cases} z_1 & \text{if} \quad |Cz_1 - y| \leq \epsilon \\ \Psi(\delta) \begin{bmatrix} z_1 \\ z_2 \end{bmatrix} & \text{if} \quad |Cz_1 - y| > \epsilon \end{cases}$$

The flow set is $C = \mathbb{Q} \times \mathbb{R}^3 \times \mathbb{R}^3 \times [0, \delta]$ and the jump set is $D = \mathbb{Q} \times \mathbb{R}^3 \times \mathbb{R}^3 \times \delta$, where $\delta > 0$ is the reset interval.

In the simulations, $m = c = k = 1.0$, $L_1 = L_c = [0.3, 0.3, 0.3]^\top$, and $L_2 = [1.0, 1.0, 1.0]^\top$. We use $\delta = 2.0$ and $\epsilon = 0.1$, that is, every δ time units, it is checked if

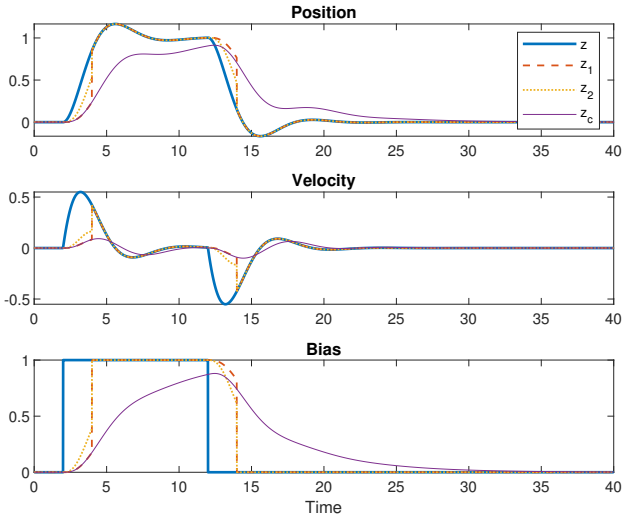

Fig. 2. Simulation results mass-damper-spring system.

$|Cz_1 - y| > \epsilon$. If this is the case, z_1 and z_2 are reset to the true system state, as calculated by (13). If not, the observers are synchronized, that is, z_2 is reset to the value of z_1.

Figure 2 shows the simulation results for the mass-damper-spring system when subject to a disturbance resulting in a 10 seconds square pulse on the bias b. The results show that the disturbance causes all estimation errors to grow. However, the resetting observer quickly reacts and resets the state to the correct values. The continuous-time observer on the other hand, captures the transient response from the disturbance too slowly, resulting in inaccurate state estimates both during the disturbance and for a long period after the disturbance has terminated.

This example also illustrates another important feature of the resetting observer. The system is subject to a severe unmodelled disturbance. However, since we have included a bias state to capture this as a type of integral action, this disturbance is accurately estimated by the resetting mechanism. The observer thus still produces good state estimates under the influence of the disturbance.

IV. Resetting observer design

A. Problem statement

Consider an LTV system of the form given in (1)-(2). The objective for this paper is to calculate a state estimate $\hat{z}$, knowing the input $u(t)$, and given measurements of the output y. It is assumed nominally that the disturbance $d(t) = 0$. The rationale behind this is that slowly varying disturbances are handled adequately by the measurement innovation in the observer, whereas the effect of rapidly changing disturbances can be considered as an initial estimation error to be handled by a resetting observer mechanism. The control design model (CDM) is thus reduced to

$$\dot{z} = A(t)z + B(t)u \tag{17}$$

$$y = C(t)z \tag{18}$$

We shall first derive how an exact state estimate for an LTV system can be obtained from two Luenberger observers, and then we propose how to use this in a hybrid resetting observer.

B. Finite-time observer equations for LTV systems

Consider two Luenberger observers for (17)-(18) with state estimates $z_i, i \in \{1, 2\}$, and dynamics

$$\dot{z}_i = A(t)z_i + B(t)u + L_i(t)(y - C(t)z_i), \tag{19}$$

where $L_i(t) \in \mathbb{R}^{n\times p}$ is a piecewise continuous and bounded injection gain matrix. Define $A_i(t) := A(t) - L_i(t)C(t)$ and the error variables $e_i := z - z_i$, and let $L_i(t)$ be chosen such that the origin is Uniformly Globally Exponentially Stable (UGES) for the error dynamics

$$\dot{e}_i = \dot{z} - \dot{z}_i = A_i(t)e_i \tag{20}$$

for $i \in \{1, 2\}$.

The solutions for these systems can be expressed in terms of the state transition matrix Φ_i [8], according to

$$e_i(t) = \Phi_i(t, t_0)e(t_0). \tag{21}$$

We seek to calculate the true system state, z, at times $t_{k+1} > t_k > ... > t_0 \geq 0$ to enable the observer to reset the state estimates to z. At the start of each interval $[t_k, t_{k+1}]$, the two observers are initialized with the same state values, that is, $z_1(t_k) = z_2(t_k)$. The initial estimation error, $e(t_k)$ is thus equal for both observers, which implies that (21) can be used to set up two vectorial equations with two unknowns, $e(t_k)$ and $z(t_{k+1})$,

$$\Phi_1(t_{k+1}, t_k)e(t_k) = z(t_{k+1}) - z_1(t_{k+1}) \tag{22}$$

$$\Phi_2(t_{k+1}, t_k)e(t_k) = z(t_{k+1}) - z_2(t_{k+1}). \tag{23}$$

Solving (22) for $e(t_k)$ yields

$$e(t_k) = \Phi_1^{-1}(t_{k+1}, t_k)(z(t_{k+1}) - z_1(t_{k+1})). \tag{24}$$

Inserting this into (23) and solving for the true system state, $z(t_{k+1})$ then yields

$$z(t_{k+1}) = (I - \Phi_2(t_k, t_{k+1})\Phi_1^{-1}(t_k, t_{k+1}))^{-1} \tag{25}$$
$$\begin{bmatrix} -\Phi_2(t_k, t_{k+1})\Phi_1^{-1}(t_k, t_{k+1}) & I \end{bmatrix} \begin{bmatrix} z_1(t_{k+1}) \\ z_2(t_{k+1}) \end{bmatrix}.$$

Hence, if $\Phi_1(t_k, t_{k+1})$ and $I - \Phi_2(t_k, t_{k+1})\Phi_1^{-1}(t_k, t_{k+1})$ are invertible matrices, the true system state can be calculated in terms of $z_1(t_{k+1})$ and $z_2(t_{k+1})$. This value can be used to update the state estimates.

C. Calculating the state transition matrices

The previous section shows that we need to know the value of the state transition matrices, $\Phi_1(t_{k+1}, t_k)$ and $\Phi_2(t_{k+1}, t_k)$, to calculate the true system state at a reset. For a generic LTV system, a closed-form expression of the state transition matrix rarely exists. Also, if the time-dependence is driven by an external signal, this may not be known in advance. Here, we show how the numerical state transition matrix can be calculated recursively in an observer.

Consider a generic LTV system

$$\dot{x} = F(t)x \tag{26}$$

which satisfies the conditions of Section II-B. Its response is given by

$$x(t) = \Phi(t, t_0)x(t_0), \quad t \geq t_0 \geq 0, \tag{27}$$

where $\Phi(t, t_0)$ is a state transition matrix.
Differentiating both sides of (27) with respect to time yields

$$\dot{x}(t) = F(t)x(t) = F(t)\Phi(t, t_0)x(t_0) = \dot{\Phi}(t, t_0)x(t_0). \tag{28}$$

Hence, the state transition matrix is governed by the differential equation

$$\dot{\Phi}(t, t_0) = F(t)\Phi(t, t_0). \tag{29}$$

Also, $\Phi(t_0, t_0) = I$, where $I \in \mathbb{R}^{n\times n}$ is the identity matrix. Therefore, the value of $\Phi(t, t_0)$ can be calculated online by integrating (29) with initial condition $\Phi(t_0, t_0) = I$.

D. Design considerations

In the resetting observer, the state estimate z_1 is used as an output of the observer during flows. z_2 is only included to accommodate a state reset if the output estimation error exceeds its bounds. A_1 should therefore be tuned in the normal relaxed manner, to avoid measurement noise to propagate into the state estimates. A_2 should be tuned to achieve an acceptable condition number of the matrix $I - \Phi_2(t_k, t_{k+1})\Phi_1^{-1}(t_k, t_{k+1})$. Because a non-aggressive observer is used during steady-state conditions, and a jump is triggered only in the transient of a disturbance, this design gives the observer a "low gain - high reactivity" property, which is our aim.

A jump is triggered only if the output estimation error exceeds predefined bounds. Define the bounds $\epsilon \in \mathbb{R}^p_{>0}$. A jump should be triggered if $|(y - C(t)z_1)_i| \geq \epsilon_i$ for some $i \in \{1, 2, ..., p\}$. The ϵ bounds should be chosen such that measurement noise can not trigger a jump.

Ideally, we would like to reset the state estimate at the instant where the output estimation error $|(y - C(t)z_1)|$ exceeds its bounds. However, in a practical implementation, there needs to be stricter control on the timing of the jumps. The determinant of $(I - \Phi_2(t_k, t_{k+1})\Phi_1^{-1}(t_k, t_{k+1}))$ will tend to zero as $t \to 0$, which gives numerical issues when calculating its inverse. This is not surprising, as the two Luenberger observers must run for some time for us to extract information about the true system state from them. Because of this, two consecutive jumps must be separated by some dwell-time. Also, the integral for the state transition matrices of (29) should be reset if the system flows for a long period of time. (25) includes the term $\Phi_1^{-1}(t_{k+1}, t_k)$. Inverting a state transition matrix results in solving the LTV system backwards in time. Since $\dot{z_1} = A_1 z$ is UGES, this inverse will therefore grow exponentially in time. This would be problematic for implementation in a digital computer, if the observer was allowed to flow for large time intervals. Also, modelling errors and measurement noise may cause drift in the state transition matrices if they are integrated over long time periods.

To control the timing of the jumps, we propose to always reset the state transition integrals after a constant time interval. That is, they are reset at times $t_{k+1} > t_k > ... > t_0 \geq 0$. The state transition matrices are reset to identity and z_2 is reset to the value of z_1, to ensure that the two observers are initialized with the same estimation error. A jump in the output estimate, z_1, is triggered only if $|(y - C(t)z_1)_i| \geq \epsilon_i$ for some $i \in \{1, 2, ..., p\}$. If not, z_1 is kept unchanged after the reset. This resetting mechanism comes at the cost of slightly lower reactivity, as we need to wait until the end of an interval, $[t_k, t_{k+1}]$, before a reset can occur. Also, conditions that ensure non-singularity of $(I - \Phi_2(t_k, t_{k+1})\Phi_1^{-1}(t_k, t_{k+1}))$ for all times are not established for generic LTV systems. To ensure that the true system state can be calculated after a jump, we propose to only jump if the determinant of $(I - \Phi_2(t_k, t_{k+1})\Phi_1^{-1}(t_k, t_{k+1}))$ is sufficiently large. This is discussed further in Section VI.

Finally, experience has shown that resetting to the true system state may cause overshooting behaviour after a reset. Also, in high noise conditions, the value calculated (25) may be inaccurate. To address this, we propose to add a linear interpolation to the jump map. That is, instead of jumping directly to the z value dictated by (25), the system jumps to $kz + (1 - k)z_1$, where $k \in [0, 1]$ is tunable scalar.

E. Hybrid observer equations

We are now ready to state the hybrid observer equations for the resetting observer using the hybrid dynamical systems framework introduced in Section II-C.

The state of the hybrid system is defined as

$$\begin{aligned} x &= (z, z_1, z_2, \Phi_1, \Phi_2, \zeta, \tau) \\ &\in \mathbb{Q} \times \mathbb{R}^n \times \mathbb{R}^n \times M \times M \times \mathbb{R}_{\geq 0} \times \mathbb{R}_{\geq 0} \end{aligned} \tag{30}$$

where z is the true system state, which is assumed to live in a compact set $Q \subset \mathbb{R}^n$, z_1 and z_2 are the Luenberger state estimates, and Φ_1 and Φ_2 are the state transition

matrices. The latter are governed by (29), and will thus have no finite escape times. Also, since they are periodically reset to identity, these matrices will live in a compact set $M \subset \mathbb{R}^{n\times n}$. ζ and τ are scalar timer and time variables.

Following the developments of Section IV, the flow map and jump map may be expressed as

$$\dot{x} = f(x) = \begin{bmatrix} A(\tau)z + B(\tau)u \\ A_1(\tau)z_1 + B(\tau)u + (A(\tau) - A_1(\tau))z \\ A_2(\tau)z_2 + B(\tau)u + (A(\tau) - A_2(\tau))z \\ A_1(\tau)\Phi_1 \\ A_2(\tau)\Phi_2 \\ 1 \\ 1 \end{bmatrix} \tag{31}$$

$$x^+ = g(x) = \begin{bmatrix} z \\ H(x) \\ H(x) \\ I \\ I \\ 0 \\ \tau \end{bmatrix}, \tag{32}$$

where

$$H(x) = \begin{cases} z_1 & \text{if} \quad |Cz_1 - y|_i \leq \epsilon_i \\ k\Psi(x)\begin{bmatrix} z_1 \\ z_2 \end{bmatrix} + (1-k)z_1 & \text{if} \quad |Cz_1 - y|_i > \epsilon_i \end{cases}$$

for $i \in \{1, 2, ..., p\}$. $\Psi(x) \in \mathbb{R}^{n\times 2n}$ is defined as

$$\Psi(x) = (I - \Phi_2\Phi_1^{-1})^{-1}\begin{bmatrix} -\Phi_2\Phi_1^{-1} & I \end{bmatrix}$$

.

The flow set is defined as

$$C = Q \times \mathbb{R}^n \times \mathbb{R}^n \times M \times M \times [0, \delta] \times \mathbb{R}_{\geq 0}, \tag{33}$$

and the jump set is defined as

$$D = Q \times \mathbb{R}^n \times \mathbb{R}^n \times M \times M \times \delta \times \mathbb{R}_{\geq 0}. \tag{34}$$

Together, this completely defines a hybrid system $\mathcal{H} = (C, f, D, g)$. The stability of the observer is adressed in Section IV-F.

F. Formal stability analysis

The resetting observer of (31)-(34) contains a conditional in the jump map. This results in a jump map that is not outer semicontinuous, and therefore a hybrid system that does not satisfy the hybrid basic conditions. We define a generalized hybrid system $\mathcal{H}' = (C, f, D, G)$ where the jump map of $\mathcal{H}$ is replaced by the set-valued mapping

$$x^+ \in G(x) = \begin{bmatrix} z \\ \{k\Psi(x)\begin{bmatrix} z_1 \\ z_2 \end{bmatrix} + (1-k)z_1, z_1\} \\ \{k\Psi(x)\begin{bmatrix} z_1 \\ z_2 \end{bmatrix} + (1-k)z_1, z_1\} \\ I \\ I \\ 0 \\ \tau \end{bmatrix}. \tag{35}$$

$G(x)$ allows both jumping to z_1 and $k\Psi(x)\begin{bmatrix} z_1 \\ z_2 \end{bmatrix} + (1-k)z_1$ at each jump. All solutions of $\mathcal{H}$ is thus contained in the set of solutions of $\mathcal{H}'$. UGpAS of $\mathcal{H}$ therefore follows from UGpAS of $\mathcal{H}'$. We begin by showing that $\mathcal{H}'$ satisfies the hybrid basic conditions.

First we note that C and D are closed sets. f is locally bounded, outer semicontinuous and has convex values for every $x \in C$ by virtue of being a singleton set-valued mapping containing only a continuous function. Similarly $G(x)$ is locally bounded and outer semicontinuous for every $x \in D$. Continuity of $\Psi(x)$ follows from the fact that the matrix inverse is a continuous function for non-singular matrices, and that continuity is conserved through products, sums and compositions with other continuous functions. This shows that the system of (31)-(32) satisfies all the hybrid basic conditions and, therefore, constitutes a well-posed hybrid system.

The following stability result shows that the state estimate z_1 converges asymptotically to the true state, z, given the assumptions made this far.

Theorem 3: The set $\mathcal{A} = \{Q \times \mathbb{R}^n \times \mathbb{R}^n \times M \times M \times [0, \delta] \times \mathbb{R}_{\geq 0} : z = z_1\}$ is UGpAS for the hybrid system $\mathcal{H}'$.

Proof:

First we note that $\|x\|_{\mathcal{A}} = \|z - z_1\| := \|e\|$ since z_2, Φ_1, Φ_2, ζ, and τ are always in $\mathcal{A}$, by construction.

We also note that the time-dependence of the LTV system can be replaced by a dependence on the timer state, τ, in the hybrid system. We can thus analyze stability of a non-compact set for a time-invariant hybrid system using Theorem 2. Forward completeness is guaranteed by the conditions on $u(t)$, $A(t)$, $B(t)$, $C(t)$, $L_1(t)$ and $L_2(t)$ given in Section II-B.

For continuous-time UGAS (or equivalently UGES) LTV systems, there always exists a quadratic, time-dependent Lyapunov function which is bounded by two Class K_∞ functions and whose time derivative is bounded by a negative definite function, as stated in Theorem 1. Since $\|x\|_{\mathcal{A}} = \|e\|$, we can choose $V(x) = e^\top P(\tau)e$ and have conditions (4a) and (4b) satisfied.

Next, we show that the quadratic Lyapunov function does not increase during jumps. We have that

$$e^+ = e$$

or

$$e^+ = z^+ - z_1^+ = z - (k\Psi(x)\begin{bmatrix} z_1 \\ z_2 \end{bmatrix} + (1-k)z_1)$$

In the first case, $V(x^+) - V(x) = 0$, and (4c) is satisfied. In the second case, we have that $\Psi(x)\begin{bmatrix} z_1 \\ z_2 \end{bmatrix} = z$, as shown in Section IV-B. It follows that

$$e^+ = z - (z_1 + k(z - z_1)) = (1-k)e$$

.

The value of the Lyapunov function after a jump then becomes

$$\begin{aligned} V(x^+) &= (e^+)^\top P(\tau)e^+ = ((1-k)e)^\top P(\tau)((1-k)e) \\ &= (1-k)^2 e^\top P(\tau)e = (1-k)^2 V(x) \leq V(x) \end{aligned}$$

since $k \in [0, 1]$.
Hence, the condition of (4c) is also satisfied.
What remains to show is that the duration of flow is sufficiently large to compensate for the potential non-decrease in the Lyapunov function during jumps.

Since a jump always occurs every δ time units we have that

$$j = \lfloor \frac{t}{\delta} \rfloor \leq \frac{t}{\delta} \implies t \geq \delta j$$

Adding δt to both sides of the inequality gives

$$\delta t + t \geq \delta j + \delta t \implies t(1+\delta) \geq \delta(t+j)$$

Solving for t finally yields

$$t \geq \frac{\delta}{1+\delta}(t+j)$$

Choosing $\gamma_r(T) = \frac{\delta}{1+\delta}T \in \mathcal{K}_\infty$ and $N_r = 0$ the condition of Theorem 2 is satisfied for every $r > 0$.

Together, this shows that we can conclude UGpAS of $\mathcal{A}$ for the hybrid system $\mathcal{H}'$. ■

V. Case study: Dynamic Positioning

The resetting observer of (31)-(34) applies to generic observable LTV systems. In this section we show how it can be applied in a DP system.

A. Mathematical modelling and observer design

The low-frequency motion of a marine surface model can be modelled as

$$\dot{\eta} = R(\psi)\nu \tag{36a}$$

$$\dot{b} = d(t) \tag{36b}$$

$$M\dot{\nu} + D\nu = \tau + R^\top(\psi)b \tag{36c}$$

$$y = \eta \tag{36d}$$

where $\eta \in \mathbb{R}^3$ is the position and heading, $\nu \in \mathbb{R}^3$ is the body frame velocity and turn rate, $b \in \mathbb{R}^3$ is a bias term, $d(t) \in \mathbb{R}^3$ is the disturbance, and $\tau \in \mathbb{R}^3$ are the body frame thruster forces. $R(\psi) \in \mathbb{R}^{3\times3}$ is a three degree of freedom rotation matrix, $M \in \mathbb{R}^{3\times3}$ is the mass matrix, including added mass, and $D \in \mathbb{R}^{3\times3}$ is the linear damping matrix.

Note that when the marine vessel is subject to surface ocean waves, wave-frequency components of the motion will enter the measurements, y. Because (36) only models the low-frequency motion, measurements should be notch-filtered before entering the observer. This is necessary because it is not desired that the wave-frequency components of the state estimates enter the control loop.

This is a nonlinear model due to the rotation matrices. However, if we use the heading measurement directly in the rotation matrices, setting $R(t) := R(\psi(t))$, this can be considered as an external time-varying signal [11]. One should note that the heading lives in the compact set $\psi(t) \in [-\pi, \pi] \quad \forall t$ The plant can then be written in LTV form as:

$$z = \begin{bmatrix} \eta^\top, b^\top, \nu^\top \end{bmatrix}^\top \in \mathbb{R}^9, \quad u = \tau \in \mathbb{R}^3 \tag{37a}$$

$$\dot{z} = A(t)z + Bu \tag{37b}$$

$$y = Cz \tag{37c}$$

where we have assumed $d(t) = 0$, and

$$A(t) = \begin{bmatrix} 0_{3\times3} & 0_{3\times3} & R(t) \\ 0_{3\times3} & 0_{3\times3} & 0_{3\times3} \\ 0_{3\times3} & M^{-1}R(t)^\top & -M^{-1}D \end{bmatrix}$$

$$B = \begin{bmatrix} 0_{3\times3} \\ 0_{3\times3} \\ M^{-1} \end{bmatrix}$$

$$C = \begin{bmatrix} I_{3\times3} & 0_{3\times3} & 0_{3\times3} \end{bmatrix}$$

Luenberger observers for z_1 and z_2 can then be designed as

$$\dot{z}_i = A(t)z_i + Bu + L_i(t)(y - Cz_i) \tag{38}$$

where

$$L_i(t) = \begin{bmatrix} K_{1,i} \\ K_{2,i} \\ M^{-1}R^\top(t)K_{3,i} \end{bmatrix} \in \mathbb{R}^{9\times3}$$

such that the origin is UGES for $\dot{e}_i = A_i(t) := A(t) - L_i(t)C$.

These Luenberger observers can now readily be used in the resetting observer of (31)-(34).

B. Simulation study

To evaluate the performance of the proposed observer design, it was tested in simulation with a high-fidelity simulation model. The model used is the *Supply Vessel* from Marine Systems Simulator [12].

We are mainly interested the resetting observers ability to handle rapidly changing loads, as discussed in Section I. To this end, the vessel was excited by an impulsive sway disturbance at $t = 50s$. The vessel was first simulated in calm sea conditions, and then in a sea state governed by a JONSWAP wave spectrum [13]. There is no position controller in the loop, so the observer-controller interactions are not addressed in this simulation study.

The measurement error of the GNSS east and north components and heading sensor are modelled as Gauss-Markov processes [14]:

$$v[n+1] = e^{-cT_s} v[n] + \rho[n] \tag{39}$$

where $v[n]$ is the measurement at discrete time n, $\frac{1}{c}$ is the time constant for the process, T_s is the sampling time and ρ is zero-mean Gaussian white noise with standard deviation σ. The values of c, T_s and σ are chosen to match the characteristics of commercially available differential GNSS and heading sensors.

For the simulation in waves, the measurements are notch filtered before entering the observer. The notch filter used is a linear second-order filter with transfer function:

$$H(s) = \frac{s^2 + \omega_0^2}{s^2 + \omega_c s + \omega_0^2} \tag{40}$$

where ω_0 is the central frequency and ω_c is the width of the rejected band.

All parameters used in the simulations are given in Appendix A. The results are presented in Figures 3 and 4. Note that the position plot shows the estimation *error* whereas the velocity and bias plots show the estimated and true values.

C. Experimental study

The resetting observer has also been tested experimentally in model scale experiments. The experiments was conducted in the Marine Cybernetics Laboratory (MCLab) wave tank as the Department of Marine Technology at the Norwegian University of Science and Technology (NTNU). The test vessel used was Cybership 3, a 1:30 scale model of an offshore supply vessel, as shown in Figure 5.

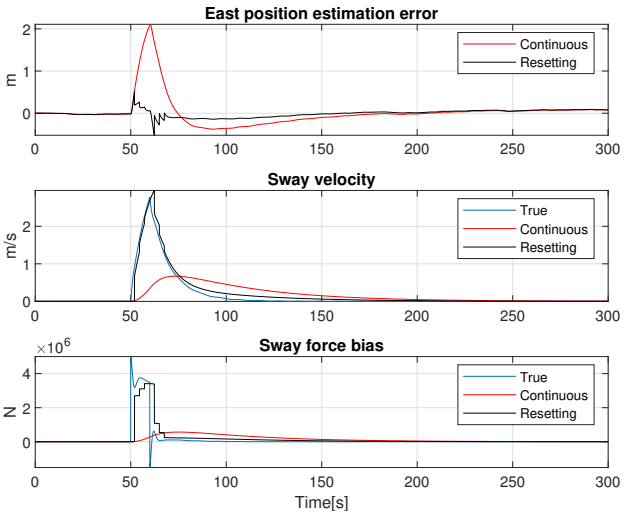

Fig. 3. Simulation results for DP observer in calm sea.

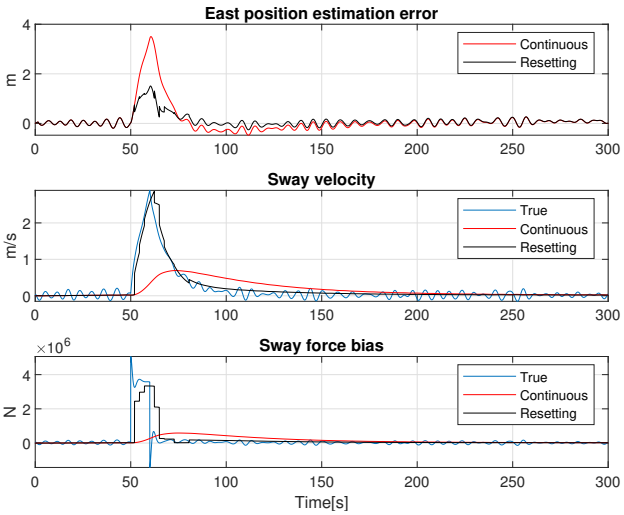

Fig. 4. Simulation results for DP observer in waves.

Fig. 5. The Cybership 3 ship model in the MCLab wave tank.

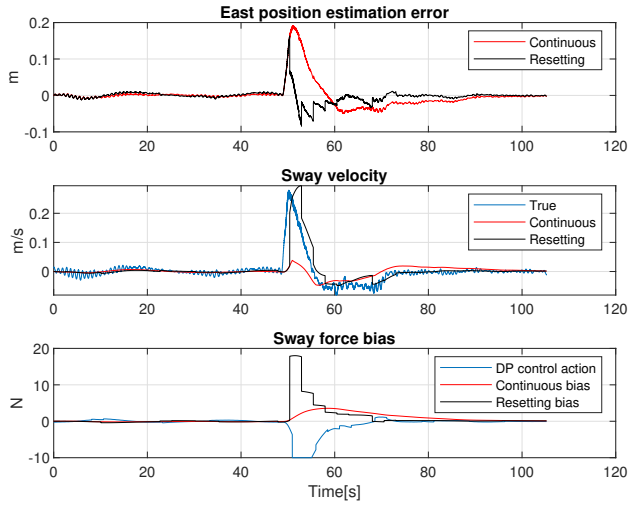

Fig. 6. Experimental results for DP observer in waves in closed loop with DP controller in moderate waves.

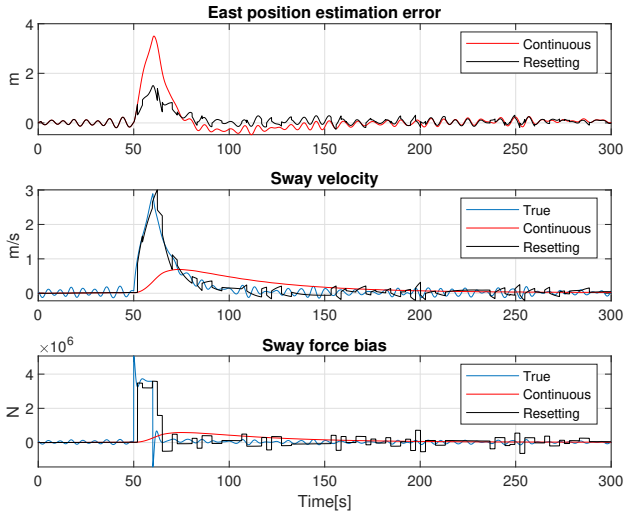

Fig. 7. Simulation results illustrating the use of too high value for the interpolation gain k

The experiment was conducted in closed-loop with a DP controller which was was fed state estimates from the resetting observer. The experiment attempted to replicate the setup used in the simulation study by giving the ship model a push in the sway-direction, giving an impulse-like, unmodelled disturbance. The experiment was conducted in a moderate sea state. For details of the experimental setup and parameter values, the reader is referred to [15].

VI. Discussion

The results from the numerical simulations in Figure 3 and 4 show promising performance. The resetting observer gives a substantial improvement during the transient phase, without amplifying measurements noise or introducing wave frequency components to the state estimates. The vessel is subject to a severe disturbance, but this is captured well by the resetting mechanism in the bias estimate. In Figure 4 it can be seen that there is a substantial wave-frequency component in the sway measurement. However, since this measurement is notch-filtered before entering the observer, this does not trigger unwanted jumps. It can also be seen that the reactivity of the observer is slightly lower in the case with waves, due to the phase-lag introduced by the notch filter. When tuning the notch filter, there must be a trade-off between phase-lag and wave attenuation. This should be adjusted to the instantaneous sea state to ensure that the wave-frequency component of the measurements can not trigger jumps.

The results from the experimental study, as shown in Figure 6 validate the findings in the simulation study. The DP sway control action from the DP controller is shown together with the resetting observer bias estimate, which shows that the state estimated from the resetting observer enable the DP controller to rapidly counteract the disturbance and return the vessel to a steady-state condition. Note that the bias estimates from the observer is not fed forward as an integral action in the DP controller. The increase in reactivity occurs due to the accurate and reactive state estimates in position and velocity. Section IV-D introduces the linear interpolation with gain k to the jump map. In an ideal world we would like to reset to the true system state. However, in practice this is not always optimal. This is illustrated in Figure 7. Here, the exact same case as in Figure 4 is simulated, except that the value of k is increased from 0.7 to 1.0. The figure shows that the wave motion combined with the measurement noise causes inaccurate estimates by the finite-time equations. This causes an overshooting behaviour which triggers a series of unwanted jumps. This behaviour is effectively mitigated by the use of an interpolation in the jump map, as Figure 4 illustrates.

Our work does not include conditions to ensure non-singularity of $(I - \Phi_2(t,0)\Phi_1^{-1}(t,0))$ for all times, and all variations of the external time-varying signal. [6] give sufficient, but highly conservative conditions for this in the case of linear time-varying systems. However, the extension of this to the time-varying case is not trivial. [16] proposes a workaround for this problem for uniformly observable systems. Here, the system is transformed to observability canonical form. The time-varying parts of the dynamics are then separated out and cancelled in the observer, resulting in time-invariant error dynamics. This may be a good approach for some systems. However, for the DP case, the transformation requires knowledge of the turn rate and yaw acceleration. Since these signals are usually not available in a ship control system, this is not an attractive solution here. In our work we propose a practical solution to avoid inverting a singular matrix by adding a check on the condition number of $(I - \Phi_2(t,0)\Phi_1^{-1}(t,0))$ before doing a jump.

VII. Conclusion

We have presented a resetting observer for linear time-varying systems. A reset is triggered if the output estimation

error exceeds predefined bounds. The jump map for the reset uses a finite-time observer approach. The finite-time equations has been derived for LTV systems, and a method for calculating the state transition matrices online has been presented. The observer equations has been formulated in a hybrid dynamical systems framework, and sufficient conditions for Uniform Global pre-Asymptotic Stability have be given.

The method has applications to observer design for dynamic positioning of marine surface vessels. A case study for this application was conducted with numerical simulations. The simulations showed promising results, with improved transient performance, compared to the state-of-the-art continuous-time observer.

The discussion highlights the need for further developments in the theoretical foundation. In particular conditions which guarantee non-singularity in the jump map is a key topic for future research.

APPENDIX

Parameter	**Value**
Vessel Lpp	$82.8m$
Vessel mass	$6362t$
Disturbance magnitude	$5 \times 10^6 N$
Disturbance duration	$10s$
Significant wave height	$2.0m$
Peak wave frequency	$1.0rad/s$
GNSS noise standard deviation (σ_{GNSS})	$0.003m$
Heading noise standard deviation ($\sigma_{Heading}$)	$0.00022rad$
Gauss-markov time constant ($1/c$)	$1100s$
Sensor sample time (T_s)	$1.0s$
Notch filter central frequency (ω_0)	$1.0rad/s$
Notch filter band width (ω_c)	$0.5rad/s$
Reset time (δ)	$2.5s$
Jump map gain (k)	0.7
Position estimation error bounds (ϵ_1, ϵ_2)	$0.1m$
Heading estimation error bounds (ϵ_3)	$0.01rad$

REFERENCES

[1] A. J. Sørensen, "A survey of dynamic positioning control systems," *Annual Reviews in Control*, vol. 35, no. 1, pp. 123–136, 2011.

[2] S. A. Vaerno, A. H. Brodtkorb, R. Skjetne, and V. Calabro, "Time-varying model-based observer for marine surface vessels in dynamic positioning," *IEEE Access*, vol. 5, pp. 14 787–14 796, 2017.

[3] Ø. K. Kjerstad and R. Skjetne, "Disturbance Rejection by Acceleration Feedforward for Marine Surface Vessels," *IEEE Access*, vol. 4, pp. 2656–2669, 2016.

[4] A. H. Brodtkorb, S. A. Værnø, A. R. Teel, A. J. Sørensen, and R. Skjetne, "Hybrid controller concept for dynamic positioning of marine vessels with experimental results," *Automatica*, vol. 93, pp. 489–497, 2018. [Online]. Available: https://doi.org/10.1016/j.automatica.2018.03.047

[5] Ø. K. Kjerstad, "Dynamic Positioning of Marine Vessels in Level Ice," Ph.D. dissertation, NTNU, 2016.

[6] R. Engel and G. Kreisselmeier, "A Continuous-Time Observer Which Converges in Finite Time," *IEEE Transactions on Automatic Control*, vol. 47, no. 7, pp. 1202–1204, 2002.

[7] T. Raff and F. Allgöwer, "An impulsive observer that estimates the exact state of a linear continuous-time system in predetermined finite time," *2007 Mediterranean Conference on Control and Automation, MED*, no. 2, pp. 2–4, 2007.

[8] C.-T. Chen, *Linear System Theory and Design*, 3rd ed. Oxford University Press, 1999.

[9] H. K. Khalil, *Nonlinear Systems*, 2nd ed. Prentice-Hall, 2002.

[10] R. Goebel, R. G. Sanfelice, and A. R. Teel, *Hybrid Dynamical Systems : Modeling, Stability, and Robustness.* Princeton University Press, 2012.

[11] S. A. Værnø, R. Skjetne, O. K. Kjerstad, and V. Calabro, "Comparison of control design models and observers for dynamic positioning of surface vessels," *Control Engineering Practice*, vol. 85, no. 1999, pp. 235–245, 2019.

[12] T. Perez, O. Smogeli, T. I. Fossen, and A. J. Sørensen, "An overview of the marine systems simulator (MSS): A simulink® toolbox for marine control systems," *Modeling, Identification and Control*, 2006.

[13] T. I. Fossen, *Handbook of Marine Craft Hydrodynamics and Motion Control*. Wiley, 2011.

[14] R. W. Beard and T. W. McLeain, *Small Unmanned Aircraft, Theory and Practice*, 2012.

[15] E. H. T. Wittemann, "Master thesis: Hybrid Observers for Autonomous Surface Vessels Experiencing Varying Operational Conditions," 2021.

[16] P. H. Menold, R. Findeisen, and F. Allgower, "Finite time convergent observers for linear time-varying systems," *Proceedings of the 11th Mediterranean conference on control and automation (T7-078)*, no. December, pp. 5673–5678, 2013.

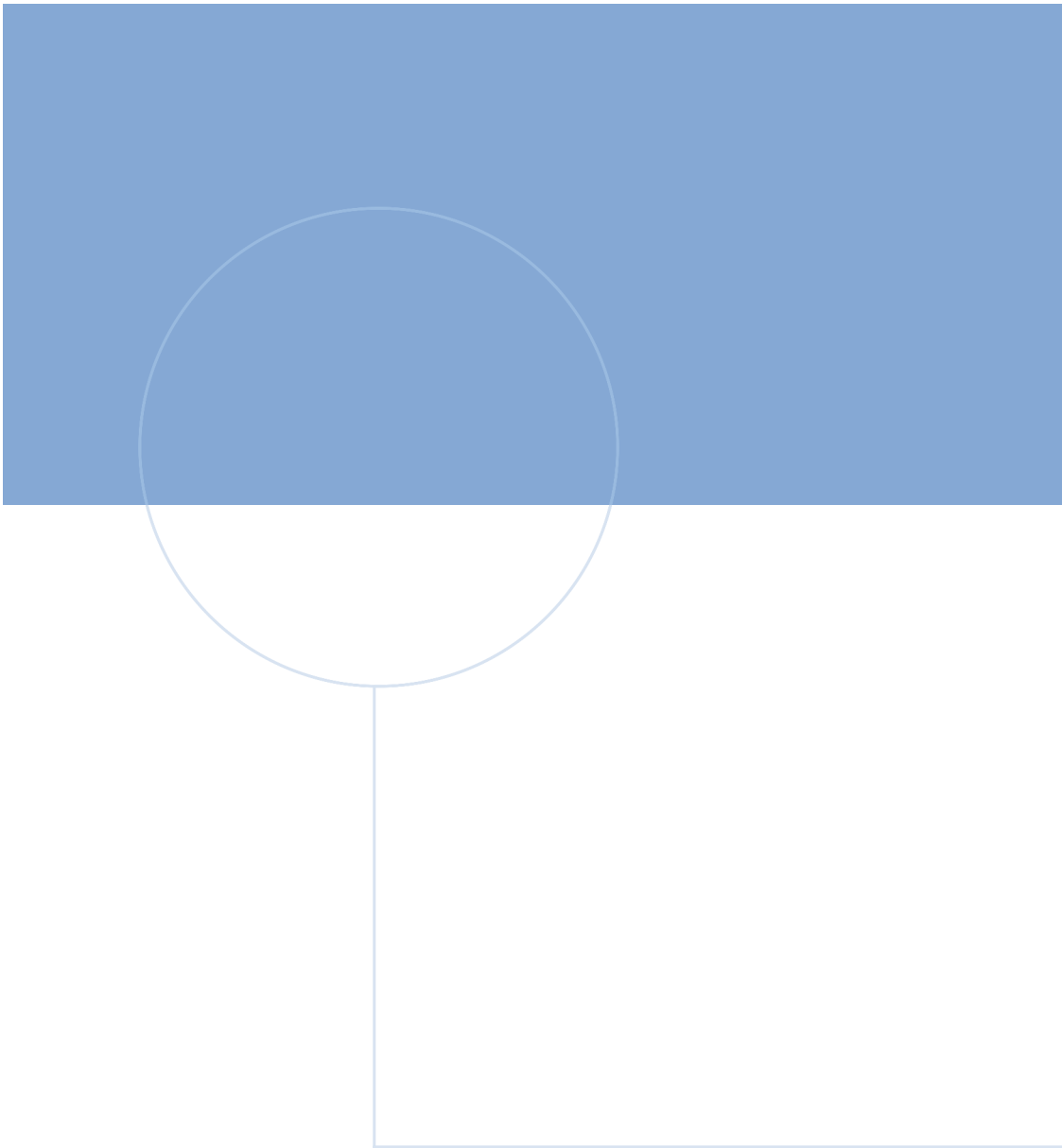

NTNU

Norwegian University of
Science and Technology